PKA phosphorylation of ATAXIN1 in Purkinje cells modulates early onset of ataxia

A DISSERTATION SUBMITTED TO THE FACULTY OF THE UNIVERSITY OF MINNESOTA BY

Judit M. Pérez Ortiz

IN PARTIAL FULFILLMENT OF THE REQUIREMENTS FOR THE DEGREE OF DOCTOR OF PHILOSOPHY

Advisor: Harry T. Orr

January 2017

Acknowledgements

Thank you to my advisor Dr. Harry Orr for letting me train in an excellent research laboratory and having the opportunity to learn an array of relevant techniques. I am particularly grateful for his expert editing in writing and advice to focus.

I thank my committee members, Dr. Paul Mermelstein, Dr. Brent Clark, Dr. Marija Cvetanovic, and Dr. Deanna Koepp for helpful feedback during my graduate training. I also thank Dr. Yoji Shimizu for his progressive leadership and individual support in trying times.

Thanks to the members of the Orr lab for the evolution of our lab family relationships in the last five years. Thank you to former lab member, Dr. Sara Lagalwar, for initial instruction in the lab and for her work on PKA studies. Thanks to Lisa Duvick for technical help especially in cloning experiments, for keeping mental historical records of all people, experiments and projects ever done in the lab, for knowing exactly where everything is, and for caring friendship. Many thanks to Orion Rainwater for mouse breeding and colony maintenance critical to this thesis work, and making sure we always have reagents. Thanks to Jillian Friedrich for training me in surgical procedures and microscopy, and for executing osmotic pump implantations shown here. Thanks to Brennon O'Callaghan for helpful conversations on kinase inhibitors and qPCR and for executing the *in vitro* phosphorylation assays shown here. To the rest of present, past, and honorary lab members for adding to a dynamic environment- Tyler Tschumperlin, Dr. Melissa Ingram, Dr. Emily Wozniak, Dr. Nissa Mollema, and Andrea Johnson. Many thanks to Dr. Christine Henzler for a crash course in RNA sequencing studies and for performing the statistical sequencing analyses presented here.

I am grateful to mentors along the way for believing in me. My science teachers Mrs. Bibiana Méndez, Mrs. Alexandra Rodriguez, and Dr. Alba Miranda Azola, for empowering my curiosity early on. To Dr. José E. García Arrarás, for providing me a platform for basic science research at the University of Puerto Rico, for nurturing my passion for science, and for being a positive role model. Dr. Pablo Ortiz for the many conversations and friendship.

Above all, I am thankful to my family, for a lifetime of love and encouragement. To my brother Carlos, for being my first role model as a studious multiple science fair winner during my formative years and for continued professional ambitions. To my father, Mario, for instilling in me a sense of curiosity for the natural world. To my sister, Maricelis, for her inspiring kindness. To Rita and Tim for their ongoing support.

Dedication

To my sources of strength and greatest champions:

To my mother Aracelis, for leading by example on how to be a hardworking, caring, unique, tenacious woman and for her unrivaled support.

To Blake, for devoted love, comfort, and encouragement during this journey. Here's to looking forward together.

Abstract

Spinocerebellar ataxia type 1 (SCA1) is a fatal adult-onset, autosomal dominant ataxia characterized in part by dysfunction and degeneration of Purkinje cells of the cerebellum. The fundamental basis of pathology is an aberration in the regulation of RNA splicing and gene transcription. SCA1 is caused by an unstable CAG trinucleotide repeat mutation in the *ATXN1* gene that codes for a toxic ATXN1 protein with an abnormal polyglutamine repeat. Decreasing mutant ATXN1 can reverse disease phenotypes in SCA1 mouse models. Phosphorylation of ATXN1 at Serine 776 (S776) is critical for disease and this modification influences ATXN1 protein levels and protein-protein interactions, which can exacerbate toxicity. Previous *in vitro* studies implicated PKA, cAMP protein kinase, in phosphorylation of ATXN1 at S776. The hypothesis being tested is that PKA-mediated ATXN1-S776 phosphorylation stabilizes ATXN1 and drives pathogenic pathways involved in disease. SCA1 mouse models expressing wild type human ATXN1[30Q] or mutant human ATXN1[82Q] were crossed to a PKA mutant mice that exhibit attenuated PKA activity. I found that PKA hypofunction leads to a decrease of phospho-S776-ATXN1 and total ATXN1 expressed in cerebellar Purkinje neurons. Mouse Atxn1 protein expressed in other cerebellar cell types was unchanged, pointing to cell specificity. In order to evaluate the disease relevance of these effects, I tested SCA1 disease metrics in the affected model, including motor behavior, histopathology and gene expression changes. Motor performance was improved to wild type levels early in disease, but progressive Purkinje cell atrophy was not averted. These results hinted at a dissociation between mechanisms causing ataxia versus Purkinje cell degeneration. Indeed, RNA sequencing studies revealed transcriptional changes linked to motor dysfunction that are distinct from those associated with progressive pathology. This work suggests ATXN1 is phosphorylated by PKA in Purkinje neurons early in disease and drives pathways that underlie early onset ataxia that are independent of pathways promoting progressive neurodegeneration.

Table of Contents

List of Tables

List of Figures

Chapter 1

GENERAL INTRODUCTION

Spinocerebellar Ataxia type 1

Spinocerebellar Ataxia type 1 (SCA1) is a fatal neurodegenerative disorder with an autosomal dominant inheritance. The genetic basis of SCA1 is a CAG repeat expansion mutation in the coding region of the Ataxin-1 (*ATXN1*) gene (Banfi et al., 1993; Orr et al., 1993). As with other trinucleotide repeat disorders, SCA1 shows genetic anticipation where the unstable repeats expand over generations, and disease onset occurs earlier and is more severe. Unaffected individuals harbor 19-36 CAG repeats, with CAT interruptions in tracts longer than 21 repeats. SCA1 patients have 43-81 uninterrupted CAG repeats (Chung et al., 1993). The gene product, ATXN1, is a predominantly nuclear protein that harbors the polyglutamine expansion mutation in its amino-terminal region. While ATXN1 is widely expressed in the brain, cerebellar Purkinje cells exhibit vulnerability to mutant ATXN1 toxicity with their degeneration underlying the ataxic phenotype. Subsequent degeneration of olivary nucleus, pons, deep cerebellar nuclei, and spinocerebellar tracts also contributes to ataxia (Schut, 1951; Zoghbi and Orr, 1995). In advanced disease, cranial nerve motor-sensory nuclei in the brainstem become involved and affected individuals succumb due to complications such as chronic lung infections and respiratory failure. There is no cure for SCA1.

Mutant ATXN1 Drives Pathology by Widely Disrupting Gene Expression

Purkinje neurons are a major early cellular target in SCA1. The role of polyglutamine tract expansion mutation in ATXN1 in Purkinje cells has been intensely studied since the generation of the SCA1 transgenic mouse model *Pcp2-ATXN1[82Q]* over twenty years ago (Burright et al., 1995). Investigating Purkinje cell basis of cerebellar

pathology has provided important insights into mechanisms of genetically triggered neurodegeneration. For example, ATXN1 nuclear inclusions (a pathological hallmark of disease) are not necessary to cause disease (Klement et al., 1998). However, ATXN1 nuclear localization is required for pathogenesis and the toxicity is driven by altering normal ATXN1 functions (Klement et al., 1998). The nuclear localization signal (NLS) directs ATXN1 translocation into the nucleus. Mice expressing mutant ATXN1[82Q] with a nonfunctional NLS do not develop disease, which demonstrates that ATXN1 exerts its toxicity in the nuclear compartment (Klement et al., 1998). Once inside the nucleus, ATXN1 interacts with cellular proteins involved in regulation of gene expression, both at the level of transcription and RNA processing.

Studies using SCA1 animal models consistently implicate aberrations in gene expression as an early part of the disease process. PCR-based cDNA subtractive hybridization first revealed abnormal gene expression in transgenic SCA1 animals (Lin et al., 2000). A set of neuronal genes highly expressed by Purkinje cells were downregulated in SCA1 cerebella, as early as P11, just one day after transgene expression and weeks before histological or behavioral deficits are detectable. These findings exhibit a causative role of mutated ATXN1 in pathogenic misregulation of gene expression. Over the years, studies have focused on groups of genes affected in disease Ca^{2+} handling/homeostasis (Lin et al., 2000), glutamate signaling (Serra et al., 2004; Zu et al., 2004), dopamine receptor (Hearst, et al., 2010), VEGF angiogenic factor (Cvetanovic et al., 2011), and synaptic proteins (Ruegsegger et al., 2016). Early expression of mutant ATXN1 contributes to disease, at least in part, by affecting RORα-mediated gene expression important for Purkinje cell maturation and cerebellar development (Serra et al., 2006). That disease onset begins by affecting development is a mechanism suggested by several SCA1 mouse models (Ebner et al., 2013; Serra et al., 2006).

More recent studies show that disease onset and progression are likely distinct processes, best illustrated by transgenic mice expressing ATXN1[30Q]-D776 in Purkinje cells. *ATXN1[30Q]-D776* mice develop an ataxia that closely resembles that seen in *ATXN1[82Q]* transgenic mice, but their disease does not progress to Purkinje cell death

(Duvick et al., 2010). RNAseq analysis of cerebellar tissue at early, mid, and late stages of disease was performed using *ATXN1[82Q]* mice (with a progressive disease) and *ATXN1[30Q]-D776* mice (having a non-progressive disease) to uncover pathways that underlie progressive disease as well as those that might prevent disease progression (Ingram et al., 2016). Weighted Gene Coexpression Network Analysis (WGCNA) of the RNAseq data across all ages and genotypes identified two modules, designated Magenta and Lt Yellow, as being associated with disease (Ingram et al., 2016). Importantly, the degree of misexpression of genes in the Magenta module are in hand with the progressive phenotypic changes seen in *ATXN1[82Q]* disease. Therefore, genes within in the Magenta gene module are associated with progressive disease changes in SCA1.

Pathogenic Properties of Mutant ATXN1 Protein and S776 Phosphorylation

Mutant ATXN1 toxicity is not solely dictated by the polyglutamine tract mutation. The C-terminal region of ATXN1 harbors several motifs that are required for the protein to be pathogenic. The ATXN1 AXH domain allows its homodimerization and interaction with regulators of transcription such as the transcriptional repressor Capicua (Cic) (Kim et al., 2013). ATXN1 and Cic together exist in large protein complexes in which mutant ATXN1 is thought to affect Cic repressor activity (Lam et al., 2006). A knockin SCA1 mouse model that expresses 154Q at the endogenous *Sca1* mouse locus ($Sca1^{154Q/2Q}$) develops an ataxia phenotype as well as other features of the human disease, including wasting and brainstem degeneration-dependent lethality (Watase et al., 2002; Jafar-Nejad et al., 2011). $Sca1^{154Q/2Q}$ mice with partial (50%) genetic ablation of *Cic* show improvement in motor coordination, weight, survival, and neuropathology. Microarray analysis reveals that many *Cic* target genes that were repressed in $Sca1^{154Q/2Q}$ were restored to near wild type levels with $Cic^{+/-}$ (Fryer et al., 2011). This finding argues for Atxn1 toxicity acting through a gain of function mechanism, whereby mutant Atxn1 affects the normal function of an Atxn1 binding partner (Cic) and exacerbates its normal gene-repressor function *in vivo*. Paradoxically, genes normally repressed by Cic are also overexpressed in $Sca1^{154Q/2Q}$ and their levels restored with partial *Cic* ablation. Thus, mutant Atxn1 likewise results in Cic loss of function. Together these observations illustrate the complex role of Atxn1 on gene

regulation. Ultimately, because partial ablation of *Cic* in *Sca1*$^{154Q/2Q}$ resulted in an improvement in disease suggests Atxn1 exerts its toxicity predominantly via Cic gain of function and hyper-repression of Cic target genes. These results show that mutant Atxn1 pathogenicity acts through aberrant interactions with its native binding partners.

A key site at the C-terminus of ATXN1 is the serine at amino acid position 776 (S776). A large body of evidence supports that S776 phosphorylation is critical for ATXN1 toxicity. A pivotal finding is that mice expressing ATXN1[82Q]-S776A phospho-resistant mutation do not develop ataxia and largely resemble wild type mice, despite harboring a mutant polyQ tract (Emamian et al., 2003). On the other hand, while *SCA1* mice expressing wild type ATXN1[30Q] are not affected, ATXN1[30Q]-S776D phosphomimicking mutation drives disease. Furthermore, D776 mutation enhances toxicity in *ATXN1[82Q]-D776* mice (Duvick et al., 2010). How does a single phosphate addition to S776 change ATXN1 so drastically? Two properties S776 phosphorylation confers to ATXN1 are greater stability and enhanced protein-protein interactions. Abnormally elevated levels of ATXN1, even in the wild type form, are pathogenic when overexpressed in both *Drosophila* and mice, suggesting ATXN1 protein load itself is toxic (Fernandez-Funez et al., 2000; Gennarino et al., 2015). The nonpathogenic ATXN1-A776 protein is unstable *in vivo* and its lowered levels are thought to be an important factor involved in averting toxicity (Emamian et al., 2003, Jorgensen et al., 2009). Another biologically relevant biochemical change brought upon ATXN1-S776 phosphorylation is enhanced interactions with other proteins, discussed below.

One mechanism that stabilizes phosphorylated pS776-ATXN1 is interaction with the molecular chaperone 14-3-3. Co-expression of ATXN1[82Q] and d14-3-3ε in Drosophila retina enhances ATXN1[82Q]-induced eye degeneration (Chen et al., 2003). In mice, 14-3-3ε haploinsufficiency (*Sca*$^{154Q/2Q}$*;14-3-3ε*$^{+/-}$) rescues the motor phenotype and Purkinje cell numbers (Jafar-Nejad et al., 2011). *In vivo,* 14-3-3ε haploinsufficiency results in lower Atxn1 levels in the cerebellum (Jafar-Nejad et al., 2011). *In vitro,* competitively disrupting 14-3-3/ATXN1 interaction with a peptide or by siRNA-mediated knockdown of 14-3-3 prompts ATXN1-S776 dephosphorylation and increased clearance of ATXN1 (Lai

et al., 2011). While 14-3-3/pS776-ATXN1 binding protects ATXN1 clearance by blocking dephosphorylation, it seems that phosphorylation itself makes ATXN1 more stable: ATXN1-D776 does not bind 14-3-3 and is as stable as phosphorylated ATXN1, suggesting the phosphorylation alone stabilizes the protein (Lai et al., 2011). Experiments exploring 14-3-3ε/pS776-ATXN1 interactions show that perhaps this interaction is unique to the cerebellum; while partial loss of *14-3-3ε* leads to lowered Atxn1 (154Q and 2Q) levels in the cerebellum, this is not the case in brainstem (Jafar-Nejad et al., 2011). Whether a different 14-3-3 isoform mediates this stabilizing interaction in the brainstem remains unexplored. Perhaps *14-3-3ε*$^{+/-}$ does not affect Atxn1 levels in the brainstem as it does in the cerebellum due to distinct protein interactions in these different brain regions. Biochemical studies demonstrate a shift in the incorporation of mutant Atxn1 from large (toxic) to small protein complexes in the cerebellum with partial loss of 14-3-3, but this was not seen in the brainstem (Jafar-Nejad et al., 2011). These observations suggest protein complex composition in the brainstem differs from that in the cerebellum. Moreover, this might provide a rationale to explain why cerebellum-related motor deficits were rescued in *Sca*$^{154Q/2Q}$*;14-3-3ε*$^{+/-}$ mice, but not there was no protection from brainstem-related deficits, including weight loss, premature death, and respiratory dysfunction. Differences in Atxn1-binding complexes suggest Atxn1 serves more than one functions and reveals potentially diverging mechanisms by which mutant Atxn1 exerts toxicity in different regions of the brain.

Perhaps the most intriguing interaction modulated by S776 phosphorylation is interaction in the nucleus with splicing factor RBM17. Work done by Lim and colleagues in Drosophila show that RBM17 overexpression worsens retinal degenerative phenotype when co-expressed with mutant ATXN1[82Q], but not with wild type ATXN1[30Q] (Lim et al., 2008). Conversely, partial genetic ablation of *dRBM17* (*SPF45*) in transgenic flies expressing mutant ATXN1[82Q] attenuates pathology. These findings indicate enhanced ATXN1[82Q]/RBM17 interaction is toxic *in vivo*. In the same study, co-immunoprecipitation experiments revealed RBM17 binding is enhanced by two key characteristics necessary for ATXN1 pathogenicity, polyglutamine tract length and S776 phosphorylation. That ATXN1[30Q]-D776 also shows enhanced binding to RBM17

suggests pathogenic effects of this phospho-mimicking protein are due to downstream effects of aberrant RBM17 interaction. Finally, ATXN1/RBM17 binding occurs in macromolecular complexes that are distinct from those in which ATXN1 interacts with Cic. Interestingly, RBM17 and Cic complexes compete for ATXN1 binding (Lim et al., 2008).

Taken together, ATXN1 exists in at least two large protein complexes that contain either Cic or RBM17 and which is likely regulated by S776 phosphorylation state. ATXN1's ability to interact with transcription and splicing factors echoes the characteristic ability of factors that regulate co-transcriptional splicing, some of which are affected in other neurodegenerative diseases such as Amyotrophic Lateral Sclerosis (Masuda et al., 2016; Sánchez-Hernández et al., 2016). It is possible that ATXN1 regulates gene expression by the spatiotemporal coupling of these two nuclear events. In this model, under normal conditions ATXN1 interacts transiently with at least two macromolecular complexes containing either Cic or RBM17. Glutamine expansion or D776 (i.e. constitutive S776 phosphorylation) create a shift in the normal binding dynamics, favoring a toxic enhanced interaction with the RBM17 complex, and disrupting normal equilibrium between gene transcription and splicing (**Figure 1**). Evidence in favor of a combined gain- and loss- of function mechanism through which ATXN1 acts arose in simple observation of $Sca1^{154Q/-}$ mice (Lim et al. 2008). Simultaneous deletion of wild type Atxn1[2Q] along with mutant Atxn1[154Q] expression ($Sca1^{154Q/-}$) produces a mouse with worse rotarod performance and poorer survival than the already sick $Sca1^{154Q/2Q}$. It seems that in the heterozygous state, wild type Atxn1[2Q] expression and function partially compensates for Atxn1[154Q]-induced gain and loss of function toxicity.

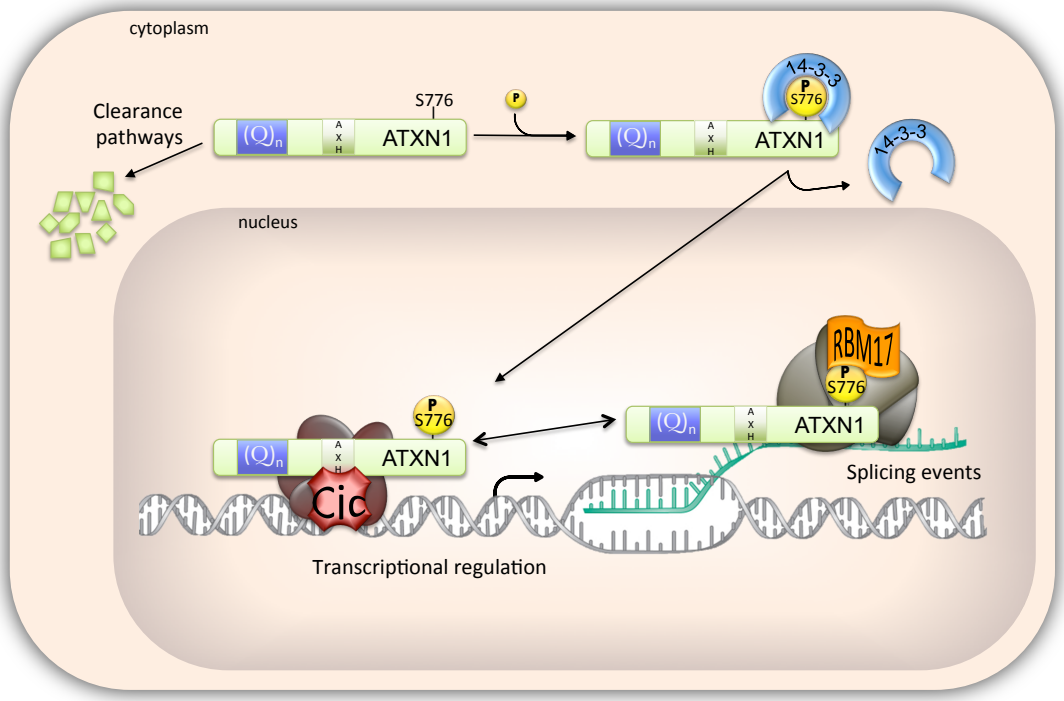

Figure 1. ATXN1 intracellular pathways. ATXN1 is a predominantly nuclear protein that shuttles between the cytoplasm and nucleus. Phosphorylation of ATXN1-S776 in the cytoplasm promotes binding by 14-3-3 at this site, which stabilizes ATXN1. Unphosphorylated ATXN1 is otherwise rapidly cleared. By some yet undefined mechanism, 14-3-3 dissociates and ATXN1 enters the nucleus. Nuclear ATXN1 can incorporate into complexes containing the transcriptional repressor Capicua (Cic) or the splicing factor RBM17 to participate in transcription and splicing events. It is in the nucleus where glutamine-expanded ATXN1 exerts its toxicity.

ATXN1 S776 phosphorylation and protein stability

Accumulation of disease-causing proteins is a hallmark of many neurodegenerative diseases, such as Parkinson's, Alzheimer's and the polyglutamine diseases, including the SCAs (López Otin et al., 2013). The accumulations are thought to be due in part to mutant proteins being resistant to degradation. In SCA1 models, decreasing mutant ATXN1 via several approaches can reverse disease phenotypes. These approaches include turning off gene expression, overexpression of molecular chaperones, and RNAi-mediated silencing (Zu et al., 2004; Serra et al., 2006; Cummings et al., 1998; Cummings et al., 2001; Keiser et al., 2013; Keiser et al., 2014; Keiser et al., 2016). Conversely, triggers of ATXN1 aggregation, such as polyglutamine tract expansion, disruption of protein clearance

pathways, overexpression, and S776 phosphorylation worsen disease (Clark et al., 1997; Cummings et al., 1999; Fernandez-Funez et al., 2000; Gennarino et al., 2015, Emamian et al., 2003). Importantly, ATXN1 protein levels and ATXN1 pathogenicity are significantly controlled by S776 phosphorylation status (Emamian et al., 2003). As a modifiable post-translational modification, phosphorylation of S776 is considered a viable therapeutic target, whereby blocking kinase activity to S776 would promote ATXN1 protein clearance and alleviate disease.

Kinases shown to phosphorylate ATXN1-S776

Efforts to identify the kinase pathway(s) involved in S776 phosphorylation have produced several promising candidates. Three main candidate kinases have been identified, PKB/AKT, MSK1, and PKA. Considering that 518 kinase genes have been identified in the human genome (and 540 kinase genes in mouse genome), the initial efforts to narrow the large number of possibilities used kinase prediction software (Manning et al., 2002a, b; Caenepeel et al., 2004; Emamian et al., 2003). The kinase recognition site surrounding S776 was identified as KRRWSAP and a handful of candidate kinases were identified, including PKB/Akt and PKA (Emamian et al., 2003). This is not surprising, as Akt and PKA belong to the same class of kinases known as the Arg-directed kinases, which also include PKC, PKG, and RSK (Manning et al., 2002a, b). AGC-family kinases share some substrate specificity with an Arg at position -3 relative to the phosphorylated serine or threonine (Akt's recognition sequence is RX**R**XXS/T and PKA's is **R**RXS/TY) (Kemp and Pearson, 1990). More recently a high-throughput siRNA kinase screen was used in a cell model stably overexpressing ATXN1[82Q]-S776 to identify kinases that when knocked down decrease ATXN1 levels. MSK1, another member of AGC family kinases with consensus sequence **R**XXS, was identified (Park et al., 2013; Roux et al., 2004).

The three candidate kinases (AKT, PKA, and MSK1) have been scrutinized over the years. All three enzymes phosphorylate purified GST-ATXN1-S776 *in vitro* (Jorgensen et al., 2009; Park et al., 2013). Cell culture or *in vitro* experiments have shown that compounds with pharmacologic selectivity to these kinases can block S776

phosphorylation (Kaytor et al., 2005). However, beyond reductionist *in vitro* studies, the crucial test lies in validating the relevance of these kinase pathways *in vivo*.

The role of Akt-mediated phosphorylation in Purkinje cells has been questioned *in vivo*. A mouse model expressing a dominant negative form of Akt (Akt-DN) in Purkinje cells was crossed to ATXN1[82Q] transgenic model and failed to show a reduction in ATXN1 levels or improvement in measures of SCA1-like pathology (Jorgensen et al., 2009). Therefore, Akt was ruled out as being a direct kinase to ATXN1-S776 in Purkinje cells *in vivo*. However, because this model was restricted to Akt in Purkinje cells, it does not rule out the possibility that Akt may play a role in other cell types.

The role of Msk1 *in vivo* was tested in $Sca1^{154Q/2Q}$ knockin mice (Lorenzetti et al., 2000). Crossing $Sca1^{154Q/2Q}$ to $Msk1^{-/-}$ mice generates mice that globally express one copy of wild type Atxn1[2Q] and one copy of mutant Atxn1[154Q] at endogenous levels and do not express Msk1 (Park et al., 2013). Immunoblotting for pS776-Atxn1[154Q] and total Atxn1[154Q] show levels are slightly (~15%), but significantly reduced in cerebellum deficient in Msk1 (Park et al., 2013). Because Atxn1 phosphorylation is tightly linked to its stability, a decrease in total Atxn1 closely tracks reduction in S776 phosphorylation. $Msk1^{+/-};Msk2^{+/-}$ mice were crossed to transgenic mice overexpressing ATXN1[82Q] in Purkinje cells and this too resulted in a small reduction of Purkinje cell expressed ATXN1[82Q], as well as whole cerebellum Atxn1[2Q]. Thus, it requires 100% loss of Msk1 or 50% reduction of both Msk1 and Msk2 to result in a slight reduction of Ataxin1 in the whole cerebellum or ATXN1 in the Purkinje cell population. With the reduction in mutant protein there is improvement in Rotarod motor performance in $Sca1^{154Q/2Q};Msk1^{+/-};Msk2^{+/-}$ mice compared to $Sca1^{154Q/2Q};Msk1^{+/+};Msk2^{+/+}$ mice, but they do not perform as well as unaffected wild type controls. Behavioral outcome of the transgenic $ATXN1[82Q];Msk^{+/-};Msk2^{+/-}$ mice was not reported. While these findings on the role of Msk1 are noteworthy, the behavioral improvement reported is modest and the biochemical effect on Atxn1[154Q] protein is minimal (**Appendix 1**). Moreover, the reported data does not explicitly address the Purkinje cell basis of disease; the behavioral improvement might also be due to Atxn1[154Q] reduction in other cell types in the cerebellum or other brain

regions involved in motor coordination. Possibly Msk1's role in S776 phosphorylation in the cerebellum is not unique to Purkinje neurons.

ATXN1 phosphorylation by PKA

Support for PKA having a role in S776 phosphorylation comes from the following key experiments. Fractionation assays in mouse cerebellum show that fractions with maximum ability to phosphorylate ATXN1-S776 are also enriched in PKA kinase (Jorgensen et al., 2009). Interestingly these studies revealed that Akt is not present in kinase active fractions, further ruling our Akt as a biologically relevant kinase in SCA1 (Jorgensen et al., 2009). These observations were independently confirmed by another study that demonstrated Msk1 also co-fractionates with cerebellar fractions containing S776 phosphorylating activity (Park et al., 2013). Careful evaluation of this data shows that PKA kinase perfectly aligns with the S776 kinase activity, while Msk1 only partially overlaps. Functionally, PKA can phosphorylate ATXN1 *in vitro* (using purified PKA), in a human cell line, and in cerebellar homogenates (Jorgensen et al., 2009; unpublished data). Immunodepletion of PKA from mouse whole cerebellar lysates dampens the ability of the PKA-deficient lysate to phosphorylate GST-ATXN1 (Jorgensen 2009 et al., 2009). Finally, use of kinase inhibitors targeting PKA also achieves a reduction in ATXN1-S776 phosphorylation (Jorgensen et al., 2009, Kaytor et al., 2005). To date, the role of PKA in controlling ATXN1-S776 phosphorylation has not been demonstrated *in vivo*.

Features of PKA Subunit Composition and its Implications

PKA consists of two catalytic (C) and two regulatory (R) subunits that together form an inactive heterotetrameric holoenzyme (C_2R_2). Upon signaling activation, cAMP molecules bind the regulatory subunits, inducing a conformational change that triggers dissociation and release of catalytic subunit monomers (Brandon et al., 1995). Phosphorylation is carried out by the PKA catalytic subunits. There are two catalytic subunits (Cα and Cβ) in mice encoded by two distinct genes (*Prakaca* and *Prakacb*), with a third found in primates (Cγ) (Uhler et al., 1986a, b). Cα and Cβ share high sequence

homology (93%), but display differences in enzyme kinetics and exhibit different expression patterns, suggesting a differential role of C subunits across tissues (Walsh et al., 1994; Gamm et al., 1996; Cadd and Mcknight, 1989). In one study, Cα displays lower K_m values on two of three peptide substrates tested, indicating differential substrate preference (Gamm et al., 1996). In turn, the V_{max} for all three peptide substrates is nearly identical for both Cα and Cβ, suggesting enzymatic activity per se is not different between isoforms. K_m and V_{max} for ATP was also identical between isoforms. However, examination of the cAMP activation constant ($Ka_{(cAMP)}$) is much lower for holoenzyme containing Cβ ($R_2C\beta_2$). In other words, R subunit sensitivity to cAMP (which activates PKA) is affected by which catalytic subunit it is bound to. Indeed, basal activity of $R_2C\beta_2$ is 5x higher than $R_2C\alpha_2$. Moreover, the IC_{50} for the native PKA inhibitor PKI and R subunit is lower for $R_2C\alpha_2$ PKA. Taken together, these findings reveal (i) C subunits exhibit subtle differences in substrate selectivity, (ii) PKA containing Cβ is more sensitive to activation, and (iii) PKA containing Cα is more sensitive to inhibition signals. Considering that Cα is the more broadly and highly expressed subunit, it is not surprising that its activity may be more strictly regulated.

PKAcα expression is critical for organismal development and viability. Gene knockout of PKAcα (*Prakaca*-/-) is not compatible with life (Skalhegg et al., 2002). The small subset (30%) of *Prakaca*-/- mice that survive into young adulthood display growth retardation and male infertility, and are too fragile to perform behavioral studies. Biochemical assessment of several distinct tissues in this model show a dramatic deficiency in cAMP-dependent PKA stimulation, supporting the major role Cα plays in PKA signaling. Tissues that also express Cβ, including the brain, show an attenuated deficit in baseline PKA activity compared to tissues not expressing this catalytic subunit (Skalhegg et al., 2002). These effects are likely due to the compensatory increase seen in Cβ protein levels with complete loss of Cα.

There are three PKAcβ isoforms (Guthrie et al., 1997). Cβ1 is expressed in all tissues, while Cβ2 and Cβ3 are only expressed in the brain, especially in limbic areas. Knockout models of PKAcβ are phenotypically normal, thus Cβ function is not critical for

life. Mice null in either in Cβ1 (*Prkacb[Cβ1]-/-*) or all three isoforms (*Prkacb-/-*) show deficits in hippocampal plasticity (Qi et al., 1996; Howe et al., 2002). Functionally, Cβ null mice have lower basal PKA activity, but cAMP-stimulated PKA activity is unaffected, possibly due to a compensatory increase in Cα.

Murine cerebellum exhibits differential expression of the PKA subunits (Lein et al., 2007; Cadd and McKnight, 1989). Cα (*Prkaca)* is highly expressed in Purkinje neurons, while Cβ (*Prkacb*) expression is very low and not detected in Purkinje cells (Cadd and McKnight, 1989). Both *Prkaca* and *Prkacb* are found in the granular layer. These observations are consistent with *in situ* hybridization from the Allen Brain Atlas (**Figure 2**). In the cerebellum, Purkinje cells are the major cellular target of SCA1. Therefore, focusing on the Purkinje cell-enriched Cα subunit is a logical strategy to study the contribution of PKA signaling in SCA1.

My thesis sought to validate the hypothesis that PKA plays a major role in regulating ATXN1-S776 phosphorylation in cerebellar Purkinje cells *in vivo*. To achieve this, I first used a pharmacologic approach to selective block Atxn1 phosphorylation by PKA in organotypic cerebellar slices. I also examined the distribution of ATXN1 and PKA in murine cerebellum. Next, I obtained a PKA mutant mouse that exhibits attenuated expression and activity of the major PKA catalytic subunit that is expressed in Purkinje cells, Cα. PKA mutant mice were crossed to SCA1 transgenic models to determine whether PKA hypofunction is of biochemical consequence to ATXN1-S776. The effects on SCA1-like behavioral and histological phenotypes were also investigated. Finally, I pursued RNA sequencing studies on the PKA mutant-SCA1 mice crosses. We identified a link between PKA control of ATXN1-S776 phosphorylation and early onset ataxia with associated transcriptional changes. Together, these represent distinct disease processes to those connected to progressive pathology influenced by mutant ATXN1[82Q] protein load in Purkinje cells.

Expression atlas

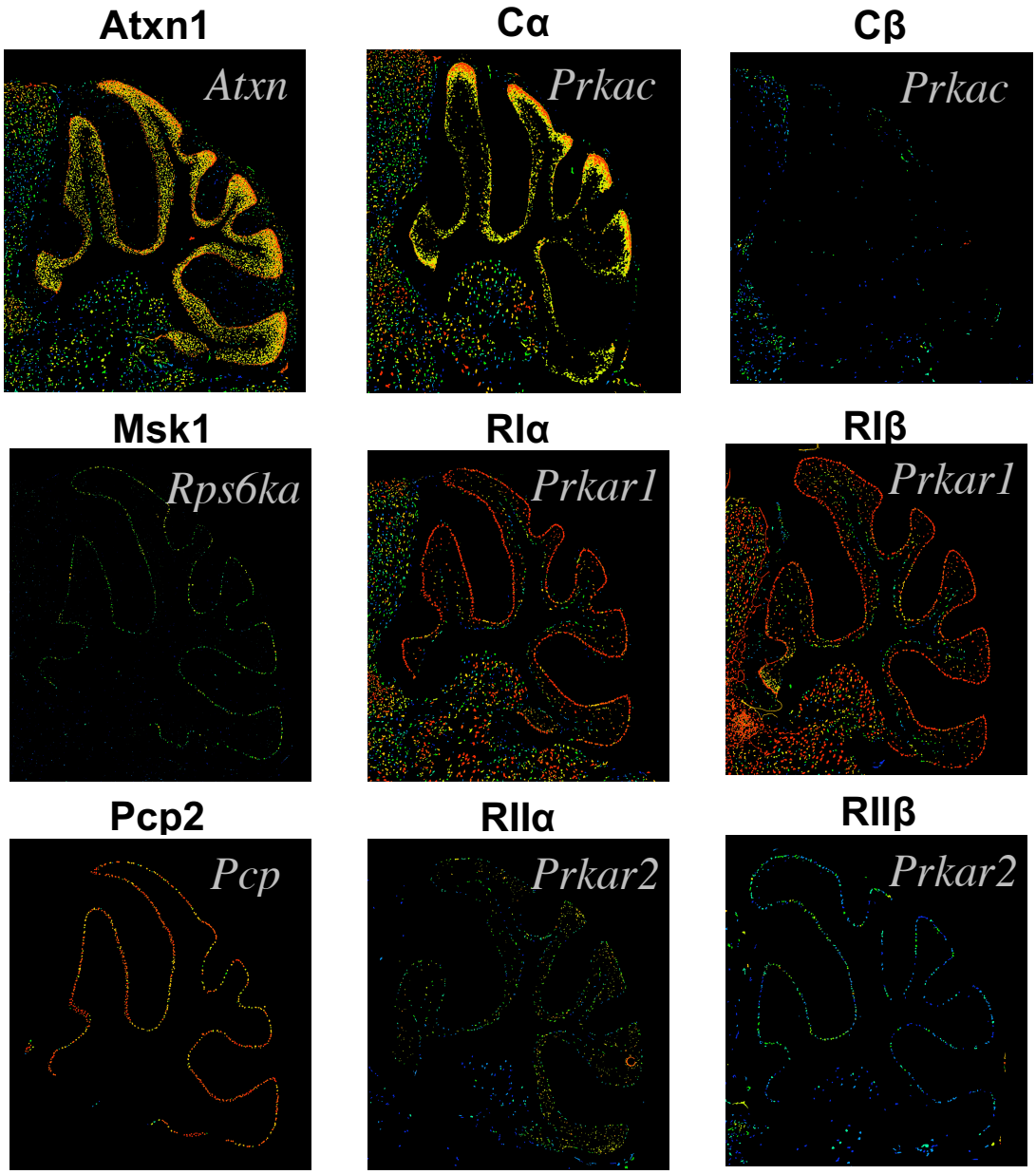

Figure 2. Allen Brain Atlas expression map. In situ hybridization data of genes indicated. Gene names are in italics inside the box and protein name is placed above each image.

Chapter 2

IN PURKINJE CELLS THE PKA PATHWAY REGULATES ATXN1 PHOSPHORYLATION AND STABILITY

Introduction

Rationale for Studying PKA in SCA1 mouse model

The SCA1-causing protein, ATXN1, harbors an expanded mutated polyglutamine tract that transforms it into a pathogenic protein prone to abnormal aggregation. Beyond the polyglutamine tract, ATXN1 phosphorylation at S776 modifies its pathogenicity in part by modulating protein stability and in part by creating a shifting towards abnormal protein interactions. Therefore, blocking S776 phosphorylation represents a druggable therapeutic target to deter ATXN1-induced toxicity. Identifying the kinase(s) involved in S776 modification *in vivo* is a key step towards exploiting this potential. To date, studies have identified two promising *in vivo* kinases, Msk1 and PKA. Data in support of Msk1 rest on the finding that Msk1/2 haploinsufficient *Sca1*$^{154Q/2Q}$ mice show partial rotarod recovery correlated with a decrease in mutant Atxn1 in the cerebellum *in vivo* (Park et al., 2013). However, the biochemical and behavioral effects in these studies are not robust nor do they address Purkinje cell biology. Studies involving the role of PKA in ATXN1 phosphorylation are compelling, but have been limited to *in vitro* tools (Jorgensen et al., 2009). Evidence in support of the contribution of the PKA pathway in SCA1 is not available *in vivo*.

To date, investigating the role of PKA in SCA1 *in vivo* has been challenging. Efforts in our lab to virally deliver shRNAs to knock down the catalytic subunits in murine cerebellum were hindered by limited breadth of delivery, inefficient cell targeting, and insufficient knockdown (unpublished data). At the same time, while *Prakaca-/-* mice would be an ideal genetic tool to study the role of the major catalytic subunit of PKA in SCA1, their severe phenotype precludes it as a viable model (Skalhegg et al., 2002). We have now obtained a PKA hypofunction mouse model to test the role of PKA *in vivo*.

Results

GSK690693 is a potent pharmacologic inhibitor of PKA that facilitates Atxn1 clearance ex vivo

As a first step in testing the role of PKA in regulating phosphorylation-mediated Atxn1 stability, a potent small molecule inhibitor was chosen to block PKA in organotypic cerebellar slices. A kinase panel analysis was done in collaboration with the Institute for Therapeutics Discovery and Development to identify compounds with strong inhibition against PKA. Activity against other kinases shown to affect Atxn1 *in vivo* was measured in the same screen. The compound GSK690693 stood out for potent, selective activity against PKA (IC_{50} = 8.745nM) (**Figure 3A**), with 50-130 times less activity against MSK1 (IC_{50} = 0.4915uM) or MSK2 (IC_{50} = 1.13uM), thus making it an attractive tool to study effects of PKA over MSK1. GSK690693 also has strong AKT inhibition (IC_{50} = 4.085nM).

Next, organotypic cerebellar slices from P13 $Sca1^{66Q/2Q}$ mice were cultured and treated with increasing concentrations of the cell-permeable GSK690693 or equal volume of vehicle (100% DMSO) in duplicate wells for 5 days. In the $Sca1^{66Q/2Q}$ knockin model a CAG (polyQ) expansion was knocked into the mouse *Sca1* locus to broadly express Atxn1[66Q] and wild type Atxn1[2Q] at endogenous levels (Lorenzetti et al., 2000). At the end of the treatment period, the slices were homogenized and protein extracts run on a western blot. A rabbit monoclonal antibody that detects phosphorylated proteins with the PKA consensus sequence (RRXS/T) was used to evaluate the efficacy of this small molecule to block phosphorylation of PKA substrates. At 10uM GSK690693, there was robust inhibition of phosphorylation of most of the detectable PKA substrates at high molecular weight (**Figure 3B**, quantified in **3C**).

Based on the dosage results above, 10uM GSK690693 was added to P10 $Sca1^{66Q/2Q}$ cerebellar slices for 1, 3, and 5 days (n = 5). At this dose, strong inhibition of PKA phospho substrates was evident after just one day of treatment, which lasted through the duration of the treatment period (**Figure 3D**, quantified in **3E**). Reduction in phospho-Atxn1-S776 was

Figure 3

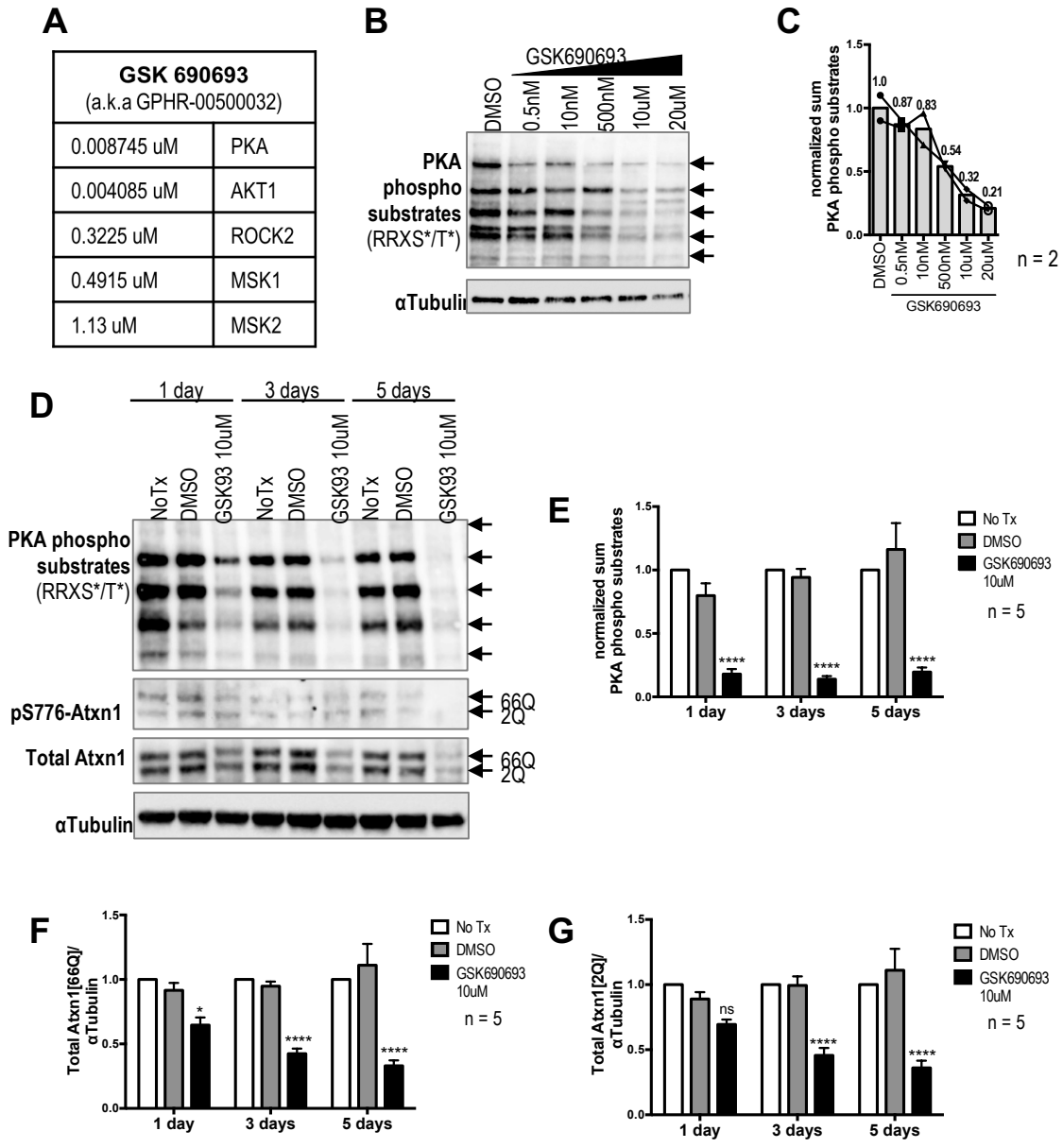

Figure 3. PKA small molecule inhibitor GSK690693 progressively lowers Atxn1 levels in *Sca1*$^{66Q/2Q}$ cerebellar slices. (**A**) Kinase panel assay of GSK690693 against five kinases shown to phosphorylate Ataxin1 indicates its strong potency against PKA with an IC_{50} in the single-digit nanomolar range. (**B**) Organotypic cerebellar slices of P10 ± 1d pups were isolated and cultured for one day before treatment onset. Dose-dependent inhibition of high molecular weight PKA substrates was observed in slices treated with increasing amount of

GSK690693 kinase inhibitor for 5 days. Samples of this pilot assay were run in duplicate, so the values are graphed connected by lines to provide a visual representation of the data (**C**). PKA substrates are proteins harboring the RRXS/T PKA consensus sequence (arrows indicate which bands were quantified). (**D**) Treatment of cerebellar slices with 10uM GSK690693 over a period of 5 days shows strong, rapid inhibition of PKA substrates (n=5), (quantified in **E**). PKA kinase inhibition leads to Atxn1-S776 dephosphorylation closely followed by clearance of total Atxn1 (quantified in **F** and **G**, respectively). Data are represented as mean, ± SEM. Two-Way ANOVA. * $p < 0.05$, ** $p < 0.01$, *** $p < 0.001$, $p < 0.0001$.

also seen after one day of treatment, which led to a decline in total Atxn1 levels (**Figure 3D**). The dephosphorylation-dependent facilitation of Atxn1 clearance proceeded over the five-day period (**Figure 3D**, quantified in **3F** and **3G**). Both Atxn1[66Q] and Atxn1[2Q] were affected to the same degree. Thus, blocking PKA activity *ex vivo* enhances Atxn1 clearance in whole cerebellum and it does not display substrate selectivity between Atxn1 with a short (2Q) or expanded (66Q) polyglutamine tract.

PKA inhibition by GSK690693 destabilizes ATXN1 in a human cell line

The next objective was to quantify the effect PKA-mediated phosphorylation on the stability of ATXN1 protein. The first experiment sought to establish the stability of ATXN1 protein in DAOY cells. The DAOY cell line is a human medulloblastoma cell line that expresses ATXN1. I reasoned that focusing the study of ATXN1 stability to a single cell type would reduce the complexity of the study and achieve more conclusive results, in contrast to the more heterogeneous and potentially variable cerebellar slices.

Cycloheximide (CHX) is a protein synthesis inhibitor used to track decay of a target protein over time and provide an estimate a protein's half-life, $t_{1/2}$ (Zhou et al., 2004). DAOY cells were plated at a density of 0.75 x 10^5 cells/ml, treated with 40ug/ml CHX over the course of 56 hours, and subjected to western blotting for quantification of residual protein. Under these conditions, ATXN1 clearance was marginal. In fact, ~14-20% of ATXN1 loss occurred within the first 24 hours (**Figure 4A**, quantified in **4B**). At 32 hours, ATXN1 had decreased by ~30%, which was stable out to 56 hours when the study was concluded. At the end of the experiment, only ~26% of ATXN1 had been cleared. Cyclin E was used as

a positive control to verify efficacy of CHX treatment at this plating density and showed a steady protein clearance curve (**Figure 4A**, quantified in **4B**). These results indicate that ATXN1 is a very stable protein.

Figure 4

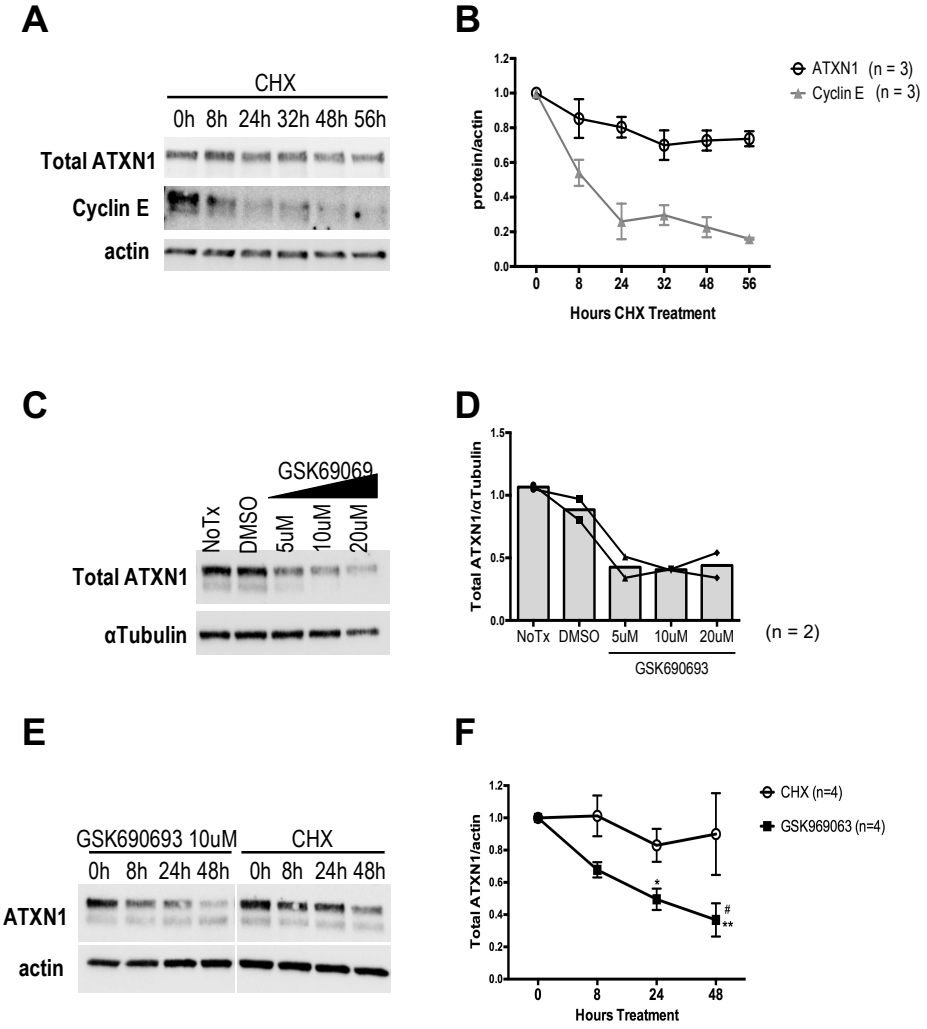

Figure 4. Kinase inhibition with GSK690693 facilitates ATXN1 clearance in a human cell line. DAOY medulloblastoma cells were used to evaluate ATXN1 stability. Cycloheximide assay was used to estimate ATXN1 clearance (n=3 for each time point) (**A**, graphed in **B**); Cyclin E was used as positive control. (**C**) DAOY cells were treated with increasing GSK690693 concentration, leading to enhanced endogenous ATXN1 clearance (**C**, quantified in **D**). GSK690693 treatment in DAOY cells lowers ATXN1 half-life (n = 4 for each time point) (**E**, quantified in **F**). Data are represented as mean, ± SEM. Two-Way ANOVA, Bonferroni post hoc test, * $p < 0.05$, ** $p < 0.01$.

Experiments in the previous section demonstrated that the small molecule inhibitor GSK690693 blocks PKA phosphorylation and lowers endogenous Atxn1 protein in mouse cerebellar slices. To test whether this drug also leads to a reduction in human ATXN1 protein levels, DAOY cells were treated with 5um, 10um, and 20uM GSK690693 for two days. Indeed, kinase inhibition with GSK690693 treatment reduced ATXN1 protein in DAOY cells (**Figure 4C,** quantified in **4D**).

Next, DAOY cells were treated with 40ug/ml CHX or 10uM GSK690693 to quantify the impact of PKA inhibition on ATXN1 stability. After 24 hours, only 17% of ATXN1 was cleared, and was not reduced any further at 48 hours (**Figure 4E**, quantified in **4F**). In contrast, treatment with GSK690693 permits steady ATXN1 clearance (16% reduction by 4hr, 32% by 8hr, 49% by 24hr, and 63% reduction by 48hr) (**Figure 4E**, quantified in **4F**).

These experiments showcase the stable nature of ATXN1. Kinase inhibition with GSK690693 rapidly destabilizes the protein. Thus, ATXN1 turnover is tightly controlled, at least in part, by PKA-mediated S776 phosphorylation.

CαM120A mice as a model of reduced PKA kinase levels and activity

One intrinsic flaw in all kinase inhibitor strategies is that small molecule inhibitors may target multiple kinases (Smyth et al., 2009; Davies et al., 2000). For example, the widely used PKA inhibitor H-89 also blocks S6L1, MSK1, and ROCK-II (Lochner et al., 2006). Even the potent PKA inhibitor used above (GSK690693) is also a strong inhibitor of Akt (**Figure 3A**).

Chemical genetics is a useful strategy to achieve selective kinase inhibition. This approach consists of mutating the ATP binding pocket of the kinase of interest, thereby making a single modified kinase sensitive to bulky inhibitors. Various research groups have used this technique to study different kinases, including CaMKII, Trk A, B and C, and TgCDPK1, where bulky derivatives of pyrazolo[3,4-d]pyrimidine (PP1) selectively block

the mutated kinase *in vitro* and *in vivo* (Wang et al., 2003; Wang et al., 2008; Chen et al., 2005; Wang et al., 2009; August et al., 2012; Liu et al., 2013; Sugi et al., 2011). One such PP1 analogue is 1-NM-PP1. 1-NM-PP1 is a cell permeable inhibitor that crosses the blood brain barrier in mice when delivered in drinking water or by intraperitoneal injection (Wang et al., 2003; Wang et al., 2008). In one study, 5uM 1-NM-PP1 was administered in drinking water for 30 days (Wang et al., 2003). Partial kinase inhibition in the brain was achieved at 6 hours and complete inhibition by 24 hours, which persisted for 30 days as long as the drug was administered. Kinase inhibition was reversible upon removal of the drug from the drinking water (Wang et al., 2003). Finally, analogue-sensitive CaMKIIa inhibition is proportional to levels of 1-NM-PP1 in the brain (Wang et al., 2008).

To study the role of the PKA pathway in ATXN1 phosphorylation *in vivo*, we obtained a commercially available, analogue sensitive PKA mouse model, originally engineered by Dr. Stanley McKnight's group (Morgan et al., 2008). A M120A point mutation in the ATP binding pocket of the Cα subunit of PKA (*Prkaca* gene) confers *in vitro* sensitivity to inhibition by derivatives of pyrazolo[3,4-d]pyrimidine, including strong inhibition by 1-NM-PP1, with an IC_{50} of ~150nM in JEG cells transfected with a CαM120A construct (Niswender et al., 2002). A CαLoxM120A mouse was generated expressing a Cre-inducible knockin CαM120A (Morgan et al., 2008). The original targeting vector consisted of a NEO cassette (flanked by lox1 and lox2) and wild type Cα minigene (exons 5–10) (flanked by lox 2 and lox3), both upstream of a second exon 5 containing the CαM120A mutation (Morgan et al., 2008). After Cre-mediated excision of the NEO cassette, the resulting *CαLoxM120A* tissues express wild type PKA Cα protein (from the wild type Cα minigene) (**Figure 5A**). These CαLoxM120A mice harbor a downstream, unexpressed, M120A-contaning exon 5. A second cross with Cre-expressing line mediates excision of the wild type minigene (exons 5-10) and allows expression of endogenous levels of activated CαM120A PKA subunit (**Figure 5A**). For unknown reasons, an unexpected consequence of the M120A mutation in exon 5 is destabilization of Cα mRNA and protein (**Figure 5B, C**), which also impacts kinase activity (**Figure 5D**) (Morgan et al, 2008). This feature is expanded on in the next section of this chapter.

Figure 5

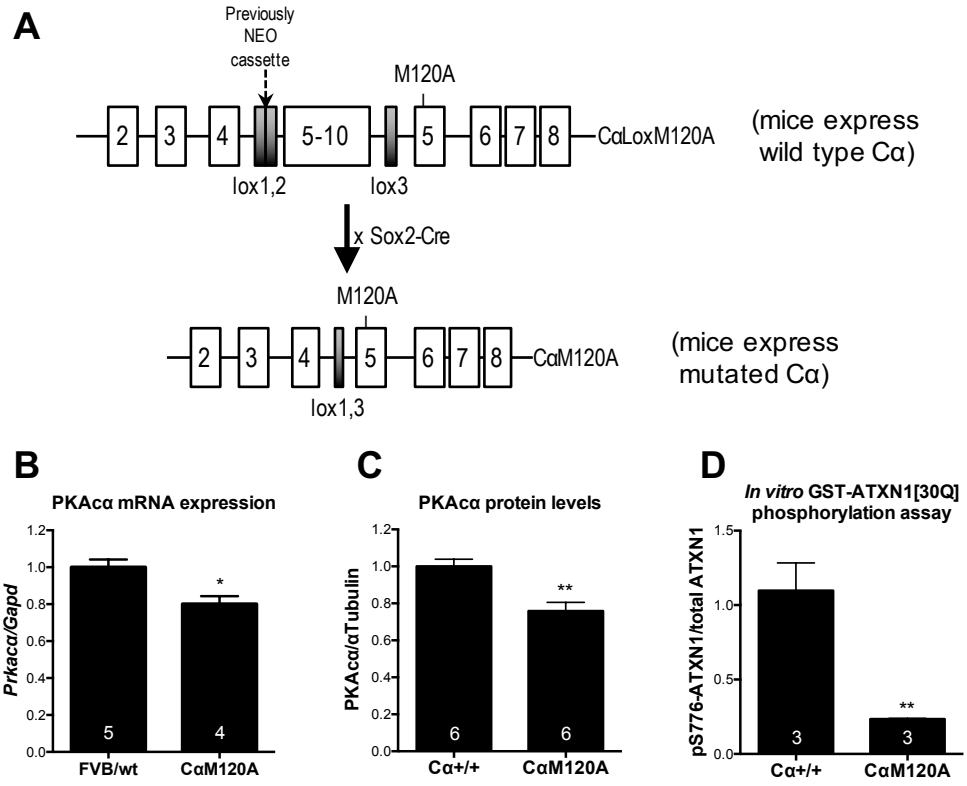

Figure 5. CαM120A mouse model is a genetic tool to study PKAcα *in vivo*. (**A**) Genetic strategy for creating a knockin CαM120 mouse. Lox P flanked minigene containing exons 5-10 of PKAcα (gene *Prkaca*) is excised after Cre-dependent recombination and allows expression of downstream exon 5 harboring M120A mutation. CαLoxM120A mice were obtained from Jackson laboratories and crossed to Sox2-Cre mice, and bred to homozygosity. CαM120A cerebellar homogenates exhibit reduced levels of PKAcα mRNA, protein, and kinase activity compared to lysates expressing wild type $C\alpha^{+/+}$ as measured by RT-qPCR (**B**), western blot (**C**), and GST-ATXN1[30Q] *in vitro* phosphorylation assay (**D**). Biological replicates are indicated within bars. Data are represented as mean, ± SEM. Student's t-test. * $p < 0.05$, ** $p < 0.01$

We obtained *CαLoxM120A* mice from Jackson laboratories and crossed them to Sox2Cre mice to generate mice expressing mutant CαM120A in all tissues. The Sox2Cre transgene expresses Cre recombinase under the control of a mouse Sox2 promoter expressed in epiblast cells at embryonic day 6.5, which give rise to all three primary germ layers, including the ectoderm, from which nervous tissue studied here arises (Hayashi et al., 2002). Using germline active EIIa promoter to drive Cre-expression in all tissues, Dr.

Stanley McKnight's group validated CαM120A sensitivity to 1-NM-PP1 in isolated sperm and testes lysates (Morgan et al., 2008).

Based on the published efficacy of 1-NM-PP1 to cross the blood brain barrier and block analogue sensitive CaMKIIa (Wang et al., 2003; Wang et al., 2008) the first set of experiments consisted of delivering 1-NM-PP1 to *Sox2Cre-CαM120A* mice *ex vivo* and *in vivo*. *Sox2Cre-CαM120A* (ie, *CαM120A*) mice were bred to homozygosity so that CαM120A (and no wild type Cα) protein is expressed in all tissues, including the cerebellum. Cerebellar slices were isolated from P10 pups and treated with 20uM 1-NM-PP1 over 3 days (**Figure 6**). These conditions failed to show a reduction in phosphorylation of PKA substrates (**Figure 6A**, quantified in **6B**). The timing and dosing of 1-NM-PP1 treatments were modified over numerous experiments, but all conditions failed to show PKA inhibition by 1-NM-PP1. As such, 1-NM-PP1 treatment did not affect Atxn1[2Q]-S776 phosphorylation (**Figure 6A**, quantified in **6C**). The small molecule PKA inhibitor (GSK690693) was used as positive control and showed the expected decrease in phosphorylation of PKA target proteins and of Atxn1[2Q] (**Figure 6A**, quantified in **6B** and **6C**).

Figure 6

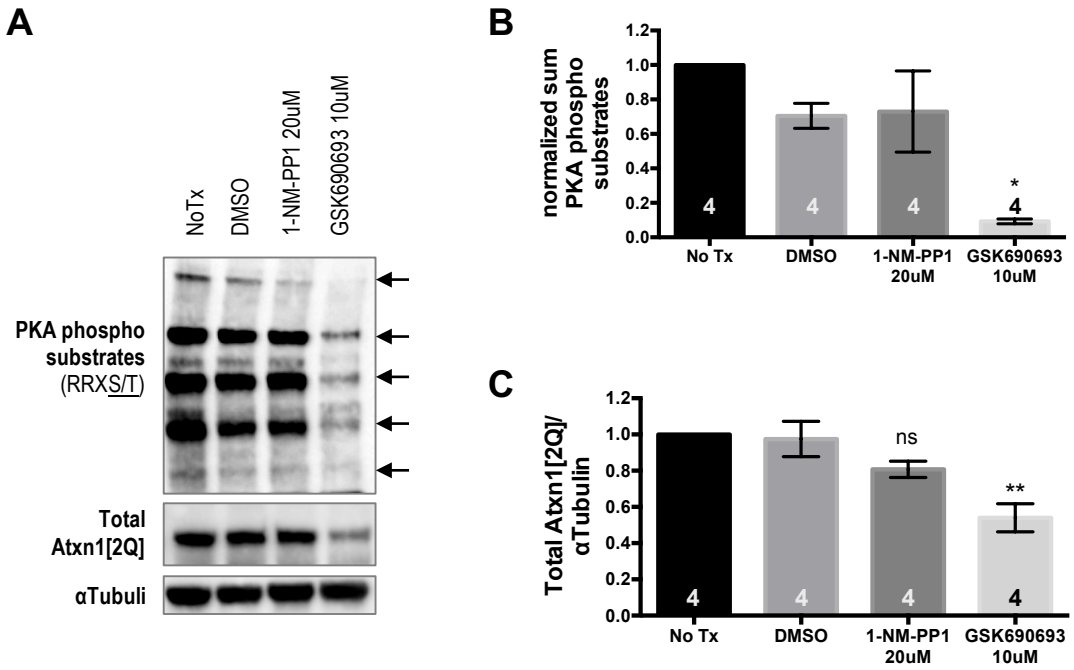

Figure 6. Administration of the PP1 analogue 1-NM-PP1 to live tissue does not block analogue-sensitive CαM120A kinase *ex vivo*. Organotypic cerebellar slices of *Sca1*$^{+/+}$*;CαM120A/CαM120A* pups (P10 ± 2d) were grown in culture for 1 day and treated with vehicle (DMSO), 20uM 1-NM-PP1, or 10uM GSK690693 for 3 more days, replacing the drug daily. Inhibition of phosphorylation of PKA substrates was detected in samples treated with 10uM GSK690693, but not in samples treated with 20uM 1-NM-PP1, demonstrating a failure of 1-NM-PP1 to block PKA activity **(A**, quantified in **B)**. Decrease in total Atxn1[2Q] was observed with PKA inhibition by 10uM GSK690693, but not by 1-NM-PP1 treatment that does not block PKA (**C**). Biological replicates (n) are indicated inside bars. Data are represented as mean, ± SEM. One-Way ANOVA, Dunnett post hoc test. * $p < 0.05$, ** $p < 0.01$.

Homozygous *Sox2Cre-CαM120A* mice were crossed to SCA1 transgenic mice that model Purkinje cell aspect of disease. *Pcp2-ATXN1[82Q]/+;Sca1*$^{+/+}$ mice express the human *SCA1* coding region with 82 CAG expansion mutation, under the *Pcp2* Purkinje cell-specific promoter (**Figure 2**, *Pcp2*). The progeny of this mating, *Pcp2-ATXN1[82Q]/+;Sca1*$^{+/+}$*;CαM120A/CαM120A* (*ATXN1[82Q];CαM120A* from here on), were used for the following *in vivo* experiments.

1-NM-PP1 was administered in three routes of delivery for ten days: drinking water, intraperitoneal osmotic pump (i.p.), and intracerebroventricular osmotic pumps (i.c.v.) (**Figure 7**). These treatments failed to demonstrate PKA inhibition by 1-NM-PP1, as indicated by phospho-PKA substrates antibody that recognizes proteins phosphorylated in the PKA consensus region (**Figure 7A**, quantified in **7B**). ATXN1[82Q] and Atxn1[2Q] levels were also unaffected (**Figure 7A**, quantified in **7C**). Subsequent internal communications with Dr. McKnight's group disclosed they too failed to achieve CαM120A inhibition when treating the whole animal with 1-NM-PP1. Additional data against the efficacy of 1-NM-PP1 showed that CαM120A in cerebellar extracts is more sensitive to inhibition by the PKA inhibitor GSK690693 than by 1-NM-PP1 (**Figure 8**). Thus, the theoretically powerful chemogenetic approach is not effective in *CαM120A* animals and was deemed unusable for *in vivo* studies surrounding the role of PKA in SCA1.

Figure 7

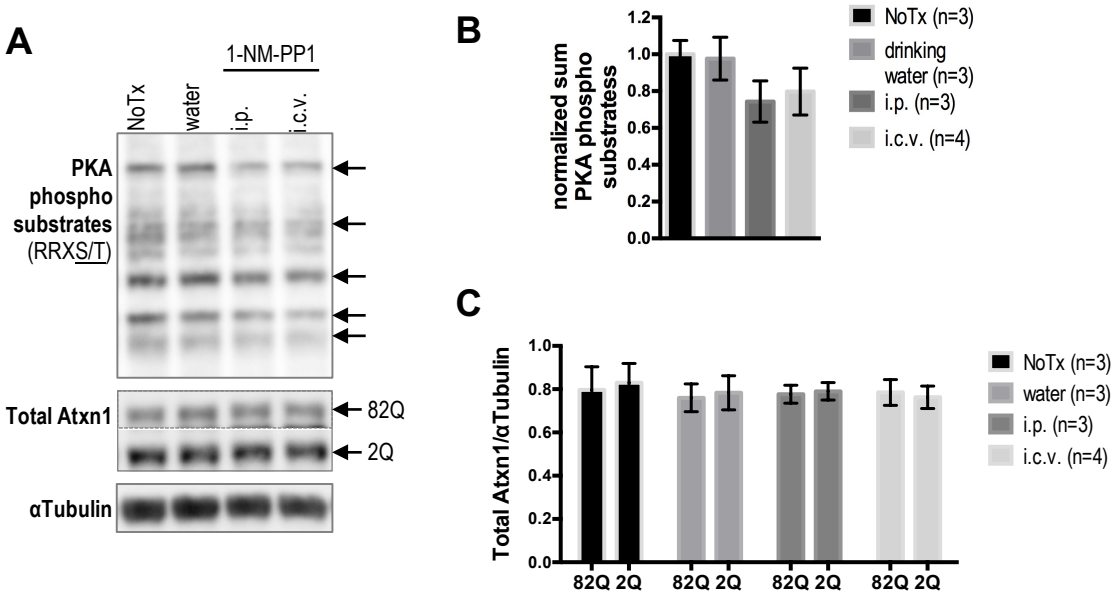

Figure 7. ***In vivo*** **delivery of the PP1 analogue 1-NM-PP1 does not block activity of analogue-sensitive CαM120A kinase in cerebellum.** 9-12 week old *ATXN1[82Q];CαM120A* mice were separated into four groups and treated via the following routes of administration for 10 days: ***No Tx*** (no treatment), ***drinking water*** (25uM 1-NM-PP1 in drinking water with 5% sucrose), ***i.p.*** (intraperitoneal pump filled with 0.4mM 1-NM-PP1 in 20% DMSO/80% PBS), ***i.c.v.*** (subcutaneous pump filled with 0.4mM 1-NM-PP1 in 20% DMSO/80% PBS connected to an intracerebroventricular cannula surgically inserted into the lateral ventricle). At the end of the treatment period, cerebella were collected for western blotting **(A)**. Immunodetection using PKA phospho substrates antibody detected no inhibition of phosphorylation of PKA targets in cerebellar homogenates of mice treated with 1-NM-PP1 **(B)**. Total ATXN1 levels are not affected by *in vivo* treatment of 1-NM-PP1 **(C)**. Data are represented as mean, ± SEM. One-Way ANOVA. All treatment conditions failed to reach statistical significance compared to no treatment control.

Figure 8

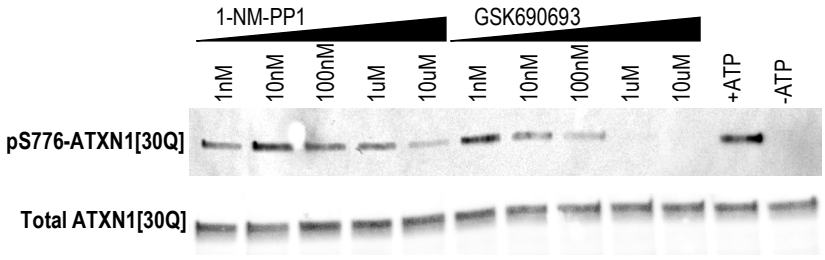

Figure 8. Cerebellar CαM120A kinase is more susceptible to inhibition by GSK690693 than 1-NM-PP1. Cerebellar extracts of mice expressing CαM120A were used as kinase source to phosphorylate purified GST-ATXN1[30Q] *in vitro*. While the M120A mutation was generated to confer sensitivity of CαM120A to 1-NM-PP1 compound, only mild inhibition is seen at a high dose of 10uM 1-NM-PP1. In contrast, ATXN1-S776 phosphorylation is blocked with as little as 10nM of GSK690693.

Purkinje cell-expressed ATXN1 is lowered by reduction in PKAcα levels

While CαM120A affinity for 1-NM-PP1 was found to be too low to enable *in vivo* studies, the effects of the M120A mutation on Cα could be harnessed. As discussed above, *CαM120A* cerebella have less *CαM120A* mRNA expression and lower kinase protein levels compared to tissues expressing wild type Cα (shown in **Figure 5B** and **5C**). Furthermore, this reduction in kinase is functionally relevant as there is decreased ability of CαM120A cerebella to phosphorylate purified GST-ATXN1[30Q] in an *in vitro* phosphorylation assay (shown in **Figure 5D**).

Interestingly, while there was only a 30% reduction in Cα levels, the reduction in baseline phosphorylation activity was much greater (80%), suggesting that the M120A mutation not only affects the expression and/or stability of the kinase, but also affects its enzymatic function. Indeed, the M120A mutation lowers binding efficacy of CαM120A to ATP (Shauble et al., 2007). These results are largely in agreement with the original studies of this mouse model (Morgan et al., 2008). However, those reports indicated a less dramatic

(30-40%) reduction of cAMP-stimulated activity in CαM120A tissues tested: testes, sperm, heart, kidney, and skeletal muscle (cerebellum was not reported). The discrepancy between the degrees of PKA activity may well be due to experimental differences (cAMP-stimulated PKA activity assay by Morgan et. al. using a small peptide substrate versus our approach probing for baseline activity on a specific protein of interest, ATXN1). However, the differences may also reflect the sensitivity of ATXN1 to a subtle decrease in PKA levels.

Although CαM120A could be inhibited with the doses used of 1-NM-PP1 *in vivo*, this model does allow a study of the effect lowered PKA levels and activity has on its putative substrates, specifically, ATXN1. For these studies, *Pcp2-ATXN1[30Q]/+;Sca1*$^{-/-}$ mice were crossed to Sox2Cre-*CαM120A/CαM120A* mice to generate *Pcp2-ATXN1[30Q]/+;Sca1*$^{-/-}$*;CαM120A/CαM120A* (*ATXN1[30Q]/Sca1*$^{-/-}$*;CαM120A* from here on). *ATXN1[30Q]* mice were previously bred to an *Sca1*$^{-/-}$ background because wild type mouse Atxn1[2Q] and ATXN1[30Q] have similar electrophoretic mobility and cannot be distinguished by western blot. Thus, immunodetection of ATXN1 in homogenates of *ATXN1[30Q]/Sca1*$^{-/-}$ unequivocally detects Purkinje cell ATXN1[30Q]. Whole cerebellar lysates of 4-6 week old *ATXN1[30Q]/Sca1*$^{-/-}$ and *ATXN1[30Q]*$^{-/-}$*;CαM120A* were subjected to western blotting and probed for pS776 and total ATXN1. **Figure 9** confirmed a 27% reduction of CαM120A protein levels and no compensatory increase in Cβ protein (only quantification of Cβ1 is shown here for simplicity, but Cβ2/3 isoforms were also unchanged across all experiments). Decrease in Cα levels was associated with a reduction in S776 phosphorylation of Purkinje cell-expressed ATXN1[30Q] (**Figure 9A**, quantified in **9B**). Because ATXN1-S776 phosphorylation is tightly linked to total ATXN1 protein, these results also showed loss of total ATXN1[30Q]. This data is the first to demonstrate a link between PKA and ATXN1-S776 phosphorylation-dependent stability *in vivo*.

To determine whether ATXN1 harboring a mutant polyglutamine expansion is also subject to phosphorylation by PKA, the above experiments were repeated in *ATXN1[82Q];CαM120A* mice (described in the previous section). *W*hole cerebellar lysates were collected from 4-5 week old *ATXN1[82Q]* and *ATXN1[82Q];CαM120A* mice. This

age was selected because ATXN1[82Q] protein in this transgenic model is more extractable at earlier stages. Similar to the *ATXN1[30Q]/Sca1*$^{-/-}$ series, a 34% reduction in CαM120A protein resulted in a dramatic 60% decrease in the phosphorylation of mutant ATXN1[82Q] in Purkinje cells, with a 41% decline of total ATXN1[82Q] (**Figure 9C**, quantified in **9D**). In contrast, levels of the broadly expressed Atxn1[2Q] protein were unaffected in the same samples (**Figure 9C** and **9D**). In conclusion, human ATXN1 is susceptible to PKA-mediated, phosphorylation-dependent stability and this effect is limited to Purkinje cells.

Ataxin1 distribution in the cerebellar cortex indicates co-localization with PKA

The cerebellar cortex is a highly organized structure arranged in a stereotypic cytoarchitecture consisting of three layers: the molecular layer (ML, containing Purkinje cell dendrites, interneurons, and granule cell axons known as parallel fibers), the Purkinje cell layer (PCL, containing PC bodies and Bergmann glia bodies), and the granule cell layer (GCL, consisting mostly of granule cell bodies as well as passing Purkinje cell axons, mossy fibers, climbing fibers, and interneurons) (**Figure 10A**, notice Purkinje neuron cartoon in blue superimposed on the high magnification section). *In situ* hybridization data from early *Sca1* studies and the Allen Brain Atlas illustrate that *Atxn1* is expressed in all three layers, as well as in the deep cerebellar nuclei (**Figure 2**, *Atxn1*) (Banfi et al., 1996).

Prakaca, the gene encoding Cα, displays a similar expression pattern to *Atxn1*, while Cβ is expressed at very low levels (**Figure 2** *Atxn1*, *Prkaca*, *Prkacb*) (Cadd and McKnight, 1989). PKA regulatory subunits are also differentially expressed in the cerebellar cortex, where RIα (*Prkar1a*) and RIβ (*Prkar1b*) show highest expression in Purkinje cells. RIIβ expression seems to be restricted to Purkinje cells, though at at low levels. RIIα expression is scant and more diffuse throughout the cerebellum. At the same time, expression of *Msk1* (gene *Rps6ka5*), a kinase shown to phosphorylate Atxn1[154Q], exhibits low expression that appears to be limited to Purkinje cells (**Figure 2**) (Lein et al., 2007; Park et al., 2013).

Figure 9

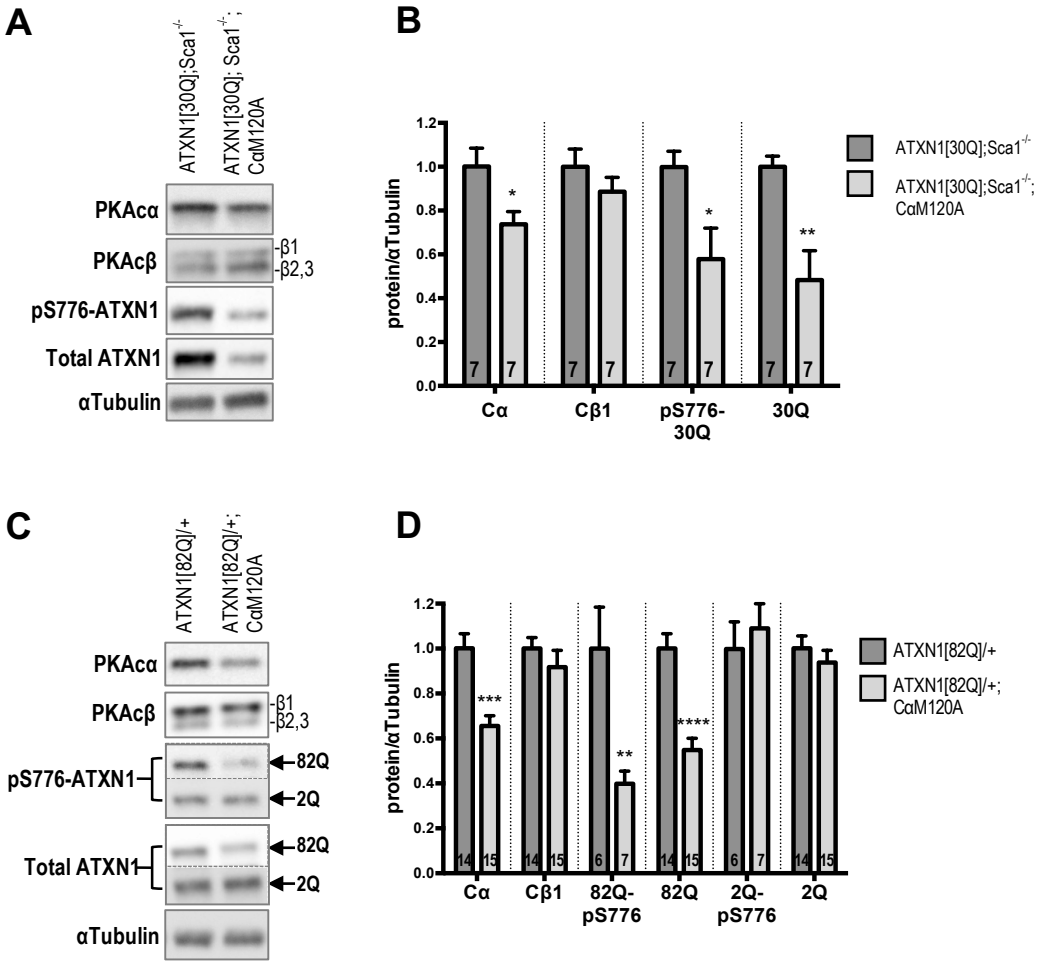

Figure 9. PKA pathway in Purkinje cells controls phosphorylation-dependent stability of ATXN1 protein. Immunoblots of whole cerebellum homogenates (4-5 weeks old) show decrease of PKAcα in CαM120A mice leads to a reduction in Purkinje cell expressed ATXN1[30Q] (**A**), quantified in (**B**). ATXN1[82Q] with a mutant polyglutamine tract expansion is also sensitive to this effect (**C**). Endogenous mouse Atxn1[2Q] is expressed in all cells of the cerebellum and its levels are unaffected by the decrease in PKAcα (**C**). Notice there is no compensation in expression of PKA catalytic subunit β isoform (**A, C**). Quantitative analysis of (**A**) and (**C**) are graphed in (**B**) and (**D**), respectively. Biological replicates (n) are indicated inside bars. Data are represented as mean, ± SEM. Student's t-test. * $p < 0.05$, ** $p < 0.01$.

To better understand what the susceptibility of Ataxin1 to PKA activity might be in Purkinje neurons, fresh *Sca1*$^{66Q/2Q}$ were subjected to laser capture microdissection (LCM) to compare the cerebellar distribution of Ataxin1 and its putative kinases, PKA and Msk1. Even though the *Sca1*$^{66Q/2Q}$ model does not manifest overt SCA1-like disease in the mouse lifespan, it is biochemically useful for expressing Atxn1 with a polyglutamine expansion comparable in length to the mutant transgenic model, while at the same time being expressed at endogenous levels and in all cells that express *Atxn1* (**Figure 2**, *Atxn1*) (Lorenzetti et al., 2000).

Cerebella from five-week-old *Sca1*$^{66Q/2Q}$ mice were used to isolate the three layers of the cerebellar cortex, with special interest in layers containing Purkinje cells (PCL and ML). Western blotting was used to examine the presence and density of proteins being studied. Pilot experiments failed to find a protein expressed to the same degree in all layers that could be used as loading control. To preserve protein loading uniformity, the same volume of tissue was collected from each layer of each sample (± 20,000,000 um^3, or 1,000,000um^2 of 20um thick sections- see methods). Using an antibody that detects ATXN1 phosphorylated at S776 showed pS776-Atxn1 was equally abundant in PCL and GCL. However, total Atxn1 was higher in GCL. Hence, the proportion of Atxn1 phosphorylated at S776 to total Atxn1 was two-fold higher in PCL than in GCL (**Figure 10B**, quantified in **10C**). While both 66Q and 2Q exhibited this trend, the difference was statistically significant for Atxn1 harboring 66Q expansion. pS776-Atxn1 in the molecular layer was too faint to quantify; perhaps more tissue is needed to detect the phosphorylated fraction of Atxn1 in this layer. These results suggest in the cerebellar cortex Purkinje cells are enriched with intracellular pathways that promote phosphorylation of Atxn1 at S776.

Figure 10

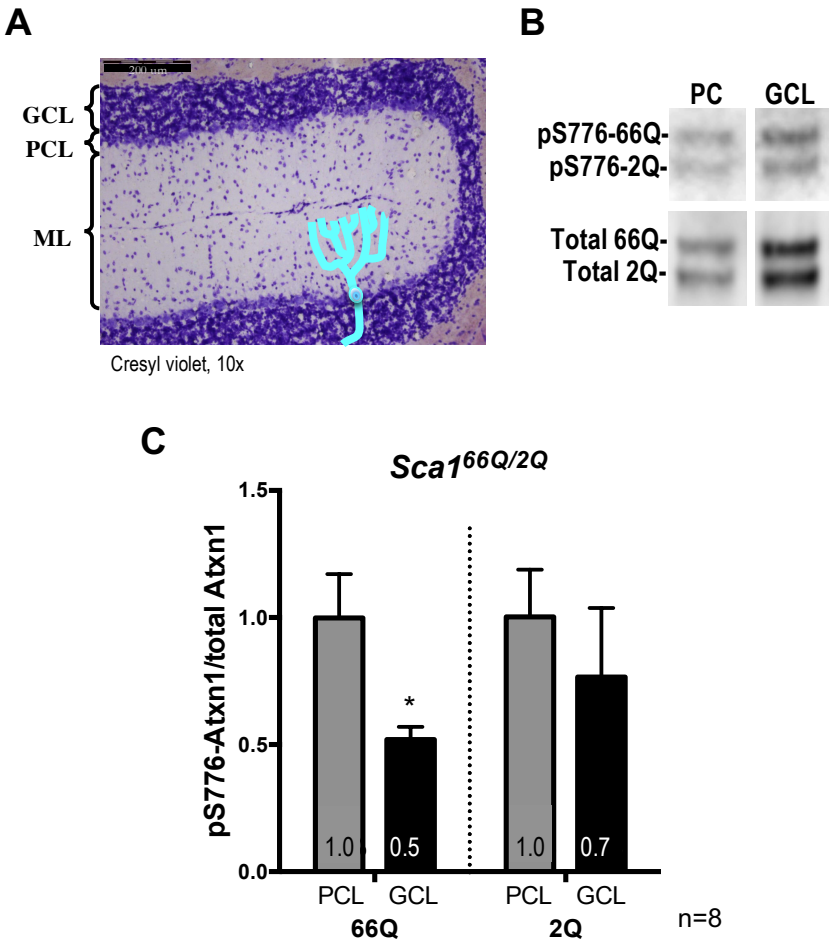

Figure 10. Microdissection reveals there is a higher proportion of pS776-Atxn1 in Purkinje cell layer than in granule cell layer. (**A**) Cresyl violet staining of a parasagittal cerebellar section illustrates the organized nature of the cerebellar cortex. The three layers of the cerebellar cortex consist of the molecular layer (ML), Purkinje cell layer (PCL), and granule cell layer (GCL). Dark purple staining represents the numerous granule cells saturating the space in the GCL. Purkinje cell bodies (blue cartoon) are located in the PCL, their dendrites extend into the ML, and their axons project out of the cerebellar cortex coursing through the GCL. Nuclei stained in the ML represent interneurons. Laser capture microdissection of *Sca1*$^{66Q/2Q}$ was used to isolate proteins in the three subdivisions of the cerebellar cortex (2 x 10^7 um^3 tissue was isolated for each sample). (**B**) Western blot densitometry analysis of phosphorylated Atxn1 divided by the total Atxn1 shows there is proportionally more phosphoprotein in the PCL than in GCL (quantified in **C**). Data are represented as mean, ± SEM. Student's t-test. * $p < 0.05$.

The next objective was to establish the distribution of Ataxin-1 in the cerebellar cortex. I used the total-Ataxin1 data from the *Sca1*$^{66Q/2Q}$ LCM samples above to graph Atxn1[66Q] and Atxn1[2Q] levels in GCL, ML, and PCL. For the LCM studies described from here on, the protein levels are normalized to PCL, which is set to 1x. Therefore, protein distribution can only be analyzed between layers within a given genotype. There was about 2x Atxn1[66Q] and Atxn1[2Q] in GCL, and near-negligible 0.08x in ML (**Figure 11A**, first and second columns). These results show that, per volume of tissue, most total Atxn1 in whole cerebellum is found in granule neurons in the GCL.

Next, I sought to determine the distribution of ATXN1[82Q] in the Purkinje cell restricted overexpression model, *Pcp2-ATXN1[82Q]/+ (i.e., ATXN1[82Q])*. Laser capture microdissection of the cerebellar layers in *ATXN1[82Q]* uncovered a novel finding: high distribution of ATXN1[82Q] in the molecular layer, i.e., Purkinje dendrites. In contrast to the low amount of Atxn1 found in ML in the knockin model, there was 0.8x ATXN1[82Q] in ML (**Figure 11A**, third column, light grey shading, and western blot shown in **11B**). Hence, in the Purkinje cell dendrites of the ATXN1[82Q] transgenic model there is approximately 10x more mutant ATXN1 as there is in Purkinje cell dendrites of the Atxn1[66Q] knock-in mouse. Because ATXN1[82Q] is only expressed in PCs, it was not detected in the GCL (**Figure 11B**).

There was 0.18-0.2x Atxn1[2Q] in the ML of *ATXN1[82Q]* and FVB/wt cerebella, which is ~2x more than initially seen in the *Sca1*$^{66Q/2Q}$ tissue (**Figure 11A**, fourth and fifth columns, light grey shading). This is logical because the *Sca1*$^{66Q/2Q}$ mice have one copy of 2Q, while *FVB/wt* (*Sca1*$^{2Q/2Q}$) and *ATXN1[82Q]* (i.e., *Pcp2-ATXN1[82Q]/+;Sca1*$^{2Q/2Q}$) have two copies. As seen in the knockin model, most Atxn1[2Q] was found in GCL (~2.5x) (**Figure 11A**, fourth and fifth columns, black shading). The distribution of Atxn1[2Q] was identical in *ATXN1[82Q]* and *FVB/wt* genotypes.

Figure 11

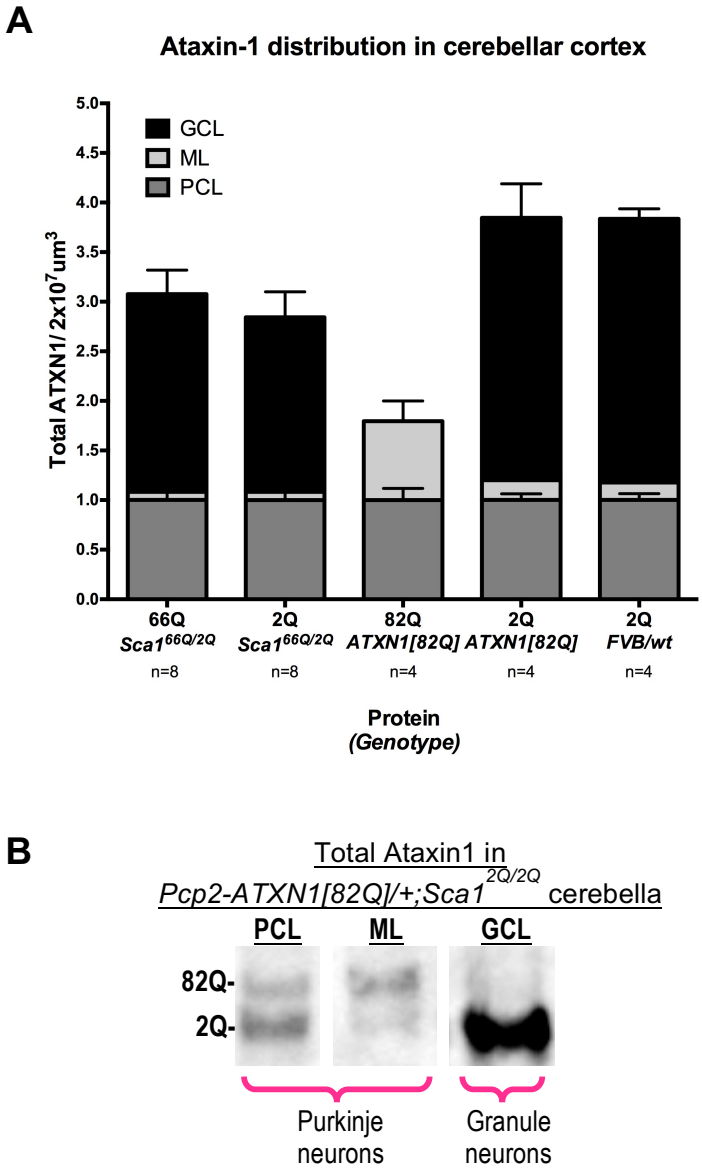

Figure 11. Characterization of the distribution of Ataxin1 in mouse cerebellar cortex. Microdissection of the layers of the cerebellar cortex was performed in *Sca1*$^{66Q/2Q}$ knockin, *Pcp2-ATXN1[82Q]* transgenics, and *FVB/wt* sections. The same volume of tissue was isolated from each sample (2 x 10^7 um^3). Graph representing western blot densitometry analysis of total Ataxin1 across the three genotypes examined (note the entire protein is shown here, represented by the size of the polyglutamine tract, 2Q, 66Q or 82Q). (**A**) In this stacked bar graph, values are normalized to PCL, which is set to 1.0. Consistently, most of Atxn1 is located in the GCL (shaded black) compared to PCL (shaded grey). There is very little Atxn1 in the ML (light grey), except in *ATXN1[82Q]* mice, where ATXN1[82Q] protein is also highly localized to the ML (**A**, **B**). Data are represented as mean, ± SEM.

The observation that the proportion of pS776 to total Atxn1 is higher in Purkinje cells than in granule layer suggests there are kinase or kinase pathways that promote S776 phosphorylation in Purkinje neurons. Therefore, I examined the distribution of putative *in vivo* Atxn1 kinases, PKA Cα and Msk1 and compare their localization with Atxn1 as substrate. While I predicted Cα levels might be higher in PCL, Cα protein was evenly distributed between the GCL, PCL and ML (**Figure 12A, B**). I also hypothesized that Cα density or localization might be disturbed in *ATXN1[82Q]* samples compared to wild type, but this was not the case; the uniform distribution of Cα protein between layers was not disrupted with ATXN1[82Q] overexpression (**Figure 12B**, second column).

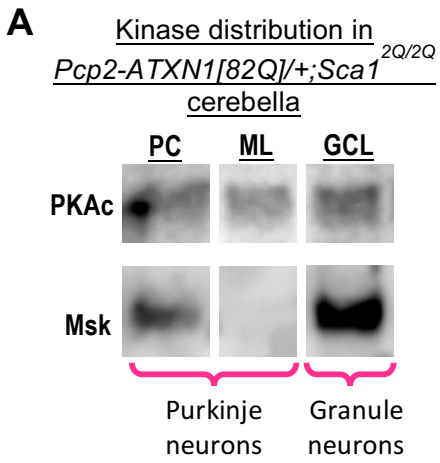

Figure 12. Distribution of ATXN1 putative *in vivo* kinases in mouse cerebellum. Microdissection of 4-5 week old cerebellum was used to isolate protein for western blot analysis. Immunoblot results of *Pcp2-ATXN1[82Q]/+;Sca1*$^{2Q/2Q}$ genotype is shown in (**A**). The alpha catalytic subunit of PKA is equally distributed in all three layers of the cerebellar cortex and higher in regions containing Purkinje neurons (**A, B**), while Msk1 is more highly expressed in the GCL (**A, C**). Calbindin is highest in GCL and ML, consistent with it being a Purkinje cell marker (**D**). There is more calbindin in FVB/wt than in *ATXN1[82Q]*, but this is not evident in these graphs because PCL each each genotype is set to 1.0. Data are represented as mean, ± SEM.

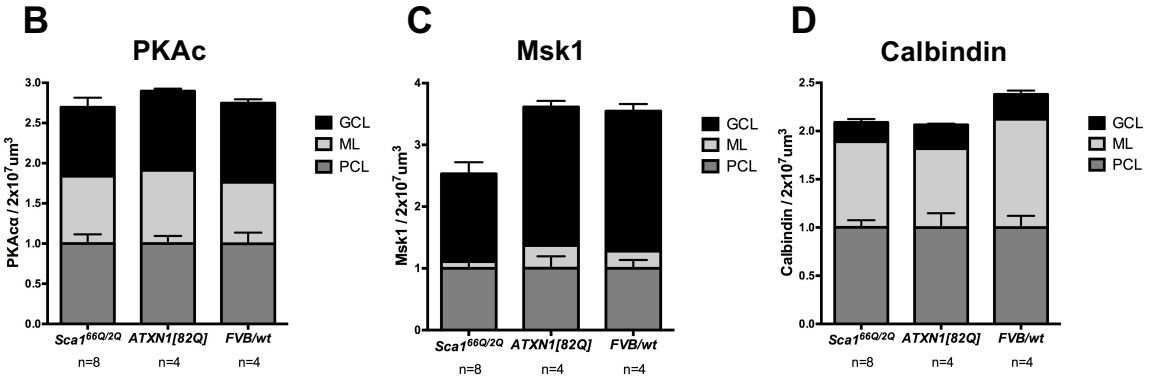

In contrast to Cα, Msk1 protein was more plentiful in the GCL. In *Sca1*$^{66Q/2Q}$, Msk1 was about 1.4x in GCL and 0.11x in ML (**Figure 12A** and **12C**, first column). This was consistent in *ATXN1[82Q]* and *FVB/wt* in which Msk1 was consistently abundant in GCL (~2.5x), with less occupancy in PCL and at very low levels in ML (~0.3x) (**Figure 12A**, and **13C,** second and third columns). These observations were unexpected, as the expression pattern in the Allen Brain Atlas shows a PCL-only expression (**Figure 2**, *Rps6ka5*).

The Purkinje cell marker calbindin was used as a control to confirm layer specificity, showing highest levels in PCL and ML, where Purkinje body and dendrites sit, and scarce in GCL, where Purkinje axons course through (**Figure 12D**). Regardless of genotype, there was only ~0.2x calbindin in GCL, with 1x in ML and 1x PCL (**Figure 12D**). As expected, calbindin levels were lower in *ATXN1[82Q]* compared to *FVB/wt* (~50% decrease), however this is not evident in the graph because levels are normalized to PCL of each genotype (**Figure 12D**, second and third columns).

These microdissection studies describe the distribution of Ataxin1 protein and its putative kinases in wild type and SCA1 mouse cerebellum. PKA is equally distributed throughout the cerebellar cortex, while Msk1 is enriched in the granular layer. Because Purkinje cells occupy both PCL and ML, this suggests PKA is more highly expressed in Purkinje neurons (PCL plus ML) than in granule cells (GCL alone). Msk1 is poorly detectable in the ML and is highest in GCL, suggesting its activity in Purkinje cells may be limited to the soma and play a predominant role in signaling pathways within granule cells. A novel finding described here is that ATXN1[82Q] also highly localizes to Purkinje neuron dendrites, a site where Cα, but not Msk1, resides. In summary, PKA Cα and Purkinje cell-ATXN1[82Q] co-localize in PCL and ML, whereas Atxn1[2Q] and Msk1 co-localize in GCL. These observations postulate a potential mechanism by which ATXN1 in Purkinje cells is predominantly targeted by the PKA pathway.

Discussion

This chapter provides data supporting my hypothesis that PKA is a major kinase involved in control of ATXN1 phosphorylation in cerebellar Purkinje cells. A small molecule with potent inhibition against PKA blocked Ataxin1 phosphorylation and reduced its stability in human cells and murine cerebellar slices. SCA1 transgenic mice crossed to *CαM120A* mutants showed reduced levels of ATXN1, in support of PKA playing a role in ATXN1 phosphorylation in Purkinje cells *in vivo*.

ATXN1 phosphorylation at S776 by PKA regulates ATXN1 stability

Kinase inhibition by the potent PKA inhibitor GSK690693 led to a reduction of ATXN1 expressed at endogenous levels in a cerebellar-derived human cell line. I next measured the stability of ATXN1 in this cell and found it to be a very stable protein, but blocking PKA-mediated phosphorylation of S776 destabilized the protein. Thus, pS776-ATXN1 itself plays a major role in ATXN1 turnover and further supports blocking S776 phosphorylation is a promising avenue for therapy in SCA1.

ATXN1 half-life has been previously studied in light of its interaction with other proteins (Riley et al, 2004). However, those results described a much more unstable protein, with ATXN1[82Q] and [30Q] exhibiting a half-life of only 8 hours. In this study, I found ATXN1 half-life is no shorter than 64 hours. There are two main reasons to explain this discrepancy, the experimental techniques and the cell types used. First, Riley et al. used pulse-chase radiolabeling approach in COS cells transiently transfected with ATXN1 constructs, while I used cycloheximide (CHX) to block further translation of endogenously expressed ATXN1 in DAOY cells. One caveat of using CHX that global protein synthesis is blocked, which may affect not just ATXN1 stability, but also availability of proteins involved in clearance pathways (Zhou et al., 2004). Therefore, the CHX approach may not faithfully represent ATXN1 turnover under normal conditions. On the other hand, while the pulse-chase approach is less disruptive, monitoring half-life of an overexpressed protein is no less artificial. In Riley at al.'s work, exogenous ATXN1 was overexpressed

in a cell, after which it was subjected to conditions that promoted rapid cell division. Different plating conditions or different cell types might express different contents of the protein clearance machinery that in turn influence ATXN1 turnover.

A larger issue is that neither DAOY nor COS cell lines reflect the biology in Purkinje cells (or other neurons), which are post-mitotic and under influence of innumerable synaptic inputs. When conditional cATXN1[82Q] expression is completely shut off in Purkinje cells it takes two days for ATXN1 nuclear inclusions to be undetectable by immunofluorescence staining (Zu et al., 2004). While this does not account for soluble ATXN1[82Q], it does suggest the possibility there is a more dynamic control of ATXN1 protein levels *in vivo*. Thus, ATXN1 half-life *in vivo* may be different from cell culture conditions and this may be in part due to control of competing phosphorylation and dephosphorylation pathways, in addition to the protein clearance machinery (Cummings et al., 1999).

The studies of Riley et al. and the data presented here are in agreement surrounding the role S776 phosphorylation plays on ATXN1 clearance. For example, analysis by Riley et al. of ATXN1[82Q]-A776 (which cannot be phosphorylated) showed that this modification decreases ATXN1 $t_{1/2}$ to at least half of that seen in ATXN1[82Q]-S776. Similarly, I showed that blocking S776 phosphorylation reduced ATXN1 $t_{1/2}$ by at least 2.5 times. Whatever the discrepancies on the exact ATXN1 half-life, my results suggest PKA activity plays a major role in the control of ATXN1 stability both *in vitro* (cells) and *ex vivo* (organotypic slices).

The PKA pathway controls phosphorylation-dependent stability of ATXN1 in cerebellar Purkinje neurons

Identification of the kinase involved in Atxn1-S776 phosphorylation has been a complex endeavor. Testing the role of PKA *in vivo* has been hindered by lack of the right tools. We obtained the *CαM120A* mutant as a model of PKA hypofunction to test PKA role in ATXN1 biochemistry. The *CαM120A* model was engineered to selectively inhibit

analogue sensitive kinase using 1-NM-PP1. This chemogenetic approach has been successfully used in other mutated kinases, but the susceptibility of CαM120A to 1-NM-PP1 had not been previously reported *in vivo*. My work shows that 1-NM-PP1 is not potent enough to block CαM120A *in vivo*.

As *CαM120A* tissues display a baseline reduction in PKA activity, we harnessed this property by crossing these mice to our SCA1 transgenic models expressing ATXN1 in Purkinje cells. Data presented here is the first to provide a link between PKA activity and ATXN1 levels *in vivo*. Moreover, my results uncovered a unique susceptibility of ATXN1 phosphorylation by PKA in Purkinje cells. Global reduction in PKA activity did not alter Atxn1[2Q] protein, which is widely expressed in the cerebellum, suggesting other kinases may execute this function in other cell types, such as granule neurons.

PKA localization in Purkinje cell body and dendrites might reveal ATXN1 susceptibility to kinase activity by PKA

Microdissection of the layers in the cerebellar cortex revealed a few important points that might hint at susceptibility of ATXN1 phosphorylation by PKA in Purkinje cells. I made the novel observation that Atxn1 is phosphorylated at S776 in Purkinje cells to a higher degree than Atxn1 residing in granule cells. This suggests in the cerebellum Purkinje cells harbor pathways that favor S776 phosphorylation.

Previous whole-cerebellum fractionation studies showed there is more ATXN1 in the cytoplasm than the nucleus and that phosphorylation of ATXN1-S776 is restricted to the cytoplasm (Lai et al, 2011). Considering the extensive dendritic arborization of Purkinje neurons, one can deduce that most the cytoplasm is distributed there. Following this logic, ATXN1's kinase would theoretically also be found there.

The even distribution of Cα protein in GCL, PCL and ML suggests it can participate in enzymatic activity throughout cells in the cerebellar cortex potentially impacting Atxn1 phosphorylation. Purkinje cells are found in PCL and ML, therefore Cα is more abundant

in Purkinje cells. Msk1, on the other hand, is more abundant in GCL, where granule cells are. Therefore, PKA is more likely to be in proximity to ATXN1 protein and catalyze addition of a phosphate group to S776.

A novel finding is that in the SCA1 model, ATXN1[82Q] localizes to a relatively high degree in molecular layer, where there is more PKA, but no Msk1. Together, these observations are in favor of a model where PKA can phosphorylate ATXN1 within Purkinje dendrites as well as in the soma. Upon phosphorylation, ATXN1[82Q] could be locally stabilized or quickly transferred to the nucleus.

The original finding that Msk1 density in the cerebellum is concentrated in the granule cell layer further argues against it regulating ATXN1 phosphorylation in Purkinje neurons. While this does not preclude Msk1 from phosphorylating S776 in the Purkinje cell body, it does suggest Msk1 might be more crucial to granule cell signaling pathways. I found abundant expression of endogenous Atxn1 in GCL, which also raises the issue that changes in whole cerebellar lysates are likely more telling of alterations in granule cells. This brings to question previous findings, where Msk1 knockout produces a reduction in Atxn1[154Q] protein in whole cerebellum (Park et al., 2013). I propose that findings described in Park et al. might reflect changes occurring in the granule cell layer and not Purkinje cells. The behavioral improvement seen in $Sca1^{154Q/2Q};Msk1^{+/-};Msk2^{+/-}$ model brings up an intriguing possibility about mutant Atxn1 insult in granule cells. It is possible that the motor phenotype described by Park et al. represents a beneficial reduction of mutant Atxn1[154Q] in cerebellar granule cells, an understudied aspect of disease (Hashida et al., 1997; Gatchel et al., 2008). In contrast, my findings argue that PKA plays a predominant role in Purkinje cell pathways controlling ATXN1-S776 phosphorylation.

Does PKA phosphorylate ATXN1 only in Purkinje cells? While the *ATXN1[82Q];CαM120A* model shows an exclusive reduction of ATXN1 in PCs, blocking PKA in $Sca1^{66Q/2Q}$ cerebellar slices achieved a robust clearance, likely involving Atxn1 cell types beyond Purkinje neurons. There are a few ways to interpret these results. The primary issue is that GSK690693 is a kinase inhibitor that shows predilection against PKA, but it

also targets Akt. In fact, purified Akt can phosphorylate purified ATXN1 *in vitro* (Chen et al., 2003). However, overexpression of dominant negative Akt in Purkinje cells failed to reduce ATXN1 phosphorylation *in vivo* (Jorgensen et al, 2009). It was therefore concluded that Akt is not involved in phosphorylating ATXN1 in Purkinje cells. However, the role of Akt was not addressed in other cerebellar cell types. It is possible that blocking Akt with GSK690693 disrupts S776 phosphorylation in other cell types. Along the same line, while we know the IC_{50} profile of GSK690693 to 5 kinases, it is possible that it also targets other unidentified kinases that phosphorylate Atxn1 in the cerebellum.

Another consideration is that multiple pathways converge in Purkinje cells and/or granule cells to promote this vital post-translational modification. My results suggest that PKA plays a more substantive role of phosphorylating S776 in Purkinje cells and a small decrease in PKA is sufficient to disrupt ATXN1 levels more readily. However, I speculate that other compensatory pathways likely emerge. It is also conceivable that a 30% reduction in PKA is not sufficient to attenuate PKA enzymatic activity in other cell types to achieve a reduction in Atxn1 (i.e., granule cells). In contrast, the high potency of GSK690693 against PKA could achieve robust kinase inhibition in which Atxn1 would be cleared more widely in cerebellar slices.

Taken together, the experiments presented here support that PKA plays a principal role in modulating ATXN1-S776 phosphorylation in Purkinje cells. Other cerebellar cells, like granule neurons, may have multiple pathways converging on S776, which may include PKA, Msk1, Akt, and/or other unidentified kinases.

Chapter 3

PKA-MEDIATED REDUCTION IN ATXN1[82Q] DELAYS EARLY ONSET OF ATAXIA

Introduction

The previous chapter introduced the novel finding that attenuation of expression of PKA in *CαM120A* mice results in a decline of ATXN1 protein in Purkinje cells (PCs). Approaches that lower ATXN1 levels directly (via RNAi or by turning off gene expression in the conditional SCA1 model) have associated changes in motor recovery and correlated improvement in pathological measures (**Appendix 1**) (Zu et al., 2004; Serra et al., 2006; Xia et al, 2004; Keiser et al., 2013, 2014, 2016). The next inquiry was to investigate whether the 41% reduction of mutant ATXN1[82Q] in PCs is sufficient to improve behavioral, histological, and molecular measures of cerebellar pathology.

Results

PKAcα-mediated reduction of ATXN1[82Q] in Purkinje cells averts SCA1-like motor deficits

The first series of experiments consisted of evaluating the ataxic phenotype using beam-walking test and the rotarod test. The beam-walking test measures the ability of the mice to maintain balance while crossing a narrow beam to reach a safe platform (Brooks et al., 2009). As the diameter of the beam narrows, the difficulty of neurologically challenged mice to cross becomes more evident. Mice with cerebellar disease find it more challenging to maintain their balance and tend to slip as they cross the beam. Six- to seven-week-old FVB/wt, *ATXN1[82Q]*, and *ATXN1[82Q]/CαM120A* mice, consisting of 6 females and 4 males per group (n=10) were subjected to the beam walking test. Mice were

trained to cross a large square beam for three days. On test day four, mice were challenged to cross beams of narrowing sizes, with two test trials per beam size. The average number of hind paw faults (foot slips) was graphed once the genotypes were decoded at the end of the behavioral experiments. While the ability of the three groups of mice to cross large and medium diameter beams was indistinguishable, *ATXN1[82Q]* mice exhibited more foot slips when crossing the small diameter beams at this age. (**Figure 13A, B**) Intriguingly, *ATXN1[82Q]/CαM120A* mice performed significantly better than *ATXN1[82Q]* mice, and equally well to wild type mice.

The rotarod is a standard test for motor coordination and balance in rodents (Brooks et al., 2009). Mice are placed on a rotating cylinder that accelerates over the test period. Reduced latency to fall from the rod indicates motor dysfunction, while neurologically intact mice are able to attain proper foot placement and stay on the rod for a longer period of time. The same groups of mice used above were used for this study immediately after the beam walk test, at 7-8 weeks of age. The latency to fall was recorded by an investigator blinded to the genotypes. Wild type mice stayed on the rotarod for 168 seconds (trial day 1) and improved up to 228 seconds over course of the study, as expected in this motor learning task (**Figure 13C**). *ATXN1[82Q]* mice are neurologically compromised and consistently fell off the rotarod 73-78 seconds earlier than wild type mice (95 seconds on trial day 1; 150 seconds on trial day 4). Strikingly, *ATXN1[82Q]/CαM120A* mice remained on the rotating rod as long as the wild type controls (156 second on trial day 1; 187 seconds on trial day 4). These behavioral tests illustrate that 60% reduction in phospho-S776-ATXN1[82Q] and 41% reduction of total ATXN1[82Q] protein in Purkinje cells of *ATXN1[82Q]/CαM120A* mice averts or delays onset of deficits in fine motor coordination and balance in two individual cerebellum-dependent motor tasks.

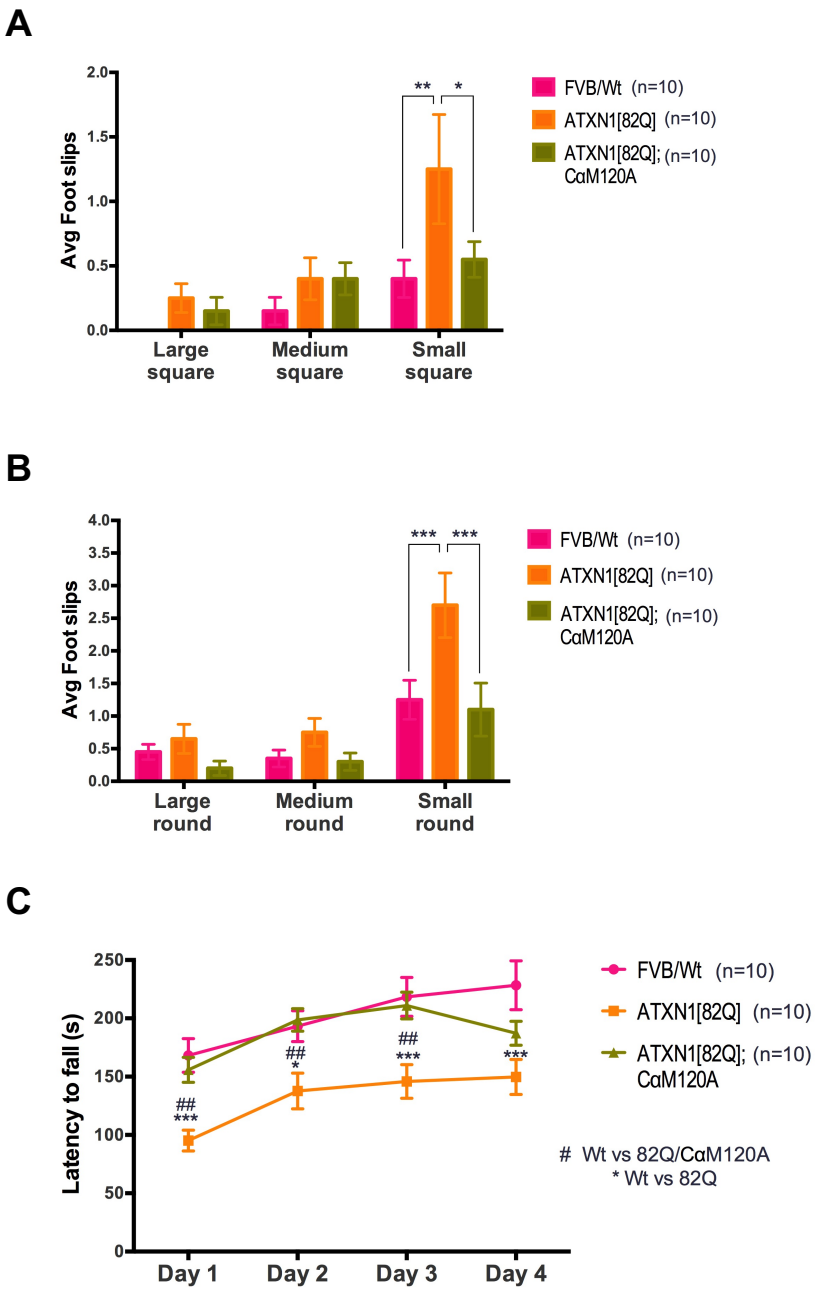

Figure 13. Cα-mediated reduction of ATXN1[82Q] in Purkinje cells reverts SCA1-like motor deficits. Beam walk test for motor balance was performed at ages 6-7 weeks (**A, B**). *ATXN1[82Q]* mice display an increased number of foot slips in when walking across a beam of small diameter, indicating motor deficits. *ATXN1[82Q];CαM120A* mice have equivalent performance to FVB/Wt mice. Rotarod test for coordination was performed on the same groups of mice at 7-8 weeks of age. (**C**) The performance of *ATXN1[82Q];CαM120A* mice was significantly better than *ATXN1[82Q]* and comparable to FVB/Wt. Data are represented as mean, ± SEM. Two-way ANOVA. * $p < 0.05$, ** $p < 0.01$. Notice in C, * indicates comparison between wt and *ATXN1[82Q]*, and # indicates comparison between wild type and *ATXN1[82Q]; CαM120A* mice.

Lower Cα levels in transgenic model does not improve progressive pathological atrophy of the molecular layer at early or mid-stage disease

Purkinje cell dysfunction in SCA1 mouse models results in dendritic atrophy and thinning of the molecular layer, even before neuronal death (Burright et al., 1995; Clark et al, 1997, Barnes et al., 2011). Calbindin immunostaining is used to label Purkinje cells and allows visualization of the entire dendritic tree that extends the width of the molecular layer. Previous studies have established that as early as 6 weeks, SCA1 mice already display rotarod deficits and signs of Purkinje cell dendritic thinning. By 12 weeks, ataxia is more marked and the molecular layer atrophy more pronounced (Clark et al, 1997; Ingram et al., 2016). Interventions that lower Ataxin1 expression or protein load show partial or full recovery of dendritic arborization (**Appendix 1**) (Keiser et al., 2013, 2014, 2016; Zu et al., 2004; Jafar-Nejad et al., 2011).

To test whether preservation of dendritic integrity underlies the improvement in motor performance seen in *ATXN1[82Q]/CαM120A* animals, cerebella of 6 and 12 week old mice were collected for histological analysis (**Figure 14A)**. Analysis of the molecular layer of the primary fissure in calbindin stained sections showed significant thinning of *ATXN1[82Q]* cerebella at 6 weeks of age (171um compared to 194um FVB/wt, $p < 0.01$) (**Figure 14B**). At 12 weeks, the molecular layer showed advanced atrophy compared to 6 weeks (139um, $p < 0.001$) (**Figure 14B**). Unexpectedly, the molecular layer of non-ataxic *ATXN1[82Q]/CαM120A* mice demonstrated a similar degree of progressive atrophy than of *ATXN1[82Q]* mice (156um at 6 weeks; 135uM at 12 weeks) (**Figure 14B**).

CαM120A homozygous mice were examined to evaluate whether *CαM120A* background might impact molecular layer width. *CαM120A* controls displayed mild thinning of the dendritic arborization at 6 weeks (186um, $p < 0.05$.) and 12 weeks (173um, $p < 0.01$) compared to age-matched FVB/wt (**Figure 14B**). There was no significant difference between *CαM120A* at 6 versus 12 weeks, indicating there is no age-dependent molecular layer atrophy in *CαM120A* cerebella. Importantly, the *CαM120A* cerebellar cortex was significantly fuller than *ATXN1[82Q]/CαM120A* at both ages studied. Based on these

Figure 14

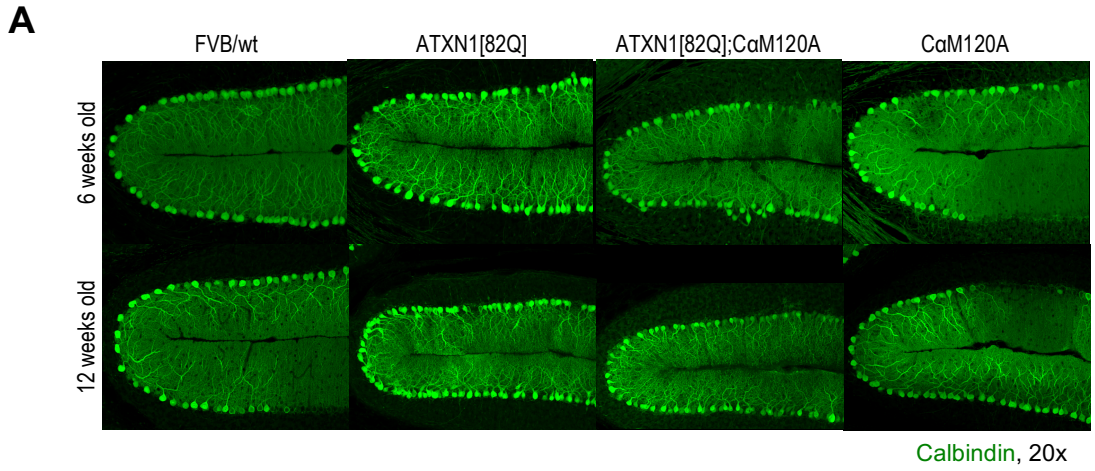

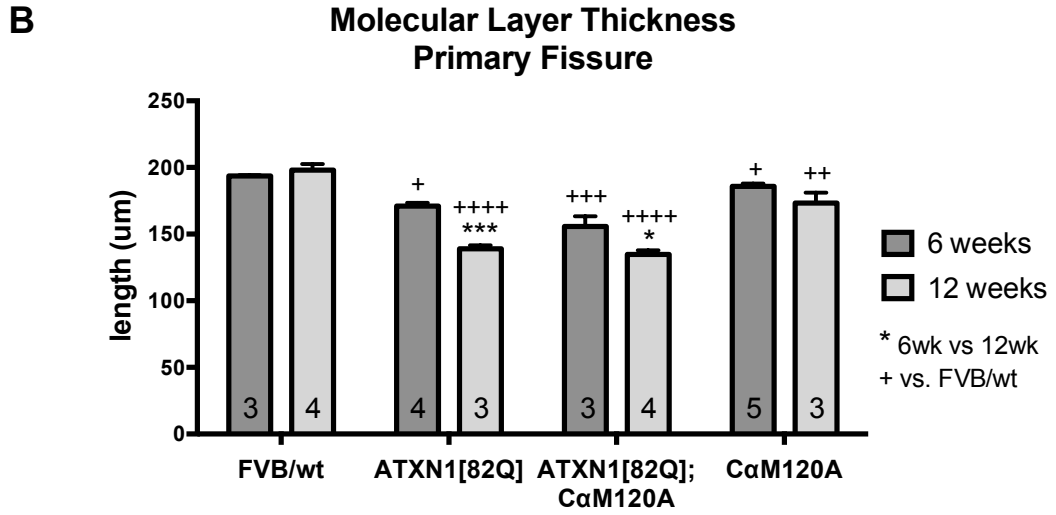

Figure 14. Cα-mediated reduction of ATXN1[82Q] in Purkinje cells does not improve pathological atrophy of the molecular layer at early or mid-stage disease. (**A**) Immunofluorescence staining using the Purkinje cell marker Calbindin was used to identify the molecular layer (ML) at 6 weeks and 12 weeks of age. ML thickness is an indicator of Purkinje cell integrity. (**B**) ML length (um) was measured in the genotypes indicated, demonstrating the expected age-dependent atrophy in *ATXN1[82Q]* and in *ATXN1[82Q];CαM120A* cerebella. *CαM120A* controls showed mild ML thinning compared to *FVB/wt*, but this was not an age-dependent phenotype. Data are represented as mean, ± SEM. Two-way ANOVA. * $p < 0.05$, ** $p < 0.01$, *** $p < 0.001$, **** $p < 0.0001$. Notice * indicates comparison between ages, and + indicates comparison to age-matched wild type.

observations we cannot rule out whether CαM120A expression has a detrimental effect on molecular layer which might hinder improvement in *ATXN1[82Q]/CαM120A* mice. Nevertheless, because there was no progressive atrophy from 6 weeks to 12 weeks of age, this implies *CαM120A* does not contribute to progressive degeneration of the molecular layer.

Taken together, the *CαM120A* background does not prevent ATXN1[82Q]-induced atrophy of the cerebellar cortex nor does it halt disease progression caused by ATXN1[82Q] expression in Purkinje cells. Homozygous CαM120A expression alone triggers mild molecular layer thinning, but it is not additive to the ATXN1[82Q]-induced atrophy. Prevention of molecular layer atrophy does not account for the normal motor function seen in *ATXN1[82Q]/CαM120A*.

ATXN1[82Q] protein reduction is not sufficient to correct SCA1-linked gene expression changes in cerebellum associated with disease progression

As reviewed in Chapter 1, ATXN1 exerts its toxicity in the nuclear compartment and this leads to aberrations in gene expression (Klement et al., 1998; Lin et al., 2000; Serra et al., 2004, 2006; Ingram et al., 2016). Treatments to lessen disease are accompanied by a correction of gene expression abnormalities, and considered a putative molecular marker of disease reversal (Zu et al., 2004; Keiser et al., 2013, 2014, 2016). The most recent RNAseq studies performed in our lab identified a set of 342 genes as correlating with SCA1 disease, termed the Magenta gene module (discussed in the Chapter 1 and further discussed in Chapter 4) (Ingram et al., 2016). The Magenta module is enriched for genes preferentially expressed by Purkinje cells and their transcriptional dysregulation correlates with the progressive aspect of SCA1 degeneration (**Figure 15A**) (Ingram et al., 2016).

To better illustrate the significance of Magenta module genes to disease, a mouse model generated in our lab in which Purkinje cell-expressed ATXN1[82Q] transgene was

Figure 15

A

Magenta module genes[#]

Gene name	Cic binding	PC expression
Homer3	Cic binding motif #1, TGAATGGA	Strong PC expression
Inpp5a	Cic binding motif #2, TGAATGGA	Strong PC expression
Itpr	No Cic binding motif	Strong PC expression
Rgs8	Cic binding motif #1, TGAATGGA	Strong PC expression
Mxra7	Binding motif #2, TGAATGGA	
Calbindin	Binding motif #2, TGAATGGA	Strong PC expression

Ingram et al, 2016[#]

B

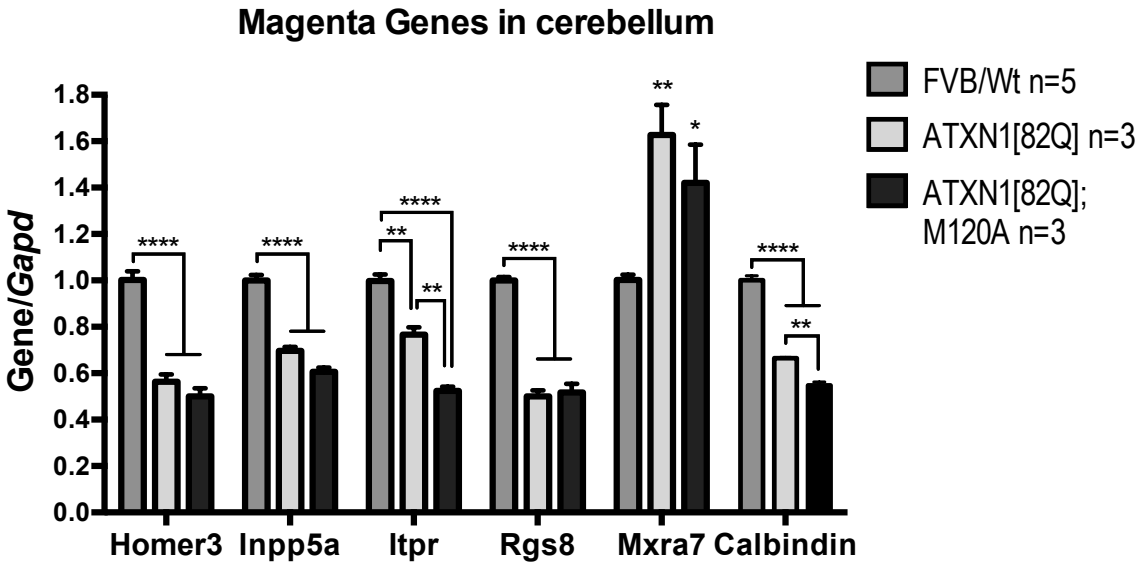

Figure 15. Transcriptional changes of disease-related genes in the Magenta module are not reversed to wild type in *ATXN1[82Q];CαM120A* cerebella. (**A**) A group of 342 genes were previously identified as being correlated with disease in SCA1 mouse models (Ingram et al., 2016). Six of these genes have been validated, five of which are highly expressed in Purkinje neurons. (**B**) The expression of genes in *ATXN1[82Q];CαM120A* were not reinstated to wild type levels. Data are represented as mean, ± SEM. One-way ANOVA. * $p < 0.05$, ** $p < 0.01$, *** $p < 0.001$, **** $p < 0.0001$.

mutated to interrupt binding to the transcriptional regulator Capicua (Cic), a native binding partner of ATXN1 (**Figure 1**) (unpublished data; Lim et al., 2008). These mice have no rotarod deficits and show preservation of the molecular layer thickness, as well as restoration to wild type levels of a number of genes in the Magenta module (unpublished data). Many genes in the Magenta module have Cic binding motifs upstream of their promoters, suggesting a causal relationship in repair of their expression when ATXN1[82Q] can no longer bind Cic (**Figure 15A**). This model sets an example of how alterations in gene expression are linked to disease in SCA1 and they can be reverted to wild type in a condition where disease is fully averted. Study of genes in the Magenta module can be used as a tool to assess disease reversal at the molecular level.

For these experiments, whole cerebellar RNA was isolated from 4-5-week-old *ATXN1[82Q]*, *ATXN1[82Q]/CαM120A*, and *FVB/wt* mice. Gene expression analysis by qRT-PCR confirmed previously validated downregulation of five (*Homer3*, *Inpp5a*, *Itpr*, *Rgs8, Calbindin*) and upregulation of one (*Mxra7*) Magenta module genes in *ATXN1[82Q]* cerebella when compared to wild type controls (**Figure 15B**, light grey bars). I hypothesized that expression of these genes would be returned to wild type levels in the cerebella of *ATXN1[82Q]/CαM120A* mice, but this was not the case (**Figure 15B**, black bars). Disease related transcriptional changes were not rectified in *ATXN1[82Q]/CαM120A* cerebellum.

Loss of genes beyond those found in the Magenta module have been associated with motor deficits. As disease advances, so does transcriptional misregulation and altered proteostasis (Ruegsegger et al, 2016). The next experiments sought to examine whether the *CαM120A* background halts progressive loss of disease-related proteins. The proteins tested were chosen for their known association with cerebellar disease. mGluR1 is a postsynaptic G-protein coupled receptor in Purkinje cell dendrites and is implicated in cerebellar function (Aiba et al., 1994). mGluR1 was the first protein to be associated with motor recovery in the conditional SCA1 model, in which turning off *cATXN1[82Q]* gene expression shows motor recovery and associated return of mGluR1α at parallel fiber-Purkinje cell synapses, as well as recuperation of mGluR1 in protein lysates of whole

cerebellum (Zu et al., 2004). In a different approach, RNAi-mediated knockdown of Ataxin-1 in *Sca1*$^{154Q/2Q}$ or *Pcp2-ATXN1[82Q]* models leads to full or partial recovery of mGluR1 gene expression (*Grm1*) (**Appendix 1**) (Keiser et al. 2014, 2016). Another Purkinje cell protein, Calbindin, has been linked to cerebellar function and its genetically induced haploinsufficiency exacerbates SCA1 phenotype (Airaksinen et al., 1997; Vig et al., 2012). Finally, Homer3 is a Purkinje cell specific postsynaptic scaffolding protein that links mGluR1 and IP3R, influencing neuronal activity (Brakeman et al., 1997, Tu et al., 1998). Both Calbindin and Homer3 are found in the Magenta gene module (**Figure 15**).

Whole cerebellar lysates from 4 week old and 12 week old FVB/wt, *ATXN1[82Q]*, and *ATXN1[82Q]/CαM120A* mice were processed for western blotting. As expected, *ATXN1[82Q]* cerebellar lysates a showed reduction in mGluR1 (**Figure 16**). The reduction was not significant at 4 weeks (black bars), but was statistically significant at 12 weeks of age (grey bars). Unexpectedly, *ATXN1[82Q]/CαM120A* failed to replenish mGluR1 protein abundance.

Consistent with the qPCR results, Calbindin and Homer3 levels were diminished in 4 weeks old *ATXN1[82Q]* cerebella (**Figure 16B** and **16C**, black bars). This reduction in protein was similar in the *ATXN1[82Q]/CαM120A* samples (although Calbindin reduction did not reach statistical significance at this young age). Calbindin, Homer3, and mGluR1 levels were further reduced in 12-week-old cerebella in both *ATXN1[82Q]* and *ATXN1[82Q]/CαM120A* to the same degree (**Figure 16A-C**, grey bars). Thus, a *CαM120A* background does not prevent progressive misexpression of select cerebellar function-associated proteins in non-ataxic *ATXN1[82Q]/CαM120A* mice.

The next series of experiments sought to evaluate whether components of PKA signaling pathway might be disrupted in *ATXN1[82Q]* compared to *ATXN1[82Q]/CαM120A* mice. PKA activity and signaling specificity is synchronized by regulatory and catalytic subunit composition, as well as specialized anchoring proteins known as AKAPs (A-Kinase Anchoring Proteins) (Tasken and Aandahl, 2004; Turnham and Scott, 2016). AKAPs bind PKA holoenzyme by interacting with type 2 regulatory

subunits and localizing PKA to subcellular microdomains to direct phosphorylation (Zhong et al., 2009; Pink and Dell'Acqua, 2010). The first AKAP to be examined was Praja2. Praja2 is an AKAP that also modulates PKA activity by regulating the levels of inhibitory regulatory subunit (Lignitto et al., 2010), and it is enriched in Purkinje neurons (Lein

Figure 16

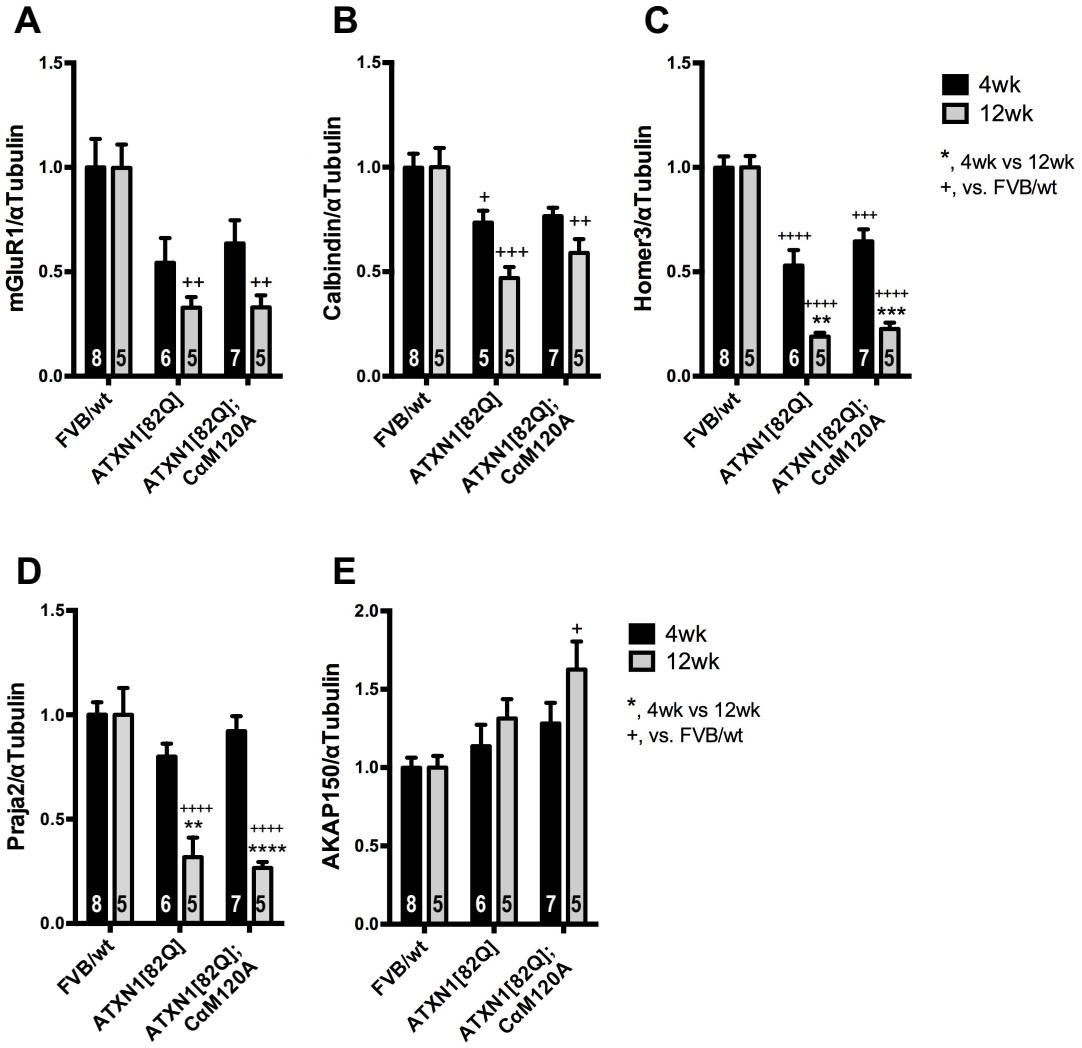

Figure 16. Levels of proteins associated with SCA1 are not restored in *ATXN1[82Q];CαM120A* cerebella, despite association with cerebellar function. Cerebellar homogenates of early (4 weeks) and mid stage (12 weeks) disease were processed for western blotting. mGluR1 (**A**) and Calbindin (**B**) were lower and 4 weeks and significantly decreased at 12 weeks (grey bars). (**C**) Homer3 was significantly reduced at 4 weeks (black bars) and progressively depleted at 12 weeks (grey bars). A-kinase anchoring proteins showed diverging trend. (**D**) Praja2 loss was not evident until 12 weeks. In contrast, at 12 weeks AKAP150 was elevated in *ATXN1[82Q];*CαM120A mice

(significantly higher than FVB, but n.s. from *ATXN1[82Q]*). Data are represented as mean, ± SEM. Two-way ANOVA. * $p < 0.05$, ** $p < 0.01$, *** $p < 0.001$, **** $p < 0.0001$.

et al., 2007). Upon PKA activation, Praja2 directs ubiquitination and degradation of PKA regulatory subunits, consequently prolonging free catalytic subunit activity (Lignitto et al., 2010). Immunoblotting of cerebellar lysates showed Praja2 levels were equivalent to wild type early in disease (4 weeks) (**Figure 16D**, black bars), but were downregulated after disease onset (12 weeks) (**Figure 16D**, grey bars). Moreover, Praja2 expression pattern was identical in *ATXN1[82Q]* and *ATXN1[82Q]/CαM120A* cerebella. The loss of Praja2 protein at 12 weeks was not averted in *ATXN1[82Q]/CαM120A* (**Figure 16D**, grey bars). These experiments are the first to show a link between Praja2 and disease progression in SCA1. Loss of Praja2 is not prevented with reduction of ATXN1[82Q] levels in *ATXN1[82Q]/CαM120A* mice.

Another Purkinje cell enriched AKAP is AKAP150, a scaffolding protein that targets several signaling molecules, including PKA, to the postsynaptic membrane, affecting membrane excitability (Glantz et al., 1992; Weisenhaus et al., 2010). AKAP150 null mice display deficits in motor coordination and strength, implicating a role in cerebellar functioning (Tunquist et al., 2008). At 4 weeks, AKAP150 levels trended higher in *ATXN1[82Q]/CαM120A* mice (**Figure 16E**, black bars), but this effect was not significant. At 12 weeks, there was a statistically significant elevation in AKAP150 compared to wild type (**Figure 16E**, grey bars). AKAP150 protein trends higher in *ATXN1[82Q]/CαM120A* than *ATXN1[82Q]* mice, but was not significant, even when restricting statistical analysis to a direct comparison by t-test ($p = 0.1879$). Therefore, AKAP150, a PKA anchoring protein the loss of which is linked to motor dysfunction, is slightly elevated in mice expressing CαM120A protein.

The focus of the next set of experiments was to evaluate whether other elements of the PKA holoenzyme are affected in disease or with CαM120A expression. Depending on the tissue examined, complete loss of Cα in *Prkaca-/-* mice leads to downregulation of PKA regulatory subunits and compensatory upregulation of Cβ (Skalhegg et al., 2002). Cβ subunits were evaluated in Figure 10 and found not to change. Here, PKA subunits were

examined to determine whether ATXN1[82Q] transgene expression or *CαM120A* (with lowered Cα) caused a shift in their levels. An antibody that recognizes PKA regulatory subunit II (α and β) was used for immunoblotting of 4 and 12 week old cerebellar lysates. There was no change in the levels of RII in whole cerebellum (**Figure 17A**). Similarly, RIβ, which is highly expressed in Purkinje cells (**Figure 2**), was unaffected by mutant ATXN1 overexpression or reduced Cα levels found in *CαM120A* brain (**Figure 17B**). Hence, ATXN1[82Q] transgene expression does not disturb the expression of PKA regulatory proteins, which influence PKA activity. Additionally, a ~30% loss of Cα in *CαM120A* tissues is not likely to be sufficient to disrupt the abundance of PKA regulatory subunits.

To date, the only other kinase implicated in Atxn1 phosphorylation *in vivo* is Msk1 (discussed in Chapters 1 and 2). Four- and 12-week old FVB/wt, *ATXN1[82Q]* and *ATXN1[82Q]/CαM120A* cerebella were subjected to immunoblotting for Msk1 to determine whether proteins levels are changed. As **Figure 17C** illustrates, Msk1 kinase levels were not disrupted in *ATXN1[82Q]* or in *ATXN1[82Q]/CαM120A* mice cerebella. Therefore, the effects of CαM120A on ATXN1[82Q] are not likely to be due to unexpected alterations in the Msk1 pathway.

PKAcα-mediated reduction of ATXN1[82Q] in Purkinje cells is transient

Results presented in Chapter 2 show the novel finding that a ~30% reduction in Cα leads to a reduction of Purkinje cell ATXN1[30Q] and ATXN1[82Q] proteins. In this chapter, *ATXN1[82Q]/CαM120A* mice do not develop motor deficits early in disease, involving a therapeutic effect of ATXN1[82Q] reduction. However, other measures of SCA1 disease, including molecular layer thickness and transcriptional changes, are not corrected. I questioned whether the reduction in ATXN1[82Q] persists into later stages of disease.

Figure 17

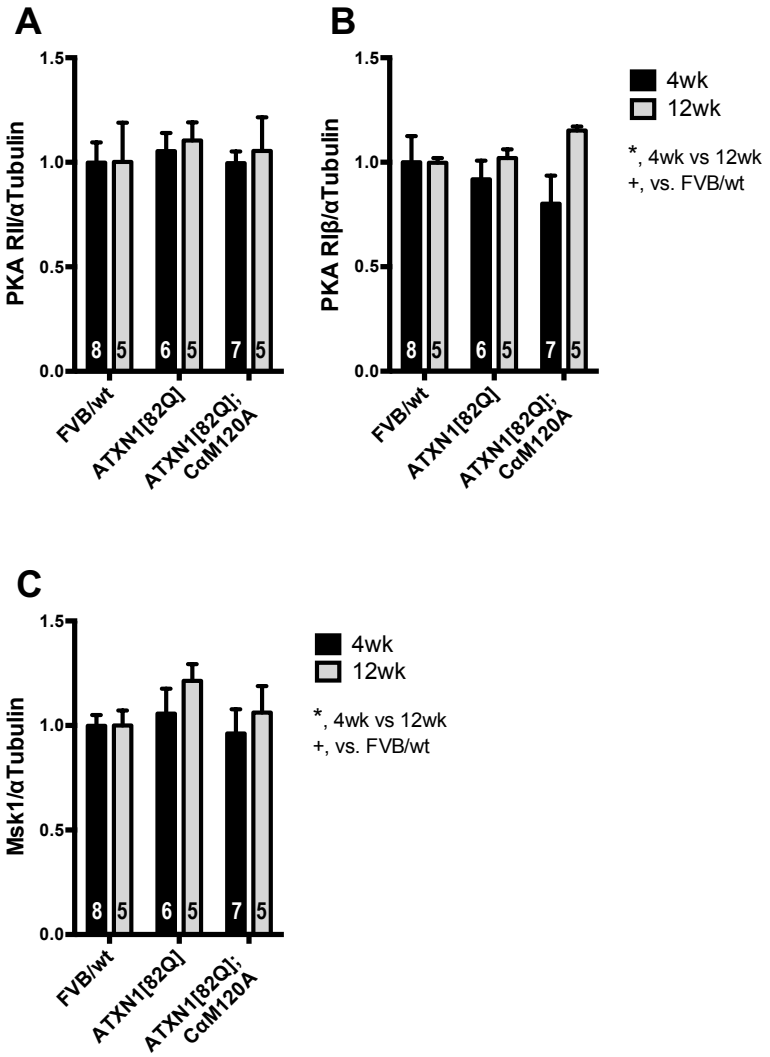

Figure 17. Reduction of Cα levels does not affect other components of the PKA holoenzyme or Msk1 expression. The same cerebellar homogenates used in Figure 17 were probed for these series of proteins. PKA regulatory subunits (RIIα/β, **A**; RIβ, **B**) were equally expressed between genotypes and ages studied, suggesting 30% reduction in Cα does not affect other components of the PKA holoenzyme. (**C**) Levels of Msk1, another kinase implicated in SCA1, are not altered with transgene expression in *ATXN1[82Q]* or with CαM120A mutation in *ATXN1[82Q]/CαM120A* mice. Data are represented as mean, ± SEM. Two-way ANOVA. * $p < 0.05$, ** $p < 0.01$, *** $p < 0.001$, **** $p < 0.0001$.

Eight- and 12- week old cerebella were processed for western blotting and antibodies against PKAcα, phospho-S776, and total Ataxin1 were used for immunodetection. Cα levels remain low (**Figure 18A**) at all ages examined. However, the 60% reduction in pS776-ATXN1[82Q] found at 4 weeks is weakened after this time point. By 8 weeks there was only a 30% reduction in phosphorylated protein and this effect failed to reach statistical significance (**Figure 18B**). Note the graphs include 4-week-old data introduced in Figure 10D for comparison.

At 8 and 12 weeks, cerebella no longer showed a reduction of total ATXN1[82Q] levels (**Figure 18C**). Consistent with findings at 4 weeks, phospho-S776-Atxn[2Q] and total Atxn1[2Q] were not affected at any age tested (**Figure 18D**, **E**). Therefore, a reduction in Cα protein impacts total ATXN[82Q] early in disease, but this effect does not persist in the course of disease. Reduced Cα might affect phospho-S776-ATXN1[82Q] at later stages, but this effect is not significant.

Figure 18. CαM120A mutation lowers PKA levels, but the effect on ATXN1 is transient. Eight and 12 week cerebella were collected and processed for western blotting. The blots were probed for PKA Cα, phospho-S776 Ataxin1 and total Ataxin1. Four week old data From figure 10D is graphed together with these results for direct comparison. Cα protein is destabilized when harboring an M to A point mutation at amino acid 120, and this reduction persists up to 12 weeks of age (**A**). Consequently, there is a significant decrease in pS776-ATXN1[82Q] at 4 weeks, but the effect is attenuated by 8 weeks and 12 weeks and is not statistically different from age-matched controls (**B**). Total ATXN1[82Q] protein is greatly reduced at 4 weeks, but there is no change in total ATXN1[82Q] at 8 and 12 weeks of age (**C**). The levels of phosphorylated and total Atxn1[2Q] are equal to wild type at all ages in both genotypes (**D**, **E**). Data are represented as mean, ± SEM. Two-way ANOVA. * $p < 0.05$, ** $p < 0.01$, *** $p < 0.001$, **** $p < 0.0001$.

Figure 18

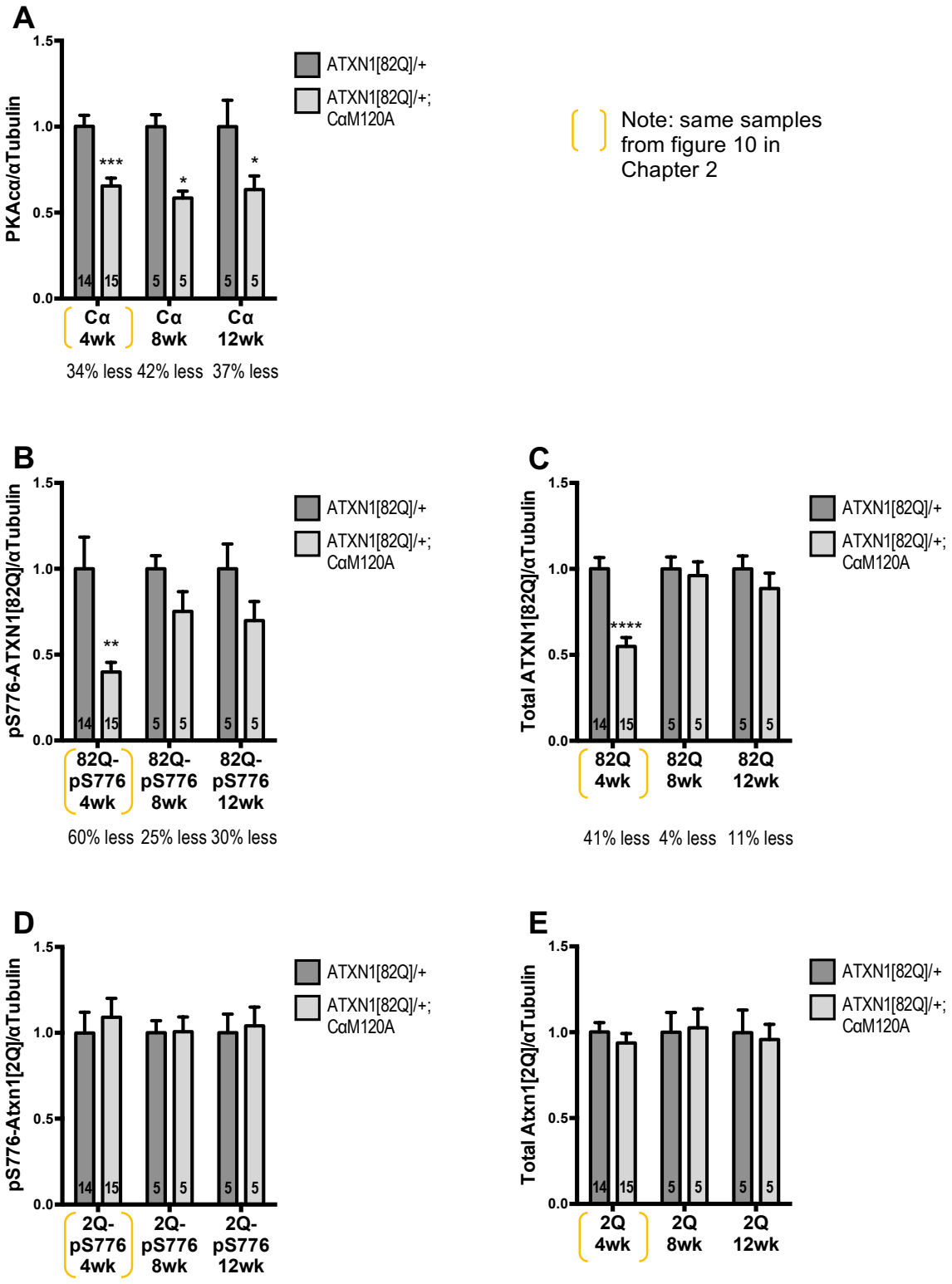
A
PKAcα/αTubulin
1.5
1.0
0.5
0.0
***
*
*
14
15
5
5
5
5
Cα 4wk
Cα 8wk
Cα 12wk
34% less
42% less
37% less
ATXN1[82Q]/+
ATXN1[82Q]/+; CαM120A
Note: same samples from figure 10 in Chapter 2
B
pS776-ATXN1[82Q]/αTubulin
**
82Q-pS776 4wk
82Q-pS776 8wk
82Q-pS776 12wk
60% less
25% less
30% less
C
Total ATXN1[82Q]/αTubulin
****
82Q 4wk
82Q 8wk
82Q 12wk
41% less
4% less
11% less
D
pS776-Atxn1[2Q]/αTubulin
2Q-pS776 4wk
2Q-pS776 8wk
2Q-pS776 12wk
E
Total Atxn1[2Q]/αTubulin
2Q 4wk
2Q 8wk
2Q 12wk

Discussion

Uncoupling hallmarks of disease in SCA1: early onset ataxia versus progressive histopathology

In chapter 2, I used a PKA mutant model, which incidentally destabilizes Cα expression and kinase activity, to test the effects attenuated PKA signaling has on phosphorylation-mediated stability of Ataxin1. I discovered a reduction in ATXN1[82Q] that is specific to Purkinje cells, implicating PKA as a major player in controlling ATXN1 phosphorylation in this neuronal cell. In this chapter I tested what the ramifications of this biochemical change are on several disease metrics. Using two behavioral tests to measure fine motor performance in rodents, I found that a 60% pS776-ATXN1[82Q] and 41% ATXN1[82Q] reduction is sufficient to reverse motor deficits in *ATXN1[82Q]/CαM120A* mice early in disease. Unexpectedly, non-behavioral correlates of disease failed to show any improvement. The molecular layer thickness, a direct measure of Purkinje cell dendritic integrity, was degenerated in *ATXN1[82Q]/CαM120A* to the same degree than in *ATXN1[82Q]* brains. Additionally, aberrant gene expression changes found in *ATXN1[82Q]* samples were not returned to wild type in *ATXN1[82Q]/CαM120A* samples. Furthermore, levels of proteins previously shown to be restored in models were ataxin1 is reduced are still suppressed in *ATXN1[82Q]/CαM120A*. These findings suggest the disease processes that induce motor deficits are distinct from those causing histological and transcriptional abnormalities in SCA1, at least early in disease.

To interpret the seemingly contradictory results presented here, one must first consider how adding a phosphate group to S776 modifies ATXN1's biochemical properties. With diminished kinase activity, phosphatases can more readily dephosphorylate S776 and additional phosphate binding is hindered. This switches S776 to an unphosphorylated state. Unphosphorylated ATXN1 is channeled to degradation pathways, the result of which is a reduction of ATXN1 protein load, further discussed below (Emamian et al., 2003). Moreover, pS776-ATXN1 displays unique protein binding characteristics, which are considered to mediate disease (Lim et al., 2008). For example,

pS776-ATXN1 and ATXN1-D776 (with a phosphomimetic aspartate, D, at position 776) show enhanced binding to splicing factor RBM17, which enhances pathogenicity *in vivo* (Lim et al., 2008). The length of the polyglutamine ATXN1 also promotes binding to RBM17 (Lim et al., 2008).

There are two SCA1 models in which the role of S776 has been specifically addressed. The potentially phosphomimicking D776 mutation worsens neuropathology and ataxia in *ATXN1[82Q]-D776* mice (Duvick et al., 2010). A major finding is that D776, which resides outside the polyglutamine tract, transforms wild type Ataxin1 into a highly toxic protein (Duvick et al, 2010). *ATXN1[30Q]-D776* mice develop ataxia and molecular layer thinning to the same extent than *ATXN1[82Q]* mice (Duvick et al., 2010; Ingram et al., 2016). However, *ATXN1[30Q]-D776* do not manifest changes that ensue with disease progression, such as Purkinje cell death or progressive molecular layer atrophy. At the transcriptional level, expression of genes in the Magenta gene module are downregulated in both *ATXN1[30Q]-D776* and *ATXN1[82Q]* mice, but they only continue to decrease in *ATXN1[82Q]*, as disease advances to cell death (Ingram et al., 2016). Comparison of the ATXN[30Q]-D776 and ATXN1[82Q]-S776 models puts forth a model where different mechanisms potentially drive the onset of disease (Purkinje cell dysfunction and nonprogressive ataxia, seen in *D776*) versus progression (progressive ataxia, Purkinje cell atrophy and cell death, seen in *82Q*). Moreover, the *ATXN[30Q]-D776* model nicely illustrates that the phosphorylation state of ATXN1 contributes to disease and ataxia, likely as a result of aberrant protein-protein interactions. Therefore, decline in pS776-ATXN1 species alone signifies a shift away from certain toxic protein-protein interactions.

The second study exploring S776-related biology is the *ATXN1[82Q]-A776* model, in which glutamine-expanded *ATXN1* is overexpressed in Purkinje cells, but the toxic effect of the protein is substantially thwarted (Emamian et al, 2003). At the protein level, ATXN1[82Q]-A776 is unstable and its levels decreased, and it does not interact with RBM17 (Emamian et al, 2003; Lim et al., 2008). These mice do not develop ataxia or rotarod deficits, even as late as 46 weeks of age (Emamian et al., 2003). No signs of Purkinje cell disease are seen initially; however molecular layer thinning is evident by 37

weeks of age (30% smaller than wild type). Therefore, although largely not pathogenic, unphosphorylated ATXN1[82Q]-A776 can cause Purkinje cell insult, if expressed for long enough time. This model hints at mechanisms that incite detrimental changes with advancing age when Ataxin1 with a polyglutamine tract mutation is present. I would argue that the main benefits obtained from A776 modification, not only stem from a reduction in ATXN1 levels, but maybe even more so from impeding toxic gain of function interactions that occur with ATXN1 phosphorylated at S776 early in disease. Because ATXN1[82Q]-A776 harbors an expansion mutation, it is still able to activate age-related degenerative processes later on.

In brief, these S776-focused SCA1 models distinguish two different functions of ATXN1 protein that control Purkinje disease processes and are relevant in light of the results presented in this chapter: (i) abnormally enhanced phosphate modification of ATXN1 at S776 underlies changes that cause motor deficits (seen in *30Q-D776* and not seen in *82Q-A776*), (ii) polyglutamine-mutant ATXN1 drives progressive features of disease, like advancing molecular layer atrophy (seen in *82Q-S776* and *82Q-A776*) and cell death (seen in *82Q-S776*). I propose that the work I have presented here is a reflection of and in support of these concepts. I found that PKA-mediated reduction in pS776-ATXN1[82Q] uniquely averts motor deficits, at least early in disease. With a decline in PKA, there is a substantial loss of pS776-ATXN1[82Q] (60% reduction), greater than the associated total protein clearance (40% reduction). I reason that the motor recovery described in this chapter is attributable to dampening toxic pS776-driven changes early in the disease process. It seems that 41% decrease in total mutant protein is not sufficient to evade the insult caused by overexpression of a polyglutamine-expanded ATXN1 in Purkinje cells.

Still, the detrimental impact of Ataxin1 protein levels are not constrained to the polyglutamine expansion mutation or phospho-S776 effects. Wild type ataxin1 overexpression itself can elicit features of SCA1 disease. *ATXN1[30Q]/ATXN1[30Q]* mice display considerable molecular layer thinning at 59 weeks, demonstrating that ataxin1 load alone can trigger disease changes (Fernandez-Funez, et al., 2000). Remarkably, elevations

in wild type murine Atxn1[2Q] are linked to rotarod deficits as early as 5 weeks of age, and Purkinje cell loss seen at only 10 weeks of age (Gennarino et al., 2015). In fact, by 32 weeks *ATXN1[82Q]-A776/ATXN1[82Q]-A776* cerebella also show signs of Purkinje cell pathology not seen in the heterozygous (Emamian et al., 2003). Interestingly, *ATXN1[82Q]-A776/ATXN1[82Q]-A776* never develop ataxia, which further supports a role of S776 residue in contributing to the ataxic phenotype. These insights are important to understanding the findings presented in this chapter.

Reducing ATXN1 protein burden has been investigated beginning with the generation of the conditional *cATXN1[82Q]* mice (Zu et al., 2004; Serra et al, 2006), and more recently with approaches to directly knock down Ataxin1 (Xia et al, 2004; Keiser et al, 2013, 2014, 2016; unpublished data). One important lesson from these studies is that in addition to timing of therapy, the degree of Ataxin1 knockdown is critical for therapeutic effect. A summary table of publications surrounding this topic is presented in **Appendix 1**. The more useful study is the most recent one by Keiser et al. 2016. A summary of this publication is presented in **Appendix 2**. A 23-28% *hATXN1* mRNA knockdown, permits rotarod recovery, but molecular layer atrophy is not prevented; instead, a ~50% knockdown is required to fully avert disease. Therefore, there is a cutoff between 30% and 50%, where reduction in total ATXN1 can rescue molecular layer atrophy, while the ataxia is more amenable to rescue. In perspective, my work shows a 40% reduction in total ATXN1[82Q] coupled with full recovery in motor coordination tests, but failure to prevent disease progression. Therefore, a 40% ATXN1 reduction in *ATXN1[82Q]/CαM120A* is not within the therapeutic threshold.

Previously identified transcriptional changes in SCA1 do not account for recovery of motor coordination and balance

Here I tested whether ATXN1[82Q] reduction with motor recovery seen in the *ATXN1[82Q]/CαM120A* mice might be coupled to restoration of genes previously correlated to disease. I first quantified the newly identified Magenta module for having genes downregulated in two ataxic SCA1 models, *ATXN1[30Q]-D776* and *ATXN1[82Q]*

(Ingram et al., 2016). I failed to find a shift in gene expression from the disease pattern. I also looked at the protein levels of genes associated with ataxia and disease, but again failed to see a return to wild type levels. The Magenta module genes continue to decrease with age in *ATXN1[82Q]*, but not *ATXN1[30Q]-D776*, so it was deduced these are linked to the progressive aspect of SCA1 (Ingram et al., 2016). My experiments agree with that conclusion, as *ATXN1[82Q]/CαM120A* also display progressive Purkinje cell atrophy. My findings suggest the Magenta module genes are not functionally related to balance and coordination phenotypes and their shared downregulation in *ATXN1[30Q]-D776* and *ATXN1[82Q]* drives some other common aspect of disease.

One protein that is generally understood as being associated with ataxic phenotype in SCA1 is mGluR1 (Zu et al, 2004). Completely turning off *cATXN1[82Q]* early on fully rescues disease and restores mGluR1. Intriguingly, I found mGluR1 protein levels suppressed to the same degree in non-ataxic *ATXN1[82Q]/CαM120A* and in ataxic *ATXN1[82Q]*, suggesting loss of mGluR1 is not a reliable marker of cerebellar ataxia. This finding is surprising as mGluR1 has an established role in cerebellar motor learning (Ichise et al., 2000). Loss of mGluR1 in Purkinje cells is linked to synaptic dysfunction and ataxia, described in mGluR1 null models, other SCAs, and autoimmune ataxias (Aiba, et al., 1994; Ichise et al., 2000; Nakao, et al., 2007; Skinner et al., 2001; Armbrust et al., 2014; Konno et al., 2014; Sillevis Smitt et al., 2000). The lack of mGluR1 recovery in a mouse that does not show ataxia challenges our understanding of this receptor, or its relative contribution to SCA1 ataxic phenotype. It remains to be examined whether there are other proteins that functionally compensate for mGluR1 deficiency in *ATXN1[82Q]/CαM120A* mice.

A potentially interesting, albeit less robust, finding is the elevation in AKAP150 protein levels in *ATXN1[82Q]/CαM120A* mice. AKAP150 is highly expressed in Purkinje cells and primarily localized to its dendrites (Glantz et al., 1992). Why AKAP150 is increased with CαM120A expression could be a subject of additional investigation. Perhaps upregulation of AKAP150 after 4 weeks functionally compensates for the reduced Cα levels, making PKA signaling more efficient by bringing Cα closer to ATXN1[82Q].

This chapter addresses the functional significance PKA-mediated decrease in pS776-ATXN1[82Q] and total ATXN1[82Q] has on SCA1 phenotypes. My findings reflect a distinction between motor deficits early in disease and histopathological features with disease progression. I propose that the more reversible S776 phosphorylation is involved in regulating dynamic pathways which when affected can lead to motor dysfunction and are more adaptable to recovery. In turn, there are separate degenerative pathways which, like a balance, "weigh" ATXN1 load and determine disease progression.

Chapter 4:

RNA SEQUENCING UNCOVERS DISTINCT PATHWAYS ASSOCIATED WITH ONSET OF ATAXIA

Introduction

SCA1 mouse models have shed light on ATXN1 normal function and dysfunction when mutated. In the nucleus, ATXN1 interacts with numerous transcriptional and splicing regulators as well as RNA, and so mutant ATXN1 can pathologically disrupt gene regulation. (Kim et al., 2013; Lam et al., 2006; Chen et al., 2003; de Chiara et al., 2009; Irwin et al., 2005; Yue et al., 2001; Tsai et al., 2004; Tsuda et al., 2005; Serra et al., 2006; Lim et al., 2008; Hong, 2003).

Recent work in our lab took advantage of the high-throughput power of RNAseq technology as an unbiased approach to study the cerebellar transcriptomes of ATXN1[82Q] and ATXN1[30Q]-D776 transgenic mouse models to identify pathways that trigger Purkinje cell disease in SCA1 (Ingram et al., 2016). This work has revealed that in both SCA1 models gene expression changes differ considerably from FVB/wt, but also from each other, which may explain the differences seen in their phenotypes. *ATXN1[82Q]* and *ATXN1[30Q]-D776* mice have in common a similar degree of ataxia, however *ATXN1[82Q]* mice have progressive molecular layer atrophy and Purkinje cell loss (Duvick et al., 2010).

The reduction of ATXN1[82Q] protein seen with low Cα levels in *ATXN1[82Q];CαM120A* mice might also alleviate the aberrant gene regulation mutant ATXN1 exerts in the nucleus. In particular, because only ataxia is reversed and not atrophy in the cerebellar cortex, I hypothesized gene changes in *ATXN1[82Q];CαM120A* might shed light on the distinction between early onset disease pathways contributing to

behavioral deficits versus later onset disease pathways causing neurodegenerative progressive disease. In order to study this hypothesis, I pursued RNAseq studies in *ATXN1[82Q]* and *ATXN1[82Q]/CαM120A* mice and *FVB/wt* controls.

Results

Whole cerebellar RNA from *ATXN1[82Q]*, *ATXN1[82Q]/CαM120A*, and *FVB/wt* of 8-9 weeks of age was isolated for RNAseq analysis. Five samples were collected for each genotype based on the average performance on rotarod and beam walking tasks (shown in Figure 13). The five most ataxic *ATXN1[82Q]* mice and the five best performing *ATXN1[82Q]/CαM120A* and five best *FVB/wt* were selected.

Samples were sent to the University of Minnesota Biomedical Genomics Center for generation of the RNA library and HiSeq 2500 sequencing. Samples were first subjected to quality control (QI) testing and passed the required limit of >8 for RNA integrity number (RIN). All 15 samples were over RIN 8 (**Table 1**). The sample with the lowest RIN was at 8.9 and the average RIN of all samples was 9.2. Therefore, very high quality RNA was used for RNA sequencing. A first run was done which yielded high quality but less than expected reads per sample (range 20-50 million reads/sample). Therefore, a second run was done to improve depth of sequencing (range 30-85 million reads/sample). Each run was processed separately, then combined after genes were summarized. The combined data was back calculated to describe the total data acquired. A total of 1,621,761,236 paired-end reads (2x125 bp reads/sample, on average 193 bp fragments) were generated, with each sample having on average 108,117,416 reads (**Table 1**).

Adapter sequences were removed and data quality control and prepping followed. Sequencing results were uploaded and stored at the Minnesota Supercomputing Institute. Reads were mapped to the UCSC mm10 mouse annotated genome using Hisat2. One of the samples had lower number of reads than the other 14 (#55964), but the mapping efficiency was very high for all samples with an average of 95.92% of read pairs correctly

Genotype	Biological replicate ID	RIN value	Number of reads	Average Mapping Efficiency (%)
FVB/wt	55964_FVB_9wk	9.2	51,477,258	95.69
	55951_FVB_9wk	9.3	100,071,473	95.76
	55931_FVB_9wk	9.3	110,426,482	95.84
	55932_FVB_9wk	9.4	95,667,349	95.80
	55933_FVB_9wk	9.2	111,949,337	95.77
ATXN1[82Q]/+; $C\alpha^{+/+}$	55953_82Q_9wk	9.3	116,091,890	94.65
	55956_82Q_9wk	8.9	135,060,867	95.48
	55957_82Q_9wk	9.3	115,319,373	95.71
	55958_82Q_9wk	9.2	97,034,139	95.68
	55949_82Q_9wk	9.3	96,168,520	95.62
ATXN1[82Q]/+; $C\alpha^{M120A/M120A}$	56094_82Qm120a_8wk	9.1	99,165,872	96.84
	56103_82Qm120a_8wk	9.4	98,230,632	96.70
	56157_82Qm120a_8wk	9.1	128,304,041	96.61
	56099_82Qm120a_8wk	9.2	129,890,811	96.46
	56092_82Qm120a_8wk	9.2	136,903,192	96.60

Table 1. Specifications of samples used for RNA sequencing. RNA integrity numbers (RIN) values are used for quality control of the samples used for RNA sequencing. Recommended RIN for high quality RNA is above 8 and the average RIN of samples used is 9.2. Number of reads indicates the number of ~193bp fragments read per sample. Mapping efficiency is the percent of genes identified for each sample that correctly mapped to the mouse genome.

mapped (**Table 1**), signifying this sequencing yielded very high quality data.

Expression analysis was done using Rsubread in collaboration with a bioinformatics analyst at the Minnesota Supercomputing Institute. To corroborate some of the transcriptional changes in the RNAseq data, genes examined in chapter 3 were verified in the RNAseq differential expression (DE) list. In the DE list, *Prkaca* gene encoding PKAcα was downregulated in CαM120A-expressing samples, which serves as an internal positive control (**Table 2**, #1). Most of the changes in RNAseq were identical to the qPCR Magenta module data in Figure 15 and the western blot data in Figure 16 and 17. The comparisons that do not match results found in chapter 3 are indicated with an asterisk (*****). Aside from PKAcα, genes encoding PKA subunits were largely unaffected (**Table 2,** #12, 13, 15, 16). Only one (*Prkar1b*) came up as being more highly expressed in the two ATXN1[82Q]-expressing samples compared to *FVB/wt* (**Table 2,** #14), in contrast to the unaltered PKArIb protein levels seen at 4 and 12 weeks in western blot data presented in Figure 17B. *AKAP150,* the gene encoding a PKA anchoring protein, was is not altered between RNAseq samples from 8-9 week old cerebella, although in Figure 16E AKAP150 protein was significantly elevated in *ATXN1[82Q]/CαM120A* cerebella at 12 weeks compared to wild type.

As an initial view of the expression patterns in the RNA seq data, principal component analysis (PCA) was performed using DESeq2. Transcriptional changes for each genotype clustered distinctly for each genotype. PCA analysis failed to show gene expression patterns in common in the ten *FVB/wt* and *ATXN1[82Q]/CαM120A* mice that didn't exhibit motor impairment, or in the ten *ATXN1[82Q]* and *ATXN1[82Q]/CαM120A* mice that showed molecular layer atrophy (**Figure 19**).

	Gene name	A_ATXN1[82Q] vs. B_FVB/wt	A_ATXN1[82Q];CαM120A vs. B_FVB/wt	A_ATXN1[82Q] vs. B_ATXN1[82Q];CαM120A
1	*Prakaca*	No difference	A < B	A > B
2	*Homer3*	A < B	A < B	No difference
3	*Inpp5a*	A < B	A < B	No difference
4	*Itpr1*	A < B	A < B	A > B, but n.s. *
5	*Rgs8*	A < B	A < B	A < B * (p=0.002946)
6	*Mxra7*	A > B	A > B	No difference
7	*Calbindin*	A < B	A < B	No difference *
8	*mGluR1 (Grm1)*	A < B	A < B	No difference
9	*Praja2*	A < B, but n.s.*	A < B	No difference
10	*AKAP150*	No difference	No difference	No difference
11	*Msk1 (Rps6ka5)*	No difference	No difference	No difference
12	*Prkacb*	No difference	No difference	No difference
13	*Prkar1a*	No difference	No difference	No difference
14	*Prkar1b*	A > B *	A > B *	A < B *
15	*Prakar2a*	No difference	No difference	No difference
16	*Prkar2b*	No difference	A < B *	No difference
17	*Atxn1*	No difference	No difference	No difference

Table 2. RNAseq expression of Magenta module genes examined in Chapter 3. As an internal control, *Prkaca* gene encoding PKAcα is downregulated in CαM120A-expressing samples. For these pair-wise comparisons the first genotype is denoted "A" and the second denoted "B" in each column. Most of the expression differences were confirmed in qPCR or western blot analyses described in chapter 3 (Figure 16-18), including Magenta gene module (#2-7) and PKA-related genes (#1, 9, 10, 12, 14-16). The comparisons that do not match results found in chapter 3 are indicated with an asterisk (*).

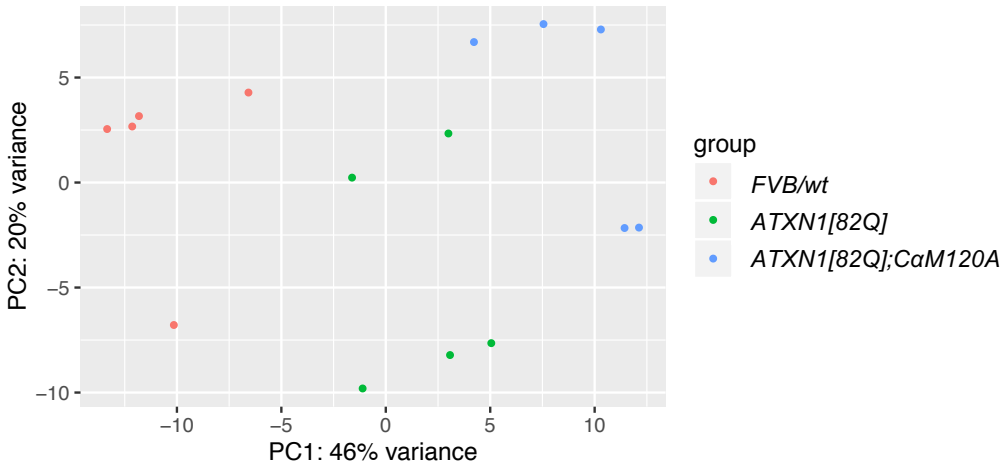

Figure 19. Principal component analysis (PCA) of transcriptional changes found in RNA-seq data. Principal component 1 (PC1) and Principal component 2 (PC2) are in the x and y axis, respectively. Expression patterns are distinct for each genotype. Each colored dot on the graph represents the transcriptional pattern of a single sample of the corresponding genotype (n=5).

Next, the data were analyzed in pairwise comparisons using DESeq2 in the following groups: *ATXN1[82Q]* vs. FVB/wt, *ATXN1[82Q]/CαM120A* vs *FVB/wt*, *ATXN1[82Q]/CαM120A* vs. *ATXN1[82Q]*, to ask whether there are gene changes that might correlate with their shared or dissimilar features (**Figure 20A**). I predicted there may be transcriptional changes that share a high degree of overlap in the genotypes that performed normally in the motor tasks or between that exhibited similar histopathology. Interestingly, there were about 2x higher number of genes differentially expressed between the two genotypes that did not show ataxia (6,391 genes in *FVB/wt* vs. *ATXN1[82Q]/CαM120A*) (**Figure 20B**). There were approximately 3,500 differentially expressed genes in *ATXN1[82Q]* when compared to either *ATXN1[82Q]/CαM120A* or *FVB/wt* (**Figure 20B**).

The high number of genes whose expression diverge between the non-ataxic pair doesn't seem to correlate to their normal behavioral phenotype. Evaluation of the percent of genes upregulated or downregulated for each group in each pair-wise comparison shows a potentially more informative trend, in which there are more genes upregulated in the groups that do not display ataxia compared to the group that does (*ATXN1[82Q]*) (**Figure 20C**, first and third pairs- black vs. grey bars). Comparing the two neurologically intact

groups directly shows they have proportionally equal amounts of genes being upregulated or downregulated (**Figure 20C**, middle pair). Therefore, the directionality of gene expression changes seems to be a better correlate to distinguish mice that are neurologically compromised versus intact.

Figure 20

A

Genotype	Histopathology (molecular layer thickness)	Rotarod & Beam Walking
FVB/wt	Intact	Intact
ATXN1[82Q]	Progressive atrophy 6-12weeks	Impaired
ATXN1[82Q]; CαM120A	Progressive atrophy 6-12weeks	Intact

B

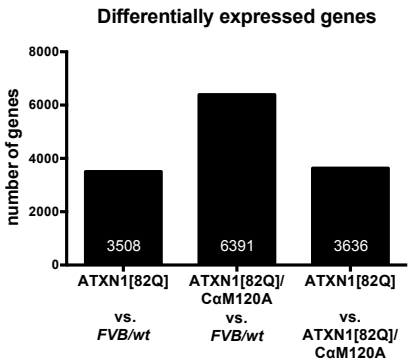

C

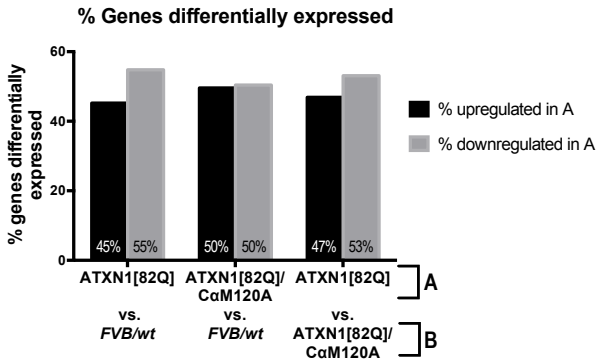

Figure 20. Summary of genotypes and differential gene expression in SCA1 cerebella. (**A**) Report summary of the key characteristics in the three groups studied. **(B)** Total number of genes differentially expressed for each pairwise comparison ($p < 0.05$). **(C)** Percent of genes upregulated per comparison, reflecting a trend: more upregulation of genes in *ATXN1[82Q];CαM120A* and *FVB/wt* than in *ATXN1[82Q]* model. There are approximately equal proportion of genes upregulated in *ATXN1[82Q];CαM120A* as there are in *FVB/wt*.

Next, we used Weighted Gene Coexpression Network Analysis (WGCNA) to generate clusters (modules) of genes that exhibit similar expression patterns between two defined groups. The gene modules generated can then be correlated to defined parameters. The objective of the first WGCNA analysis was to identify genes that are similarly expressed in cerebella of mice that exhibit motor incoordination and balance deficits versus

those that don't, termed the "Ataxia" analysis. *ATXN1[82Q]* was defined as one group (ataxic) and *FVB/wt* and *ATXN1[82Q]/CαM120A* grouped into a second category (non-ataxic). Two pairwise t-tests were done comparing *ATXN1[82Q]* vs *FVB/wt* and *ATXN1[82Q]* vs *ATXN1[82Q]/CαM120A*. Three gene modules emerged with only one, the Pink module, being statistically significant (p=4.663758e-05). The Pink module has 498 genes and shows expression patterns directionally shared by *FVB/wt* and *ATXN1[82Q]/CαM120A*, opposing the direction of gene expression in *ATXN1[82Q]* (**Figure 21**).

Figure 21

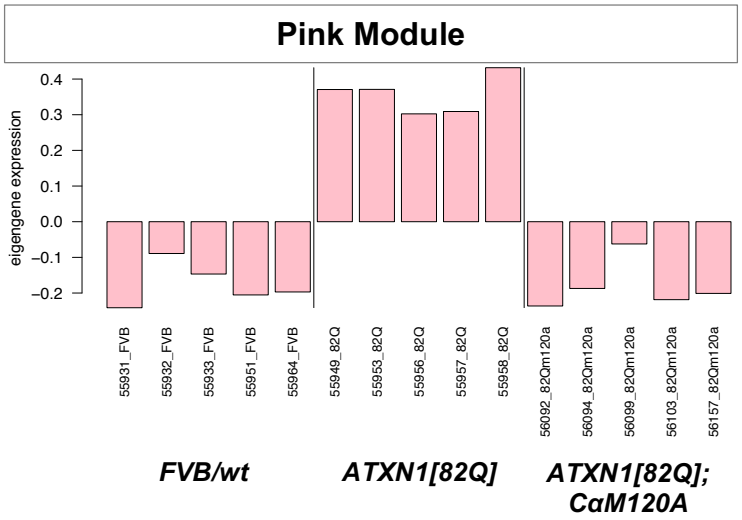

Figure 21. WGCNA "Ataxia" Module. WGCNA analysis was performed to identify genes that are similarly expressed in cerebella of mice that were neurologically intact versus those that displayed rotarod and beam walking deficits. Barplot of the Pink module shows significant relationship with the pattern of FVB/wt and *ATXN1[82Q];CαM120A* vs. *ATXN1[82Q]*. Pink (p=4.663758e-05).

Ingenuity Pathway Analysis was used to identify classes of intracellular pathways in the Pink module. The top upstream regulator is CREB1, cAMP Responsive Element Binding Protein 1 (**Table 3**). CREB is a highly conserved transcriptional regulator and its function is associated with molecular mechanisms of neuronal plasticity and learning (Frank and Greenberg, 1994). Purkinje cell-directed overexpression of CREB leads to suppression of CRE-mediated gene expression and rotarod deficits without beam walk

abnormalities (Brodie et al., 2004). In our RNAseq dataset, CREB expression levels are not changed between genotypes examined (data not shown). However, identification of CREB1 as the top upstream regulator in the Pink "Ataxia" module gene set suggests pathways related to CREB1 function, perhaps modulating neuronal plasticity, are affected in the mice that express ataxia versus the groups that display normal motor behavior.

Table 3. Top Pathways of "Ataxia" Pink Module.

Top 5 Upstream Regulators	p-value
CREB1	1.62E-05
NADPH oxidase	6.23E-05
JUN	1.54E-04
calcitriol	1.56E-04
AGT	2.11E-04
Top 5 Canonical Pathways	**p-value**
Gq Signaling	1.77E-04
fMLP Signaling in Neutrophils	2.79E-04
phagosome formation	2.98E-04
Leukocyte Extravasation Signaling	6.26E-04
FcRIIB Signaling in B Lymphocytes	9.13E-04
Top 5 Networks	**Score**
Protein Synthesis, Cell Morphology, Cell-To-Cell Signaling and Interaction	46
Connective Tissue Disorders, Developmental Disorder, Hereditary Disorder	38
Embryonic Development, Organ Development, Organismal Development	36
Cell Morphology, Cell-mediated Immune Response, Cellular Development	33
Cellular Growth and Proliferation, Tissue Development, Gene Expression	32

The most significant canonical pathway in the Pink module was Gq signaling, followed by fMLP Signaling in Neutrophils (**Table 3**). The majority genes listed in the 'fMLP Signaling in Neutrophils' overlap with the 'Gαq signaling' list. A complete list of genes in the top 5 canonical pathways are shown in **Appendix 3-7**. Cholinergic receptor muscarinic 1 (mAchR, also a Gq receptor) is only found in the latter (**Appendix 3** and **4**). GPCR signaling in which the Gα subunit is coupled to q-protein leads to downstream activation of PKC and Ca^{2+} release from intracellular stores. Gαq signaling pathways have previously been implicated in SCA1, but this has been associated to mGluR1 receptor signaling (Serra et al., 2004). Recent work has shown that mAchR1 may be involved in

synaptic signaling in the cerebellum, where postsynaptic mAChR activation in Purkinje cells triggers the synthesis and release of endocannabinoids that act presynaptically on parallel fiber terminals to attenuate LTP (Rinaldo et al., 2013), suggesting a functional dynamic role that may impact motor function in the whole animal. The top gene in the fMLP Signaling in Neutrophils list is fibroblast growth factor receptor 1 (Fgfr1), which is also the second top gene in the Gαq signaling list (**Appendix 3** and **4**). *Fgfr1*$^{+/-}$ or *Fgfr1*$^{-/-}$ mice are embryonic lethal and examination of Fgfr1 role in the cerebellum is limited to the effects of simultaneously knocking out Fgfr1 and Fgfr2 in glial cells, which leads to a very disrupted cerebellar phenotype that affects neuronal proliferation and cerebellar organization during development (Müller, et al., 2012). The type of genes clustering in the Pink module suggests gene pathways involving Gq signaling in the cerebellum may lead to changes that block or promote ataxia early in disease.

The goal of the second WGCNA analysis was to identify gene patterns in common between genotypes where there are traits of advancing disease (progressive molecular layer atrophy) versus the one that does not (intact molecular layer). *FVB/wt* was defined as one group (wt) and *ATXN1[82Q]* and *ATXN1[82Q]/CαM120A* sorted into a second group (progressive atrophy). Two pairwise t-tests were done comparing *FVB/wt* vs. *ATXN1[82Q]* and *FVB/wt* vs. *ATXN1[82Q]/CαM120A*. Six modules emerged as statistically significant. The Turquoise Module contains 3,246 genes, was the most statistically significant, and displayed very clear direction in gene expression, p=7.4e-07 (**Figure 22**).

Ingenuity Pathway Analysis of the Turquoise "disease progression" module identified L-DOPA as the top upstream regulator (**Table 4**). L-DOPA is the dopamine precursor molecule used to treat Parkinson's disease (PD) in symptomatic patients. A recent fMRI study showed PD patients ON or OFF L-DOPA medication displayed differences in cerebellar-cerebellar and cerebellar-whole brain connectivity, in which OFF medication state showed higher cerebellar connectivity although with inconclusive behavioral motor effects (Festini et al., 2015). Because L-DOPA is a catecholamine precursor, this suggests modulation of these pathways may affect cerebellar function. It is unclear what the role is in the context of SCA1.

Figure 22

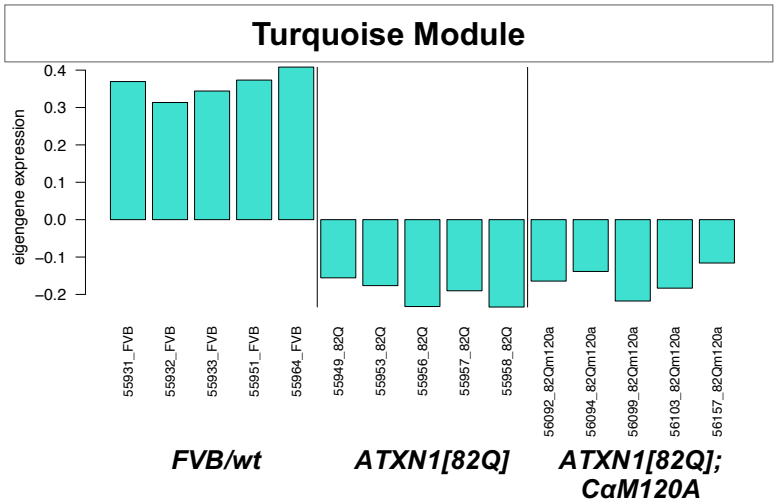

Figure 22. WGCNA "Disease Progression" Module. WGCNA analysis was performed to identify genes that are similarly expressed in cerebella that exhibit progressive dendritic atrophy and molecular layer thinning vs. wild type cerebella. Barplots for the modules that had a significant relationship with the pattern of *ATXN1[82Q];CαM120A* and *ATXN1[82Q]* and FVB/wt. Turquoise (p=7.4e-07).

Several of the top canonical pathways in the "disease progression" Turquoise module are linked to neuronal function or neurodegeneration. These include Axonal Guidance Signaling, Huntington's Disease Signaling and CREB Signaling in Neurons (**Table 4**). A complete list of genes in the top 5 canonical pathways are shown in **Appendix 8-12**. Like SCA1, Huntington's disease (HD) is an adult-onset progressive neurodegenerative disease caused by a CAG tract expansion mutation. That genes known to be affected in HD were identified in our disease-associated module suggests SCA1 and HD may share common mechanisms of disease. A less intuitive canonical pathway, the Superpathway of Cholesterol Biosynthesis, was also identified in the Turquoise gene set. Interestingly, cholesterol deregulation has been implicated in Alzheimer's disease and Parkinson's disease process (Liu et al., 2010). Additionally, the degenerative neuronal storage disease Niemann–Pick disease type C has severe involvement of the cerebellum in most cases and involves anomalies in cholesterol trafficking (Vanier, 2013). Collectively,

IPA analysis identified progressive disease-related pathways in SCA1 that appear to share changes seen in other heritable neurodegenerative disorders.

Table 4. Top Pathways of "Disease Progression" Turquoise Module.

Top 5 Upstream Regulators	p-value
L-dopa	2.20E-23
TGFB1	2.60E-17
lipopolysaccharide	3.93E-17
IFNG	4.68E-17
TNF	5.89E-16
Top 5 Canonical Pathways	**p-value**
Axonal Guidance Signaling	1.80E-08
B Cell Receptor Signaling	2.31E-07
Huntington's Disease Signaling	2.37E-07
Superpathway of Cholesterol Biosynthesis	7.43E-07
CREB Signaling in Neurons	1.18E-06
Top 5 Networks	**Score**
Cell Cycle, Cell-To-Cell Signaling and Interaction, Cellular Function and Maintenance	36
Protein Trafficking, Developmental Disorder, Hereditary Disorder	36
Developmental Disorder, Hereditary Disorder, Immunological Disease	34
Protein Synthesis, Hematological Disease, Hereditary Disorder	34
Cell Morphology, Cellular Assembly and Organization, Cellular Function and Maintenance	34

We next compared the overlap of genes in the Magenta module (Ingram et al., 2016) with all the modules in my dataset to look for correspondence of the previously identified progressive disease module to this study (**Figure 23**). We found 247 genes significantly overlap with the progressive disease Turquoise module in this study (1.347278e-97), but not with the ataxia Pink module (p=0.1997589).

Next, we generated a Venn diagram to identify the degree of overlap between the progressive disease-linked module described in Ingram et al. 2016 (Magenta) vs. this study (Turquoise) and the ataxia module (Pink) (**Figure 24A**). The 247 genes that overlap in Magenta and Turquoise include the six genes examined by qPCR in figure 16. Out of 342 Magenta genes, most (72%) overlap with the Turquoise module. This suggests there is concordance in a subset of gene expression changes that are associated with progressive disease between the Ingram et al. study and this study. However, of the 3,246 genes in the Turquoise module, only 8% overlap with the Magenta module (**Figure 24A**). This analysis

Figure 23

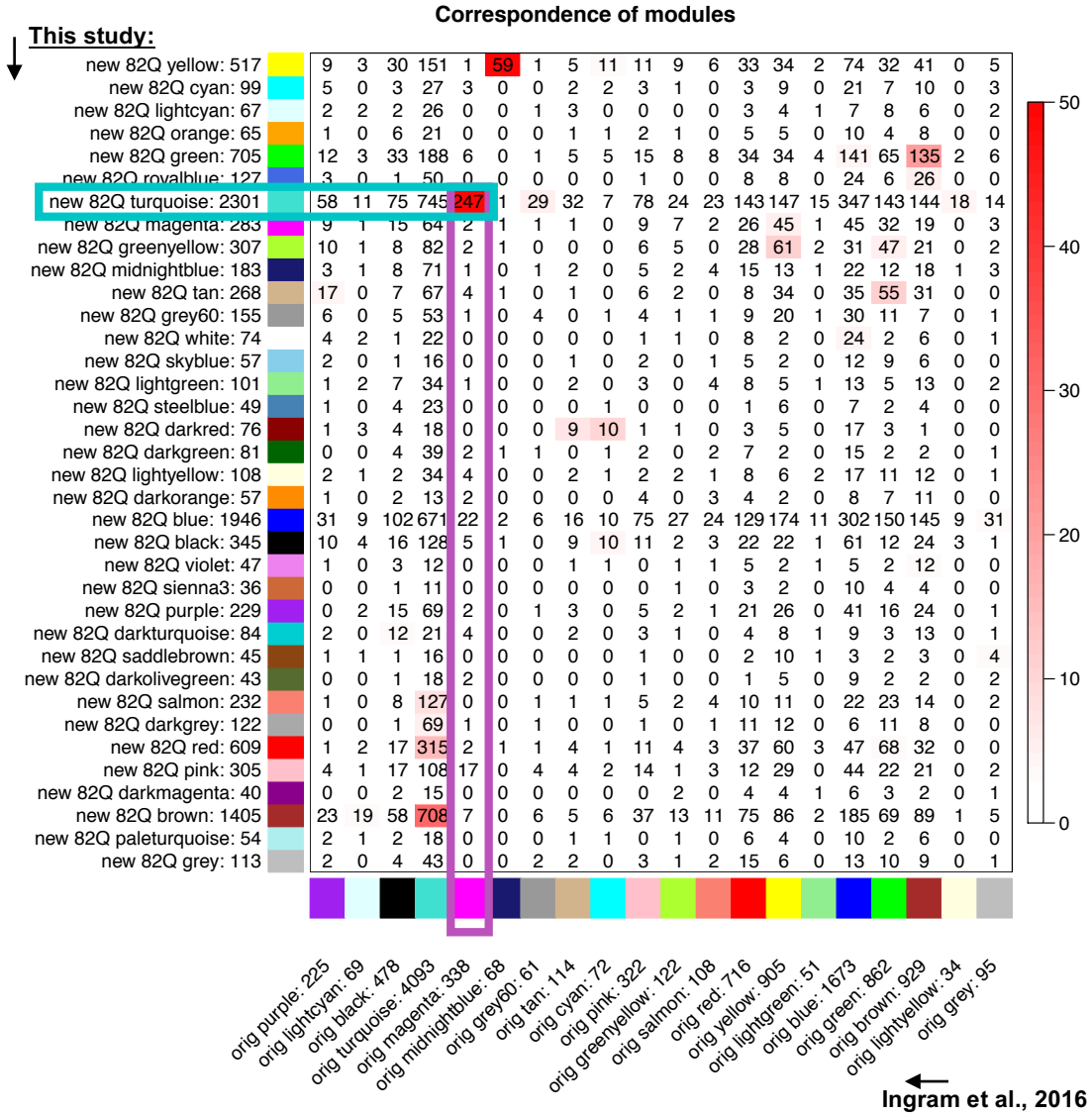

Figure 23. Comparison of WGCNA analyses in this study versus Ingram et al., 2016. Heatmap of the correspondence of modules if both studies. The numbers in each cell indicate genes present in the two modules being compared that are present in both datasets. The red gradient color coding corresponds to -log10(p-value) for Fisher's exact test, in which bright red indicates highly significant overlap and white indicates little or no overlap (see gradient on the right). Notice there is significant overlap between the original Magenta module (x axis) and the Turquoise module in this study (y axis), p= 1.347278e-97.

shows there are 2,999 genes that could belong to gene pathways not previously associated with progressive neurodegeneration in SCA1. Work by Ingram at al. linked overexpression of cholecystokinin (Cck) to a halting of progressive neurodegenerative phenotype in SCA1

mouse model, but Cck was not assigned to the Magenta progressive disease module in those RNAseq analyses. Interestingly, cholecystokinin (Cck) was assigned to the Turquoise module in our studies (**Figure 24B**). As expected, Cck was downregulated in *ATXN1[82Q]* cerebella. Remarkably, Cck expression in *ATXN1[82Q];CαM120A* mice was partially but significantly elevated from the levels found in *ATXN1[82Q]* (**Figure 24B**). This finding further supports the notion that genes identified in the Turquoise module contain genes or pathways that may be involved in driving or blocking progressive pathology that were not identified previously in the Magenta module. Finally, gene changes associated with progressive disease are distinct from those driving ataxia (Pink vs. Magenta, Pink vs. Turquoise), and provides a new set of previously unexplored intracellular mechanisms that may be linked to early motor deficits, and not disease progression, in SCA1.

Figure 24

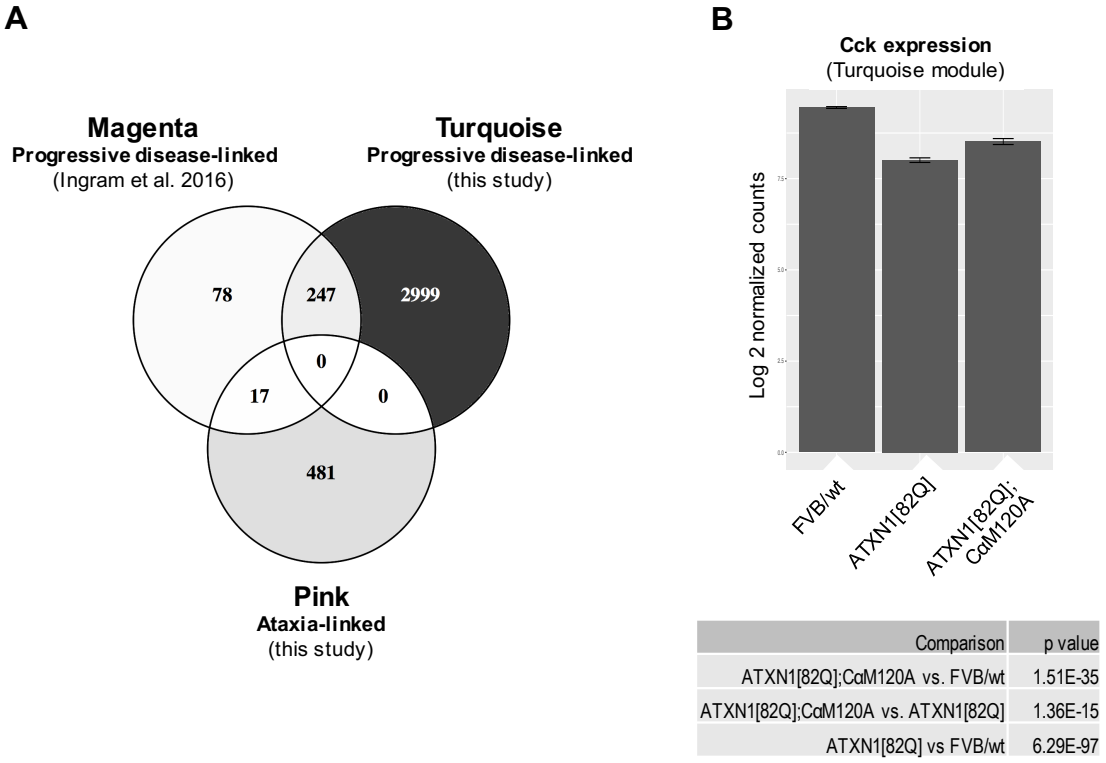

Comparison	p value
ATXN1[82Q];CαM120A vs. FVB/wt	1.51E-35
ATXN1[82Q];CαM120A vs. ATXN1[82Q]	1.36E-15
ATXN1[82Q] vs FVB/wt	6.29E-97

Figure 24. Turquoise and Pink modules represent unique gene expression changes associated with disease progression or ataxia in SCA1 mouse model. (**A**) Venn diagram show significant ($p < 0.05$) genes for each pairwise comparison and indicates overlap

between progressive disease-linked modules in Ingram et al. 2016 vs. this study (Turquoise). There are 247 genes that significantly overlap (p = 1.347278e-97), and which include the six genes described in figure 16. Most of the Magenta genes (72%) overlap with the Turquoise module, but this represents only 8% of the genes found in the Turquoise module. Neither of the progressive disease modules (Magenta, Turquoise) significantly overlap with the ataxia-linked Pink module. (**B**) In this study, Cck is assigned to the Turquoise module (but is not in the Magenta module). Downregulation of Cck mRNA is partially recovered in cerebella of *ATXN1[82Q];CαM120A* mice. Table shows pairwise comparisons and corresponding p values.

Discussion

RNAseq studies presented in this chapter provide an unbiased approach to identifying gene pathways linked to what we believe are different mechanisms of disease, involving on one hand motor dysfunction and on the other hand progressive neurodegeneration.

PCA showed all three genotypes to distribute into separate clusters, therefore the variation and overall pattern of gene expression of each mouse strain is distinct. I expected to find grouping together by shared characteristics, but this was not so straightforward. *ATXN1[82Q*] and *FVB/wt* are the most unrelated regarding behavioral outcome and histological measures. However, *ATXN1[82Q]/CαM120A* and *ATXN1[82Q]* have in common degenerative progressive traits of disease. At the same time *ATXN1[82Q]/CαM120A* overlaps with *FVB/wt* in the ability to perform well in the rotarod and beam walking tasks. The PCA analysis suggests the overall gene expression patterns between these strains are unique.

Differential expression analysis led to the finding that there is a high number of gene expression changes between *ATXN1[82Q]/CαM120A* and *FVB/wt* mice, both of which displayed the same rotarod and beam walking behavior. Moreover, the transcriptional changes between *ATXN1[82Q]/CαM120A* and *FVB/wt* are much greater than *FVB/wt* and *ATXN1[82Q]* (without CαM120A expression), suggesting there are potentially new pathways that are activated or suppressed to override ATXN1[82Q]-induced motor deficits that are rescued in *ATXN1[82Q]/CαM120A* mice.

WGCNA analysis evaluates small groups of co-expressed genes. Grouping the data to test specific hypothesis of correlations between groups we found a total of 9 hubs that were correlated with the gene expression patterns (3 related to the "ataxia" phenotype and 6 related to the "disease progression" phenotype), but only one hub was significant for each comparison. Perhaps the most interesting finding is that while there was significant overlap of genes in the Turquoise "degenerative disease" module with the previously identified Magenta module associated with progressive neurodegeneration, there was no significant correlation between the Magenta module and any other of the newly identified modules. Moreover, of the 3,246 genes in the Turquoise module, the grand majority (2,999) do not overlap with the Magenta module. The major implication of this finding is that we have potentially uncovered genes that will be revealing of mechanisms of disease progression that have not previously been recognized. Finally, the lack of overlap of gene changes in the ataxia module vs. the published Magenta module and new progressive disease module suggests pathways causing ataxia are independent of those driving progressive disease.

Chapter 5

CONCLUSIONS AND FUTURE DIRECTIONS

Major Findings

The body of work presented in this thesis provides strong evidence for the involvement of cAMP protein kinase (PKA) in the regulation of ATXN1-S776 phosphorylation in Purkinje cells *in vivo*. I used a PKA mutant model (*CαM120A)* that shows a ~30% decrease in PKA catalytic subunit alpha and decreased phosphorylating activity as a tool to study the effects of enzymatic hypofunction on ATXN1 protein. When crossed to SCA1 mice, I found that this reduction in PKA blocks S776 phosphorylation selectively in Purkinje neurons, resulting in a decline of total ATXN1. Importantly, I found that this effect is independent of the length of the polyglutamine tract in ATXN1. Thus, both wild type and mutant ATXN1-S776 are PKA substrates in Purkinje neurons *in vivo*. I also addressed the functional implications of this biochemical conversion. Behavioral studies at 6-8 weeks of age showed that *ATXN1[82Q];CαM120A* mice are neurologically intact. Nonetheless, their cerebellar cortex display signs of progressive atrophy, comparable to *ATXN1[82Q]* mice. Therefore, cerebellar function, but not cerebellar structure, is salvaged early in disease when ATXN1-S776 phosphorylation is blocked.

Another insight gained from my experiments surrounds Purkinje cell (PC) sensitivity to disease. Microdissection studies presented here revealed that ATXN1 is highly phosphorylated in PCs, when compared to the fraction of pS776-ATXN1 found in granule neurons which are thought to be secondarily affected in disease (Hashida et al., 1997; Gatchel et al., 2007). This suggests there are more active kinase pathways that favor phosphorylation of S776 in PCs. Perhaps these play a role in PC sensitivity to mutant ATXN1 insult.

Regarding cerebellar kinase pathways, I found that PKA catalytic subunit alpha is localized throughout the cerebellar cortex, likely throughout the Purkinje neuron body and its dendritic tree. The novel finding that ATXN1[82Q] localizes to Purkinje dendrites hints at a potential upstream mechanism of signals driving phosphorylation of ATXN1 by PKA. An interesting result shown here is that Msk1 is more abundantly expressed in cerebellar granule cells. *Sca1*$^{154Q/2Q}$*;Msk1*$^{+/-}$*;Msk2*$^{+/-}$ mice show some improvement in the rotarod task with modest reduction in cerebellar Atxn1 levels (Park et al., 2013). As more extensively discussed in Chapter 2, I would argue the effects found by Park and colleagues might reflect on Atxn1[154Q] toxicity in granule cells and Msk1/2 signaling in that cell type. At the circuit level, granule cell axons project to and contact PCs as parallel fibers forming PF-PC synapses. While PF-PC deficits were not seen until advanced disease, and much later than climbing fiber-PC synaptic deficits (Barnes et al., 2011), the reported studies used PC transgenic *ATXN1[82Q]* mice. It remains to be determined whether Atxn1[154Q] expressed in granule neurons exerts toxicity and perhaps also PF-PC dysfunction triggering motor dysfunction in the *Sca1*$^{154Q/2Q}$ model.

An inadvertent finding of this work concerns mGluR1 function in the cerebellum in SCA1. The mGluR1 null model first linked this receptor to LTD and cerebellar ataxia (Aiba et al., 1994). mGluR1 is required for cerebellar motor learning (Ichise et al., 2000) and mGluR1 deficits are implicated in other SCAs as well as autoimmune ataxias (Aiba, et al., 1994; Ichise et al., 2000; Nakao, et al., 2007; Skinner et al., 2001; Armbrust et al., 2014; Konno et al., 2014; Sillevis Smitt et al., 2000). The lack of mGluR1 recovery in a mouse that does not show ataxia (shown here) challenges our understanding of this receptor and suggests that at least in SCA1 mGluR1 expression alone is not a good predictor of cerebellar function at the behavioral level. Recent studies have paradoxically found abnormal, prolonged mGluR1 signaling in symptomatic *ATXN1[82Q]* mice, and blocking mGluR1 with negative allosteric modulators completely reverses ataxia (Power et al., 2016). In contrast, treating symptomatic 30-week old *Sca1*$^{1542/2Q}$ mice with positive allosteric modulators of mGluR1 is beneficial later in disease (Notartomaso et al., 2013). It remains to be examined whether there are other proteins that functionally compensate for mGluR1 deficiency or dysfunction in *ATXN1[82Q]/CαM120A* mice.

The findings presented in this thesis work illustrate important implications in the disease processes driven by ATXN1 in Purkinje neurons early in disease. The selective rescue of motor coordination and balance without halting degenerative histological features suggests there is a disconnect between pathogenic pathways triggering different phases of disease (**Figure 25**). Considering these results and previous work, I suggest that the pathways driving synaptic dysfunction and ataxia are a consequence of abnormal gain of function when ATXN1 is in the phosphorylated state. These pathways are likely more reversible and account for the selective improvement in motor performance seen here. As a separate mechanism, when ATXN1 load overwhelms PCs at a certain threshold, this activates different degenerative pathways in the nucleus that compromise cell integrity and stimulate progressive degeneration.

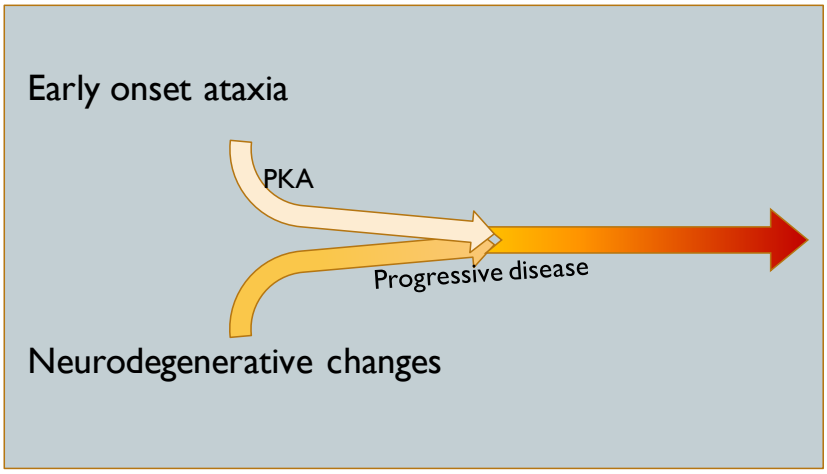

Figure 25. Early vs. late disease processes in SCA1. Distinct intracellular pathways drive early onset ataxia vs. progressive neurodegenerative changes. In this model, ataxia is driven by aberrant protein-protein interactions of pS776-ATXN1 phosphorylated by PKA. Progressive changes are likely caused by pathways triggered by protein overload of polyglutamine-expanded ATXN1.

We performed RNA sequencing analysis as an unbiased approach to uncover pathways that may be involved in these separate disease processes. We used Weighted Gene Co-expression Network Analyses as a strategy to identify (1) gene changes linked to age-dependent worsening of histopathology and (2) transcriptional changes associated with ataxia. The first criteria identified the Turquoise "progressive disease" Module, which

contains 247 genes previously correlated with disease progression (Magenta genes in Ingram et al., 2016). However, most (92%) genes in the Turquoise module do not overlap with Magenta cluster. This potentially paves the way for discovering previously unidentified pathways that contribute to or trigger neurodegeneration in SCA1. The second criteria identified gene changes potentially associated with synaptic/motor function. In the Pink ("ataxia") module, the top canonical pathway involves Gq signaling, the top hit being cholinergic receptor muscarinic 1 (i.e., muscarinic acetylcholine receptor 1), which has been linked to Purkinje cell synaptic plasticity (Rinaldo et al., 2013). These WGCNA modules identified in this work may expose unpaved pathways and mechanisms of disease that trigger to motor dysfunction versus those that drive progressive pathology in SCA1.

Preclinical Therapeutic Investigations

To date, two general strategies are being employed to mitigate SCA1 pathogenesis preclinically in animal models. One strategy is to restore expression of a gene product downregulated in disease. The second is suppressing ATXN1 expression to block pathogenic effects.

Genetic and pharmacologic treatments of *Sca1*$^{154Q/2Q}$ mice with VEGF, vascular endothelial growth factor was first used to restore disease-related deficits (Cvetanovic et al. 2011). *Sca1*$^{154Q/2Q}$ cerebella have a dramatic downregulation of *Vegfa* mRNA, likely due to increased occupancy by Atxn1 of the *Vegfa* promoter and consequent gene repression, in a histone acetylation dependent manner. VEGF is an angiogenic and neurotrophic factor. In the cerebellum, VEGF is expressed by neurons, glia, and endothelial cells (Acker, Beck, and Plate 2001; Ruiz de Almodovar et al. 2010). *Sca1*$^{154Q/2Q}$ mice crossed to transgenic mice that overexpress VEGF from an embryonic stage showed improved rotarod motor performance in adulthood, with apparent full motor recovery by 6 months (Cvetanovic et al. 2011). The motor improvement was coupled to a subtle but statistically significant improvement in molecular layer thickness of the cerebellar cortex. To test the therapeutic potential of exogenous VEGF delivery, intracerebroventricular administration of recombinant mouse VEGF was continuously delivered by osmotic pump into the lateral

ventricles for two weeks starting at 11 weeks of age. This short period of treatment produced a complete recovery in rotarod motor performance in treated animals. It is unclear whether VEGF benefits stem from the effects on microvasculature improving nutrient and oxygen delivery to the brain parenchyma and/or activation of neurotrophic pathways. Regardless, replenishing levels of a gene product downregulated in disease can attenuate mutant Atxn1 toxicity.

A more recent study sought to reinstate expression of another cellular component deficient in *Sca1*$^{154Q/2Q}$ cerebella (Ruegsegger et al. 2016). Mass-spectrometry analysis of *Sca1*$^{154Q/2Q}$ cerebella reveals a reduction in Homer-3 levels in synapses, likely caused by defective mTOR signaling. Blocking mTORC1 signaling depletes Homer-3 levels and worsens *Sca1*$^{154Q/2Q}$ pathology. While enhanced neurotransmission and activation of mTORC1 signaling enriched expression of the Purkinje cell scaffold protein Homer-3 in wild type cerebella, it failed to do so in *Sca1*$^{154Q/2Q}$ mice. Thus, to increase Homer-3 synaptic levels, AAV-Homer-3 was injected into the ventricles of neonate brains. Behavioral examination at P40 - P200 shows incomplete but statistically significant improvement in rotarod testing. Other parameters improved with AAV-Homer-3 gene treatment included Purkinje cell spine density, Purkinje cell numbers, and vesicle pool occupancy (Ruegsegger et al. 2016). Thus, replacement of Homer-3 levels during development restores synaptic deficits and partially improves motor functioning in *Sca1*$^{154Q/2Q}$ mice.

Perhaps the most promising preclinical therapeutic approaches under investigation are predicated on the finding that reducing the amount of mutant protein expressed in the cerebellum can alleviate its toxicity (**Appendix 1**). Conditional *SCA1* mice were generated to manipulate *cATXN1[82Q]* expression in Purkinje cells by Doxycycline administration to turn off *cATXN1[82Q]* expression and reduce mutant protein levels (Zu et al. 2004). Strikingly, turning off gene expression after disease onset results in reversal of the motor deficits and histopathology. Moreover, the earlier the gene is turned off, the more pronounced disease reversal is. A follow up study investigated the effect suppressing *cATXN1[82Q]* transgene expression during postnatal development has on SCA1 pathology

in adulthood (Serra et al., 2006). In one group of mice *cATXN1[82Q]* gene expression was kept off for 14 weeks and turned on for 12 weeks (14 wk gene-off/12 wk gene-on). The other group had *cATXN1[82Q]* gene on for 12 weeks (12 wk gene-on), so in both groups the "dose" of ATXN1[82Q] was the same (12 weeks). Fourteen wk gene-off/12 wk gene-on mice performed better in the rotarod than 12 wk gene-on mice. Molecular layer thickness in 14 wk gene-off/12 wk gene-on cerebella was comparable to wild type mice, even when the transgene was turned on for 24 weeks, indicating preservation of Purkinje cell health. This was also found in 2 wk gene-off/12wk gene-on and 3 wk gene-off/12wk gene-on mice, indicating the protective effect was due to delaying toxic *cATXN1[82Q]* expression during the critical period of cerebellar cortex development taking place during the first three weeks of life.

The above findings reveal two important points. First, progression of this inherited neurodegenerative disease can be reversed. Early intervention is key to preserve and recover the remaining tissue. If the disease is targeted early enough the cells are still present and able to recover. In fact, later studies have shown that there are differential circuit-specific changes that progress in the course of disease and precede gross pathology (Barnes et al. 2011). Secondly, there is a significant therapeutic opportunity in targeting the mutant protein directly.

That replacement of any one gene (ie, *Vegf*, *Homer3*) does not fully rescue disease together with consistent observations that ATXN1 disrupts a multitude of genetic pathways suggests the best strategy to treat SCA1 is by targeting ATXN1 directly. Several targets for development of therapies for SCA1 are being pursued (**Figure 26**). Antisense Oligonucleotides (ASOs) are synthetic nucleotide oligomers that hybridize with specific mRNAs, leading to nuclear RNAse H mediated cleavage and targeted gene knockdown (**Figure 26A**). In $Sca1^{154Q/2Q}$ mice, treatment with ASOs knocks down *mAtxn1* mRNA (30% knockdown in whole cerebellum, or 50% in microdissected Purkinje cell layer), improves rotarod performance, and extends lifespan (unpublished data).

The RNAi pathway is a robust gene silencing mechanism through which mRNAs are cleaved and destroyed in the cytoplasm. In recent years, studies have taken advantage of this powerful tool to reduce mutant Atxn1 expression and test the therapeutic potential of this approach (Xia et al. 2004) (**Figure 26B**). Delivery of AAV-miRNA targeting hATXN1[82Q] in SCA1 transgenic mice (AAV-miSCA1) achieves robust (70%) *hATXN1* mRNA knockdown without measurable toxicity (Keiser et al. 2013). In these studies, AAV-miSCA1 injections were targeted to deep cerebellar nuclei (DCN) for uptake and expression by Purkinje cells. With AAV injection at 5 weeks, a battery of motor performance tests shows complete recovery out to 37 weeks of age. Histological measures of cerebellar integrity such as molecular layer thickness, total Purkinje cell numbers, and ectopic Purkinje cell numbers, were only modestly improved, consistent with the accumulating notion that full rescue of histopathological changes may not be required for complete recovery of motor performance. Another possibility is that 70% knockdown of the highly overexpressed *hATXN1[82Q]* in the transgenic model is sufficient to alleviate deficits underlying ataxia, but not to fully halt development of pathology triggered by the mutant protein.

A new study suggests there is a specific window at which viral load tolerability and *hATXN1* knockdown achieve disease control or reversal in the transgenic model (Keiser et al., 2016). These studies are summarized in the table in **Appendix 1**. Early (6-week-old) AAV-miSCA1 injection at 8E8 (8×10^8) dose achieves 23% mRNA knockdown and improves motor function at 30 weeks, but does not rescue cerebellar histopathology. This finding echoes the Keiser et al., 2013 study discussed above, where *hATXN1[82Q]* knockdown at presymptomatic age rescues the ataxic phenotype, but does not prevent histopathological changes from progressing. Additionally, the same viral dosage (8E8) and degree of mRNA knockdown (28%) fails to rescue behavior, histology, or gene expression abnormalities when delivered at 12 weeks, after disease onset. Very high dose (8E10) of AAV-miSCA1 achieves a remarkable 96% *hATXN1* mRNA knockdown, but these mice display the same level of disease as untreated controls. Presumably, the viral load is too high at this dose and triggers reactive changes that override potential benefits. The critical doses of 2.6E9 and 8E9 lead to 53%-71% *hATXN1* knockdown, which prevent or reverse

histopathology and abnormal gene expression changes, while also attenuating motor deficits. These studies suggest at least 50% of ATXN1 knockdown is required for therapeutic value in *ATXN1[82Q]* transgenic model.

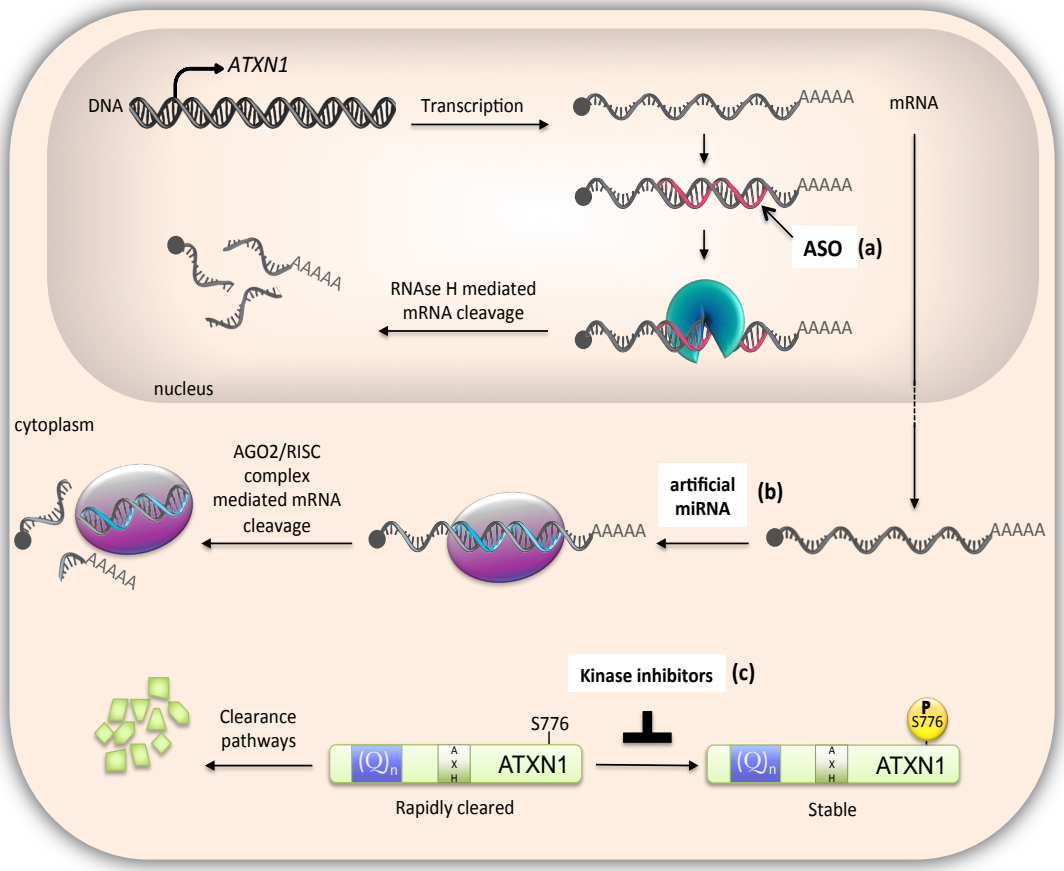

Figure 26. SCA1 Therapeutic Targets. The fundamental strategy underlying these targets is in harnessing pathways that lower ATXN1 levels (wt and mutant). ATXN1 mRNA expression can be targeted two ways. In the nucleus, ASOs complementary to the mRNA promote its cleavage via the RNAse-H pathway (**a**). The RNAi machinery operates in the cytoplasm, where the miRNA is processed, complexes with the target mRNA in the RISC complex, and this leads to mRNA cleavage (**b**). At the protein level, action of small molecule inhibitors that block ATXN1-S776 phosphorylation would promote rapid clearance of unphosphorylated ATXN1 (**c**).

More recently an upgraded AAV-miSCA1 was tested in the *Sca1*$^{154Q/2Q}$ knockin model to examine its therapeutic effect beyond Purkinje cell related pathology in a model

where mutant Atxn1 is not overexpressed (Keiser et al. 2014). As predicted, *Atxn1* knockdown fully rescued motor impairments and fully rescued the histopathology. In this study, one strategic injection site (the DCN) was sufficient to deliver the AAV-miSCA1 to reach the brain regions most critically affected in SCA1 (the cerebellum and brainstem) (**Appendix 1**). It will be important to determine whether *Atxn1* knockdown prolongs survival, a brainstem-related phenotype.

That S776 phosphorylation is linked to ATXN1 pathogenicity and stability makes it an attractive small molecule therapeutic target (**Figure 26C**). This has driven pursuit of kinase(s) involved in this phosphate modification, with promising candidates being MSK1 and, in this work, PKA. Blocking kinase activity should impact ATXN1 stability and toxic protein-protein interactions known to be mediated by pS776-ATXN1. However, the work presented here shows that dampening PKA activity is not sufficient to halt disease progression.

The conclusions stemming from this thesis have important therapeutic implications. For instance, kinases are readily druggable targets. Identifying compounds that have high potency and selectivity against PKA could be used to treat SCA1 early on. This would be expected to target pS776-ATXN1 and boost protein clearance. One hope is this might first retard development of ataxic features and keep ATXN1 protein load at bay. As I found here, reducing PKA is not sufficient to maintain pS776-ATXN1 and total ATXN1 lowered as disease advances. Possibly other mechanisms jump in that override the decrease in PKA activity, the consequence of which is a return of ATXN1 protein load that is detrimental. At that stage, therapies would need to target ATXN1 directly. In sum, work presented here proposes a putative treatment plan in which patients early in disease are first treated with kinase inhibitors to block ATXN1 phosphorylation, and with advancing disease, supplement with or switch to RNAi or ASO therapies to knock down *ATXN1* and reduce protein burden.

Future Studies

Intriguing future studies arise because of this work. For instance, what more can we learn from the RNAseq studies? How is PKA activity regulated in Purkinje neurons? Does neuronal activity play a role in these pathways? Do different kinases or pathways regulate S776 phosphorylation in different cell types? Are there beneficial, subtler synaptic changes in *ATXN1[82Q]/CαM120A* that are not detectable when measuring molecular layer length? These are important questions that remain to be answered. The following experiments propose potential approaches to begin to address these questions.

Uncovering new gene pathways associated with ataxia vs. progressive disease

Ongoing studies analyzing RNAseq involve three main approaches. First, we will evaluate the dataset for alterations in gene splicing to evaluate whether these provide additional insights about ataxic vs progressive disease changes seen in the mouse models tested here. Second, we will run direct comparisons of transcriptional changes between my dataset and the RNAseq data from the *ATXN1[30Q]-D776*, which develop ataxia but not progressive disease (Duvick et al, 2010). I expect that a more useful comparison will be between *ATXN1[82Q]/CαM120A* (no ataxia) and conditional *ATXN1[30Q]-D776* (with both 12-week gene on and 6-weesk gene on/6-weeks gene off conditions). In the conditional *ATXN1[30Q]-D776* model, turning off gene expression at 6 weeks of age for another 6-weeks reverses ataxia, but does not rescue the length of the molecular layer, showing reversal of ataxia without difference in histopathology (M. Ingram, unpublished). If my hypothesis is correct that the behavioral improvement in *ATXN1[82Q]/CαM120A* is a result of dampening deleterious effects caused by phosphorylated ATXN1, then I would expect to find gene changes that overlap with *ATXN1[30Q]-D776*, 6-weeks gene on/6-weeks gene off (when ataxia is reversed). Perhaps the more exciting feat will be to identify new pathways that have not been previously described in SCA1 that impact cerebellar signaling function. Finally, additional analysis will be performed to uncover novel pathways associated with disease progression. One caveat in these experiments is having

to discern the contribution of the *CαM120A* background to transcriptional alterations identified in the RNAseq studies.

Neuronal aspects of Purkinje cell susceptibility to kinase pathways

Moving forward, it will be important to evaluate the PKA pathway in Purkinje cells as neurons that are integrated into a dynamic network. Here I showed that there is a high fraction of phosphorylated ATXN1 in Purkinje cells. How do PKA or other kinase signaling pathways contribute to disease? Or, how are these pathways affected due to the disease process? As a first step to answering this question, I propose a series of experiments to modulate neuronal activity in cerebellar slices and ask whether ATXN1 phosphorylation is affected. My hypothesis is that changes in neuronal activity (either more active or suppressed) will lead to changes in ATXN1-S776 phosphorylation.

Shim and colleagues found that chronic inhibition of PCs leads to decrease in PC excitability (Shim et al., 2016). They found that TTX-mediated inhibition in cerebellar slices leads to constitutive activation of mGluR1, which decreases intrinsic excitability (decrease in firing rates, and other electrophysiological parameters) by increasing components of hyperpolarization-activated current (I_h) in PCs. PKA is thought to regulate I_h (Narayanan et al. 2010). Using pharmacologic tools, Shim et al. found that activity deprivation with TTX activated PKA. Thus, changes that affect PC activity can lead to PKA activation and this can affect PC function. In SCA1, mutant ATXN1[82Q] affects PC activity. It is thought that increase in K+ channel expression at the cell surface in the *ATXN1[82Q]* mouse model slows firing rates and firing frequency in PCs before onset of rotarod deficits (Hourez et al., 2011). Treatment with K+ channel blockers *in vivo* improve motor behavior. While these two studies don't seem clearly connected, I suggest they are helpful in guiding experiments to address PC activity, the PKA pathway, and ATXN1 phosphorylation I propose a model whereby mutant ATXN1[82Q] exerts excitability changes in Purkinjce cells, which compromise PC activity. In consequence, this would activate a signaling cascade that involves the PKA pathway. Higher PKA activity in PCs would enhance ATXN1-S776 phosphorylation and precipitates motor dysfunction. I would

test this idea by culturing organotypic cerebellar slices and chronically treating them with TTX (to block activity) or Picrotoxin (to enhance network activity), in the presence or absence of GSK69093 (to block PKA). Slices would be processed for western blotting to identify changes in ATXN1 S776 phosphorylation and levels of total protein. This could be tested in *Pcp2-ATXN1[82Q], Pcp2-ATXN1[30Q]*, as well as $Sca1^{66Q/2Q}$ models to address changing occurring in Purkinje cells versus Atxn1 in other cell types. Modifications could be done by using pharmacological tools to activate or block specific receptors and identify specific intracellular pathways.

Other pathways to be considered involve glutamate signaling (Serra et al. 2004), potentially cholinergic signaling (based on my RNAseq data), and dopamine signaling (based on work by Dr. Vig's research group). For example, Vig's team has suggested one pathway involved in SCA1-triggered activation of PKA pathway is a consequence of disease related exclusion of DRD2 receptors from the cell surface (Hearst et al. 2010). Dopamine D2 receptors (DRD2) are Gi/o-protein coupled receptors; their activation suppresses cAMP levels, which in turn reduces activation of PKA. This group proposes that functional loss of DRD2 leaves PKA activity unchecked. However, these studies fail to convincingly demonstrate an *in vivo* role of DRD2, restricting PKA-ATXN1 phosphorylation experiments to HEK cell models. While intriguing, the DRD2 hypothesis needs to be better validated. This research group also developed a PKA inhibitor peptide (Synb1-ELP-PKI), which crosses the blood brain barrier and gets into the cerebellum (Hearst et al., 2014). While they show its efficacy at blocking PKA activity in cell cultures, they do not assay whether *in vivo* delivery of Synb1-ELP-PKI blocks PKA activity in slices or *in vivo*.

Are there beneficial, subtler synaptic changes in ATXN1[82Q]/CαM120A that are not detectable when measuring molecular layer length?

One experiment that remains to be completed is to evaluate whether there are other histological features of disease that might show improvement in *ATXN1[82Q]/CαM120A* cerebella. I propose to examine whether the climbing fiber translocation deficits are restored in *ATXN1[82Q]/CαM120A* mice. Additionally, studies can be done to count

density of synapses in Purkinje dendrites to evaluate whether structural synaptic plasticity underlies recovery in motor phenotype seen in *ATXN1[82Q]/CαM120A* mice.

ATXN1[82Q] and *ATXN1[30Q]-D776* models share ataxic phenotype, as well as abnormalities in climbing fiber (CF)-Purkinje cell (PC) innervation (Ebner et al., 2013). Purkinje cells receive many inputs from the granule cell parallel fibers, but during development, multiple climbing fiber inputs "compete" until one CF remains and ascends the dendritic tree forming a one-to-one relationship with PCs (Hashimoto and Kano, 2003, Hashimoto and Kano, 2013; Hashimoto et al., 2009, Kakizawa et al., 2003). This process is affected in SCA1 and is linked to the ataxic phenotype. In conditional *ATXN1[30Q]-D776*, turning off gene expression after 16 weeks of age reestablishes CF-PC translocation in a gene-off dependent manner (where the longer the gene remains off, the more the CF-PC extension is normalized) (M. Ingram, unpublished). This recovery is associated with improved performance of the rotarod. Paradoxically, CF extension is not restored when the gene is turned off earlier in the disease process. Still, it prompts the question of whether CF extension is resumed in *ATXN1[82Q]/CαM120A* cerebella, that might provide an anatomical synaptic correlate of motor function.

Do different kinases or pathways regulate S776 phosphorylation in different cell types?

Here I showed worked to support the role of PKA-mediated phosphorylation of ATXN1 in Purkinje cells. However, this effect is transient, suggesting compensatory mechanisms that: (1) improve efficacy of remaining PKA in PCs despite lower levels (perhaps by AKAPs), (2) upregulate other kinases that can phosphorylate ATXN1, or (3) an age-dependent switch occurs in which other kinases phosphorylate ATXN1. This suggests that while PKA plays a predominant role in ATXN1 phosphorylation, at least early on, it is not the only kinase that can perform that function.

Using GSK690693 inhibitor on cerebellar slices I found that it is able to potently block phosphorylation of PKA targets, as well as endogenous Atxn1. However, Purkinje cells only comprise a small fraction of the cerebellum, and based on my laser capture

studies there is more Atxn1 per volume of tissue in the granule cell layer than in the PCL. Therefore, the results I obtained from GSK690693 on cerebellar slices must also indicate destabilization of Atxn1 phosphorylation in granule neurons. GSK690693 also blocks Akt, and while Akt was ruled out as a kinase involved in phosphorylating ATXN1 in Purkinje cells, its role in other cerebellar cell types is not known. It is possible that blocking Akt with GSK690693 lowered Atxn1 in the slices. It is also conceivable that other kinases are involved in this pathway. Msk1 might be one of them, especially in granule neurons. Future experiments could involve better understanding different pathways/kinases involved in regulating Ataxin1 phosphorylation. In light of Msk1 studies by Zhogbi's group, perhaps it would be important to study the role of granule cell function and health in the disease process. Finally, toxicity exerted by phosphorylated ATXN1 has been only investigated in Purkinje neurons in the *Pcp2* models. An *Sca1*$^{82Q\text{-}D776/2Q}$ knockin model is underway to examine whether the nonpathogenic Atxn1[82Q] (knockin) protein is transformed into a pathogenic one with an S776D mutation. This will pave way to addressing the degree role of pS776-Atxn1 toxicity in cell types beyond Purkinje cells.

Chapter 6

MATERIALS AND METHODS

Mice

The Institutional Animal Care and Use Committee approved all animal use protocols. All mice were housed and managed by Research Animal Resources under SPF conditions in an AAALAC-approved facility. CαM120A mice were obtained from Jackson Laboratories. Strain name: CalphaM120A-Lox1,2, B6Crl.129X1-Prkaca$^{tm4.1?Gsm}$/Mmcd, Stock number 034669-UCD. The following primers were used for genotyping CαLoxM120A mice: Fwd: 5'-TCACATCCCACACGATTTT-3', Rev: 5'-GCAGGCATTGAAACCTCAGTG-3'). Sox2-Cre mice were also obtained from Jackson Laboratories (B6.Cg-Tg(Sox2-cre)1Amc/J). CαM120A mice were crossed to Sox2-Cre females to promote germline excision of the exons 5-10 minigene (see Figure 6A), then bred to homozygosity. Then, mice were crossed to *Pcp2-ATXN1[82Q]*/+; *Sca1*+/+ or *Pcp2-ATXN1[30Q]*/+;*Sca1*-/- (ATXN1[82Q] mice are a newly rederived lined from the original BO5 mouse line described in Burright et al., 1995; Sca1-/- described in Matilla et al., 1998) mice for several generations until obtaining Pcp2-ATXN1[82Q]/+;CαM120A/CαM120A mice or ATXN1[30Q];Sca1-/-;CαM120A/CαM120A, respectively. The *Pcp2-ATXN1[82Q]*/+; *Sca1*+/+ mice used here are a newly re-derived line from the line originally described in Burright et al., 1995.

RNA isolation

Total RNA was isolated from half cerebellum per mouse using TRIzol reagent (Cat No. 15596-018 Life Technologies, Carlsbad, California). Cerebella were homogenized in 300ul TRIzol reagent using RNase-free disposable pellet pestles in a motorized chuck for 30 seconds each. Another 700ul TRIzol reagent was added to bring up to 1ml total TRIzol per half cerebellum and briefly vortexed. RNA isolation was done following manufacturer's protocol. The RNA pellet was resuspended in 100ul of RNAse-free water. RNA

concentration was quantified using nanodrop and stored at -80ºC or used to do cDNA synthesis or RNA-sequencing.

RNA used for RNA-sequencing was further purified using following the "RNA cleanup" protocol in RNeasy Mini Kit (cat no 74104, Qiagen, Venlo, Limburg). Organic RNa extraction methods (like TRIzol) could result in organic carryover that inhibits enzyme reactions used in Illumina library preparation and increase risk of failure of library generation. Therefore, 60ul of the 100ul of total RNA isolated above were brought to 100ul volume using RNAse-free water. The following steps were done following manufacturer's protocol. RNA elution was done by adding 45ul RNase free water, incubated for 1 minute, then centrifuged at >10,000 rpm for 1 minute.

cDNA synthesis

cDNA synthesis was done using iScript Advanced cDNA Synthesis Kit (Cat No 172-5037). 500ng total RNA input was mixed with 2ul 5x iScript advanced reaction mix, 0.5ul iScript advanced reverse transcriptase, and nuclease-free water to total volume of 10ul/reaction.

RT-qPCR

RT-qPCR experiments were done using LightCycler 480 Probes Master Mix and hydrolysis probe (Roche, Penzberg, Germany) following manufacturer's protocol. Universal ProbeLibrary for mouse Assay Design Center (Roche) was used for primer design. ProbeLibrary Mouse GAPD Gene Assay (Roche) as control. Primer sequences: Homer3 (Probe 13): F: 5'-tgaagaagatgctgtcagaagg-3', R: 5'-ctgtcctgaagcgcgaag-3'; Inpp5a (Probe 67): F: 5'-attcggacactttggagagc-3', R: 5'-ccttttcttgaccatttgcac-3; Rgs8 (Probe 88): F: 5'-ctgtcacacaaatcagactcctg-3', R: 5'-tgcttcttccgtggagagtc-3'; Itpr (Probe 85): F: 5'-gaaggcatctttggaggaagt-3', R: 5'-accctgaggaaggttctgc-3'; Mxra7 (Probe 25): F: 5'-tgaggggaagccagtacaag-3', R: 5'-ccagctgttctttctgaactctg-3'; Calb1 (Probe 42): F: 5'-aaggcttttgagttatatgatcagg -3'; R: 5'-ttcttctcacacagatctttcagc -3'; Prakaca (Probe 66): F: 5'-tctcggagtcctcatctacga-3', R: 5'- ctgaagtgggatgggaacc-3'.

Illumina RNA-sequencing

Whole cerebellar RNA from five biological replicates for each genotype was isolated with TRIzol reagent, followed by column purification using RNeasy Kit as described above in detail. Purified RNA was sent to the University of Minnesota Genomics Center for quality control. Samples were quantified using fluorimetry (RiboGreen assay, Life Technologies) and RNA integrity assessed by capillary electrophoresis (Agilent Tape Station/BioAnalyzer 2100, Agilent Technologies, Inc.). All samples passed QC requirements with RNA integrity number (RIN) for all samples between 8.9-9.4, well above the required RIN of >8, and total mass between 2.5-3.5ug. RNA library was created using Classic RNA-Seq method. This includes removal or rRNA via oligo-dT purification of mRNA, and second-strand cDNA synthesis. Resulting double stranded cDNA is fragmented, blunt ended, and ligated to indexed (barcoded) adaptors. Average inserts of approximately 193 bp, and size distribution validated using capillary electrophoresis and quantified using fluorimetry (PicoGreen, Life Technologies) and via Q-PCR. Indexed libraries were then normalized, pooled, clustered on a flow cell, and loaded to the instrument for sequencing. 8 - 9wk old ATXN1[82Q], ATXN1[82Q]/CaM120A and FVB/wt samples were sequenced on an Illumina HiSeq2500 High Output instrument using a 125bp paired-end read strategy. Data was stored and maintained on University of Minnesota Supercomputing Institute (MSI) Servers. Research Informatics Support Systems (RISS) bioinformatician at MSI was available to running requested analyses, questions, and support.

RNA-seq expression analyses

Hisat2 was used to align reads to the genome. Rsubread was then used to quantify the number of reads per gene in each sample (Table 3). DESeq2 was used for the differential expression analysis and PCA plots. Weighted Gene Coexpression Network Analysis was used for the WGCNA analysis. Ingenuity Pathway Analysis was used for the IPA.

Histology and immunostaining

Animals were anesthetized and transcardially exsanguinated with PBS and perfused using 10% formalin. Brains were post-fixed 1hr to overnight in 10% formalin and placed in PBS

before sectioning. Cerebella were sectioned into 50 um parasagittal sections using a vibratome. Epitopes were exposed using antigen retrieval by boiling sections four times for 10 s each in 0.01 M urea. Sections were blocked 1hr - overnight in 2% normal donkey serum and 0.3% Triton X-100 in PBS. For staining, primary antibodies were diluted blocking solution as indicated. Rabbit Anti-calbindin antibody was used to label Purkinje neurons (Sigma-Aldrich Cat# C2724, RRID: AB_258818) at a 1:500 dilution). Following incubation, sections were washed three times in PBS and exposed to secondary antibodies (Cy3 donkey anti-rabbit 711-165-152, Jackson Immunoresearch Labs) for 24 hr at 4ºC. Sections were washed three times in PBS and mounted onto charged slides (Colorfrost Plus, Fisher). Fluorescently labeled tissue was imaged using a confocal Olympus 1000 IX inverted microscope.

Primary fissure molecular layer width was measured on 20x z-stack images, of 10um 1um step sizes. The width was measured as the distance from the base of the PC soma to the pial surface. Six measurements were averaged per section and three sections were measured for each animal. The final average was considered to be the molecular layer thickness and was plotted on the graph.

Western blotting

Samples used for western blotting were first flash frozen in liquid nitrogen (both cerebellar slices and fresh cerebellum) and either processed on the same day or stored at -80ºC until experiment day. All samples in the same experiment were handled and processed at the same time. Standard Tris-Triton Lysis buffer (50 mM Tris, pH 7.5, 100 mM NaCl, 2.5 mM $MgCl_2$, 0.5% Triton X-100) is supplemented with Phosphatase Inhibitor II and III and Protease Inhibitor Cocktail (cOmplete Mini, EDTA-free (Roche) #11836170001). Ice-cold lysis buffer was added and samples homogenized with a micro pestle for exactly 30 seconds. Samples were freeze/thawed 3x in liquid nitrogen/37ºC water bath (each thaw for exactly 2 minutes). Samples were then centrifuged at 4ºC 15,000rpm for 10min. The supernatant was transferred to a new tube, kept on ice, and protein concentration was estimated using Bradford assay before loading on to the gel. We used the BioRad western blot system. The gels used were 4-20% SDS-PAGE Tris-glycine 26-well gels. Transfer

was done onto nitrocellulose membrane using Trans Blot Turbo transfer system. Blots were blocked in 5% milk in 1xPBS-0.2%Tween-20 for at least 45 minutes. Primary antibody was added overnight. Incubation in secondary antibody was done the next day followed by chemiluminescence image acquisition and densitometry analysis were done using ImageQuant LAS 4000.

Antibodies used for western blotting: Primary antibodies: Phospho-PKA substrate antibody rabbit monoclonal IgG 100G7E (Cat. No. 9624 Cell Signaling Technology, Danvers, MA) 1:1,000; MSK1 antibody polyclonal goat IgG (Cat. No. AF2518 R&D Systems, Minneapolis, MN) 1:2,000; Anti-cAMP Protein Kinase Catalytic subunit polyclonal rabbit IgG (Cat. No. ab26322, Abcam, Cambridge, MA) 1:1,000; Anti-cAMP Protein Kinase Catalytic subunit beta polyclonal rabbit IgG (Cat. No. ab94612, Abcam, Cambridge, MA) 1:1,000-1:2,000; aTubulin- mouse monoclonal, (SIGMA T5168); Rabbit anti-Homer3 AP6992c 1:1,000; Rabbit anti-mGluR1 Millipore 07-617 1:1,000; Rabbit anti-Praja2 ab125330 (1:1000); Goat anti-AKAP150 C-20 sc6445 1to500; Rabbit anti-Calbindin C2724 Sigma-Aldrich 1:1,000; Rabbit anti- PKA RIb ab38225 1to500; Goat anti-PKA RII ab33970 1to500; Rabbit anti-pS776-ATXN: PN1249 (1:5,000); Mouse anti-pS776-ATXN: MoAb13 (1:500), Rabbit anti-total ATXN: 12NQ (1:2,500). Secondary antibodies: ECL anti-Rabbit IgG HRP from donkey, NA934V; ECL anti-Mouse IgG HRP from sheep, NAV931V; ECL anti-Rabbit IgG HRP from goat.

***In vitro* phosphorylation assay**

Cerebellar homogenates are prepared fresh using Tris-Triton lysis buffer and following the same procedure described in western blot section, with the distinction that the final centrifugation is at 20,000g for 10 minutes. Bradford assay is used to estimate protein concentration. Each reaction consist of the following: 5ug protein in lysis buffer, 1ug purified GST-ATXN1[30Q], 100 mM $MgCl_2$, 1 mM ATP, TT buffer, ATP, and either DMSO or drug (3ul volume), for a total volume of 30ul per reaction. The samples are shaken in a 30ºC water bath for 1hr. The reaction is stopped using 300ul of 50mM EDTA/PBS-T. 30ul of each reaction are ran onto a 4-20% SDS-PAGE Tris-glycine 18-well gel (BioRad).

Drug treatment in slice culture

P9-P12 pups were sacrificed by decapitation and their cerebella were carefully placed in 2% low-melt agarose until hardened on ice. 350um parasagittal slices were in cut in ice cold GBSSK medium using a Leica vibratome. GBSSK consists of: GBSS, Kynurenic Acid, Glucose). Slices were pooled from different animal of the same genotype and 4-6 slices were placed on Millicell Cell culture inserts (0.4um 30mm, PICM03050). Unless otherwise indicated, media was replaced every 2-3 days. Culture media consists of: 50% MEM, 22% HBSS, 15% HI Horse Serum, 10% FBS, 1% ITS, 1% P/S, 1% D-Glucose, 2mM Glutamax1. Slices were culture for one day before adding drug. This protocol was modified from: J Falsig and A. Aguzzi (Nature Protocols Vol. 3 No. 4 2008).

1-NM-PP1 delivery in vivo

9-12 week old *ATXN1[82Q];CαM120A* mice were separated into four groups and treated via the following routes of administration for 10 days. *No Tx* (no treatment) indicates mice stay in their cage for the duration of the experiment. *Drinking water:* 25uM 1-NM-PP1 was added to autoclaved water with 5% sucrose and used to fill a red light-resistant water bottle (40ml) and placed in the mouse cage. Water and drug were replaced every two days; sucrose was added to stimulate drinking. Intraperitoneal pumps were filled with 0.4mM 1-NM-PP1 in 20% DMSO/80% PBS. For *i.c.v.*, a subcutaneous pump filled with 0.4mM 1-NM-PP1 in 20% DMSO/80% PBS was connected to an intracerebroventricular cannula surgically inserted into the lateral ventricle.

Laser Capture Microdissection

Fresh cerebellum was isolated from 4-5 week old animals of the indicated genotypes. The cerebellum was cut in half in the midline and embedded in Tissue-Tek OCT compound with midline face down. Liquid nitrogen was used to slowly solidify the mold. Embedded tissue was promptly transferred to -20ºC while the rest of the samples were collected, at which point cerebella were sectioned or stored in -80ºC until a later day. 20um thick cryosections were collected onto PEN-Membrane membrane slides (No 11505158 Leica). Slices were stained with Cresyl Violet. LMD6500 Laser Dissection Microscope was used to dissect a total of ~1,000,000um^2 of tissue. Samples fall by gravity into the top of a 0.2ml

tube containing 15ul lysis buffer. Once all the tissue was collected, the tubes were spun down to collect the sections and buffer to the bottom of the tube. The slides and tubes containing microdissected sample were kept frozen in dry ice. At the end of tissue collection samples were store in -80ºC until western blotting. The day of western blotting, samples were thawed and frozen 3-4x and vortexed vigorously in between. Samples were loaded on a western by adding 3ul of 6x loading dye to the 15ul lysis buffer with sample, boiling for 10 minutes, then loading 15ul to each well.

Behavioral analyses

Behavioral assessments were performed at the University of Minnesota's Mouse Behavior Core facility. Experimenters were blinded to the mouse genotype. Upon completion of the experiments, I decoded the data to separate performance according to genotypes and plot the graphs.

Beam walking test was used to assess balance. Mice were trained to cross a large square beam for three days. On test day four, mice were challenged to cross beams of narrowing sizes, with two test trials per beam size. The beams (round:25 mm, 17 mm and 10 mm diameter; square: 25 mm, 15 mm and 8 mm wide) are 1 meter long and elevated 50 cm above the bench, suspended between a start point and goal box. The average number of hind paw faults (foot slips) was graphed once the genotypes were decoded at the end of the behavioral experiments.

Mice were tested on an accelerating rotarod apparatus (Ugo Basile) to test motor coordination and balance. Mice underwent testing with four trials per day for four consecutive days. For each trial, acceleration was from 4 to 40 rpm over 300 s, and then speed maintained at 40 rpm. Latency to fall was recorded for each mouse per trial.

Statistical analysis

Data are expressed as the means ± standard error of measurement (SEM). Statistical analysis was performed using GraphPad Prism software (version 6.0c) to identify significant differences based on either t-test, one-way, or two-way analysis of variance

(ANOVA) followed by Bonferroni or Dunnett post-hoc test, depending on the analysis (indicated in figure legends). P-values <0.05 were considered to indicate statistically significant differences.

Bibliography

Acker, T., Beck, H. & Plate, K.H., 2001. Cell type specific expression of vascular endothelial growth factor and angiopoietin-1 and -2 suggests an important role of astrocytes in cerebellar vascularization. *Mechanisms of Development*, 108(1–2), pp.45–57.

Aiba, A. et al., 1994. Deficient cerebellar long-term depression and impaired motor learning in mGluR1 mutant mice. *Cell*, 79(2), pp.377–388.

Airaksinen, M.S. et al., 1997. Ataxia and altered dendritic calcium signaling in mice carrying a targeted null mutation of the calbindin D28k gene. *Proceedings of the National Academy of Sciences*, 94(4), pp.1488–1493.

Armbrust, K.R. et al., 2014. Mutant b-III Spectrin Causes mGluR1 ␣ Mislocalization and Functional Deficits in a Mouse Model of Spinocerebellar Ataxia Type 5. *The Journal of neuroscience*, 34(30), pp.9891–9904.

Aungst, S., England, P.M. & Thompson, S.M., 2013. Critical role of trkB receptors in reactive axonal sprouting and hyperexcitability after axonal injury. *Journal of neurophysiology*, 1, pp.813–824.

Bain, J. et al., 2007. The selectivity of protein kinase inhibitors: a further update. *Biochemical Journal*, 408(3), pp.297–315.

Banfi, S. et al., 1993. Mapping and cloning of the critical region for the spinocerebellar ataxia type 1 gene (SCA1) in a yeast artificial chromosome contig spanning 1.2 Mb. *Genomics*, 18(3), pp.627–635.

Barnes, J.A. et al., 2011. Abnormalities in the climbing fiber-Purkinje cell circuitry contribute to neuronal dysfunction in ATXN1[82Q] mice. *The Journal of neuroscience : the official journal of the Society for Neuroscience*, 31(36), pp.12778–89.

Boudreau, R.L., Martins, I. & Davidson, B.L., 2009. Artificial microRNAs as siRNA shuttles: improved safety as compared to shRNAs in vitro and in vivo. *Molecular therapy : the journal of the American Society of Gene Therapy*, 17(1), pp.169–75.

Brakeman, P.R. et al., 1997. Homer: a protein that selectively binds metabotropic glutamate receptors. *Nature*, 386(6622), pp.284–8.

Brandon, E.P. et al., 1995. Hippocampal long-term depression and depotentiation are defective in mice carrying a targeted disruption of the gene encoding the RI , B subunit of cAMP-dependent protein kinase. *Proceedings of the National Academy of Sciences of the United States of America*, 92, pp.8851–8855.

Brodie, C.R. et al., 2004. Overexpression of CREB reduces CRE-mediated transcription : behavioral and cellular analyses in transgenic mice. *Molecular and Cellular Neuroscience*, 25, pp.602–611.

Brooks, S.P. & Dunnett, S.B., 2009. Tests to assess motor phenotype in mice : a user ' s guide. *Nature Publishing Group*, 10(7), pp.519–529.

Burright, E.N. et al., 1995. SCA1 transgenic mice: a model for neurodegeneration caused by an expanded CAG trinucleotide repeat. *Cell*, 82(6), pp.937–48.

Cadd, G. & McKnight, G.S., 1989. Distinct patterns of cAMP-dependent protein kinase gene expression in mouse brain. *Neuron*, 3(1), pp.71–79.

Caenepeel, S. et al., 2004. The mouse kinome : Discovery and comparative genomics of all mouse protein kinases. *Proceedings of the National Academy of Sciences of the United States of America*, 101(32), pp.11707–12.

Chen, H.-K. et al., 2003. Interaction of Akt-phosphorylated ataxin-1 with 14-3-3 mediates neurodegeneration in spinocerebellar ataxia type 1. *Cell*, 113(4), pp.457–68.

Chen, X. et al., 2005. A Chemical-Genetic Approach to Studying Neurotrophin Signaling Neurotechnique. *Neuron*, 46, pp.13–21.

Chung, M.Y. et al., 1993. Evidence for a mechanism predisposing to intergenerational CAG repeat instability in spinocerebellar ataxia type I. *Nature genetics*, 5(3), pp.254–258.

Clark, H.B. et al., 1997. Purkinje cell expression of a mutant allele of SCA1 in transgenic mice leads to disparate effects on motor behaviors, followed by a progressive cerebellar dysfunction and histological alterations. *The Journal of neuroscience : the official journal of the Society for Neuroscience*, 17(19), pp.7385–95.

Cummings, C.J. et al., 1998. Chaperone suppression of aggregation and altered subcellular proteasome localization imply protein misfolding in SCA1. *Nature genetics*, 19(2), pp.148–54.

Cummings, C.J. et al., 1999. Mutation of the E6-AP ubiquitin ligase reduces nuclear inclusion frequency while accelerating polyglutamine-induced pathology in SCA1 mice. *Neuron*, 24(4), pp.879–92.

Cummings, C.J. et al., 2001. Over-expression of inducible HSP70 chaperone suppresses neuropathology and improves motor function in SCA1 mice. *Human molecular genetics*, 10(14), pp.1511–8.

Cvetanovic, M. et al., 2011. Vascular endothelial growth factor ameliorates the ataxic phenotype in a mouse model of spinocerebellar ataxia type 1. *Nature Medicine*, 17(11), pp.1445–1447.

Davies, S.P. et al., 2000. Specificity and mechanism of action of some commonly used protein kinase inhibitors. *Biochemical Journal*, 351, pp.95–105.

de Chiara, C. et al., 2009. Phosphorylation of S776 and 14-3-3 binding modulate ataxin-1 interaction with splicing factors. *PloS one*, 4(12), p.e8372.

Dell'Orco, J.M. et al., 2015. Neuronal Atrophy Early in Degenerative Ataxia Is a Compensatory Mechanism to Regulate Membrane Excitability. *The Journal of neuroscience : the official journal of the Society for Neuroscience*, 35(32), pp.11292–307.

Duvick, L. et al., 2010. SCA1-like disease in mice expressing wild-type Ataxin-1 with a serine to aspartic acid replacement at residue 776. *Neuron*, 67(6), pp.929–935.

Ebner, B. a et al., 2013. Purkinje cell ataxin-1 modulates climbing fiber synaptic input in developing and adult mouse cerebellum. *Journal of Neuroscience*, 33(13), pp.5806–5820.

Emamian, E.S. et al., 2003. Serine 776 of ataxin-1 is critical for polyglutamine-induced disease in SCA1 transgenic mice. *Neuron*, 38(3), pp.375–387.

Fernandez-Funez, P. et al., 2000. Identification of genes that modify ataxin-1-induced neurodegeneration. *Nature*, 408(6808), pp.101–6.

Festini, S.B. et al., 2015. Altered cerebellar connectivity in Parkinson ' s patients ON and OFF L-DOPA medication. *Frontiers in Human Neuroscience*, 9(April), pp.1–13.

Francis, S.H. & Corbin, J.D., 1994. Structure and function of cyclic nucleotide-dependent protein kinases. *Annual review of physiology*, 56, pp.237–72.

Frank, D.A. & Greenberg, M.E., 1994. CREB : A Mediator of Long-Term Memory from Mollusks to Mammals. *Cell*, 79, pp.5–8.

Fryer, J.D. et al., 2011. Exercise and Genetic Rescue ofSCA1via the Transcriptional Repressor Capicua. *Science*, 334(November), pp.690–693.

Gamm DM, Baude EJ, U.M., 1996. The Major Catalytic Subunit Isoforms of cAMP-dependent Protein Kinase Have Distinct Biochemical Properties in vitro and in vivo. *Journal of Biological Chemistry*, 271(26), pp.15736–15742.

Gatchel, J.R. et al., 2007. The insulin-like growth factor pathway is altered in spinocerebellar ataxia type 1 and type 7. *Proceedings of the National Academy of Sciences of the United States of America*, 105(4), pp.1291–1296.

Gennarino, V.A. et al., 2015. Pumilio1 haploinsufficiency leads to SCA1-like neurodegeneration by increasing wild-type Ataxin1 levels. *Cell*, 160(6), pp.1087–1098.

Glantz, S.B., Amatt, J.A. & Rubin, C.S., 1992. cAMP Signaling in Neurons : Patterns of Neuronal Expression and Intracellular Localization for a Novel Protein , AKAP 150 , that Anchors the Regulatory Subunit of cAMP-Dependent Protein Kinase 1W , 8. *Molecular Biology of the Cell*, 3, pp.1215–1228.

Guthrie, C.R., Skâlhegg, B.S. & McKnight, G.S., 1997. Two novel brain-specific splice variants of the murine Cbeta gene of cAMP-dependent protein kinase. *Journal of Biological Chemistry*, 272(47), pp.29560–5.

Gutstein, HB and Morris, J., 2009. Laser Capture Sampling and Analytical Issues in Proteomics Howard. *Cancer*, 4(5), pp.627–637.

Hashida, H. et al., 1997. Brain Regional Differences in the hxpansion of a CAG Repeat in the Spinocerebellar Ataxias: Dentatorubral-Pallidoluysian Spinocerebellar Ataxia Type 1. *Annals of Neurology*, 41, pp.505–511.

Hashimoto, K. et al., 2009. Translocation of a “Winner” Climbing Fiber to the Purkinje Cell Dendrite and Subsequent Elimination of “Losers” from the Soma in Developing Cerebellum. *Neuron*, 63(1), pp.106–118.

Hashimoto, K. & Kano, M., 2013. Synapse elimination in the developing cerebellum. *Cellular and Molecular Life Sciences*, 70, pp.4667–4680.

Hashimoto, K. & Kano, M., 2013. Synapse elimination in the developing cerebellum. *Cellular and Molecular Life Sciences*, 70(24), pp.4667–4680.

Hashimoto, K. & Kano, M., 2003. Functional Differentiation of Multiple Climbing Fiber Inputs during Synapse Elimination. *Neuron*, 38, pp.785–796.

Hayashi, S. et al., 2002. Efficient gene modulation in mouse epiblast using a Sox2Cre transgenic mouse strain. *Mechanisms of Development*, 119S, pp.97–101.

Hearst, S.M. et al., 2014. The design and delivery of a PKA inhibitory polypeptide to treat SCA1. *Journal of Neurochemistry*, 131(1), pp.101–114.

Hearst, SM, Lopez ME, Shao, Q, Liu Y, Vig, P., 2010. Dopamine D2 Receptor Signaling Modulates Mutant Ataxin-1 S776 Phosphorylation and Aggregation. *Journal of neurochemistry*, 114(3), pp.706–716.

Hong, S. et al., 2003. p80 coilin , a coiled body-specific protein , interacts with ataxin-1 , the SCA1 gene product. *Biochimica et Biophysica Acta 1638*, 1638, pp.35–42.

Hourez, R. et al., 2011. Aminopyridines correct early dysfunction and delay neurodegeneration in a mouse model of spinocerebellar ataxia type 1. *The Journal of neuroscience : the official journal of the Society for Neuroscience*, 31(33), pp.11795–11807.

Howe, D.G., Wiley, J.C. & McKnight, G.S., 2002. Molecular and behavioral effects of a null mutation in all PKA Cβ isoforms. *Molecular and Cellular Neuroscience*, 20(3), pp.515–524.

Huang, Y., Roelink, H. & McKnight, G.S., 2002. Protein kinase A deficiency causes axially localized neural tube defects in mice. *Journal of Biological Chemistry*, 277(22), pp.19889–19896.

Ingram, M. et al., 2016. Cerebellar Transcriptome Profiles of ATXN1 Transgenic Mice Reveal SCA1 Disease Progression and Protection Pathways. *Neuron*, 89(6), pp.1194–1207.

Irwin, S. et al., 2005. RNA association and nucleocytoplasmic shuttling by ataxin-1. *Journal of Cell Science*, 118, pp.233–242.

Jafar-Nejad, P. et al., 2011. Regional rescue of spinocerebellar ataxia type 1 phenotypes by 14-3-3epsilon haploinsufficiency in mice underscores complex pathogenicity in neurodegeneration. *Proceedings of the National Academy of Sciences of the United States of America*, 108(5), pp.2142–7.

Jorgensen, N.D. et al., 2009. Phosphorylation of ATXN1 at Ser776 in the cerebellum Nathan. *Journal of neurochemistry*, 110(2), pp.675–686.

Kakizawa, S. et al., 2003. Effects of insulin-like growth factor I on climbing fibre synapse elimination during cerebellar development. *European Journal of Neuroscience*, 17, pp.545–554.

Kaytor, M.D. et al., 2005. A cell-based screen for modulators of ataxin-1 phosphorylation. *Human Molecular Genetics*, 14(8), pp.1095–1105.

Keiser, M.S., Boudreau, R.L. & Davidson, B.L., 2014. Broad therapeutic benefit after RNAi expression vector delivery to deep cerebellar nuclei: implications for spinocerebellar ataxia type 1 therapy. *Molecular therapy : the journal of the American Society of Gene Therapy*, 22(3), pp.588–95.

Keiser, M.S. et al., 2015. Broad distribution of ataxin 1 silencing in rhesus cerebella for spinocerebellar ataxia type 1 therapy. *Brain*, 138(12), pp.3555–3566.

Keiser, MS, Mas Monteys A, Corbau R, Gonzalez-Alegre, P, Davidson, B., 2016. RNAi prevents and reverses phenotypes induced by mutant human ataxin-1. *Annals of Neurology*, 80(5), pp.754–765.

Kemp, B.E. & Pearson, R.B., 1990. Protein kinase recognition sequence motifs. *Trends in Biochemical Sciences*, 15(9), pp.342–6.

Kim, E. et al., 2014. Structural basis of the phosphorylation dependent complex formation of neurodegenerative disease protein Ataxin-1 and RBM17. *Biochemical and Biophysical Research Communications*, 449(4), pp.399–404.

Kim, E. et al., 2013. Structural basis of protein complex formation and reconfiguration by polyglutamine disease protein Ataxin-1 and Capicua. *Genes & Development*, 27(6), pp.590–595.

Klement, I. a et al., 1998. Ataxin-1 nuclear localization and aggregation: role in polyglutamine-induced disease in SCA1 transgenic mice. *Cell*, 95(1), pp.41–53.

Konno, A., Shuvaev, A.N. & Miyake, N., 2014. Mutant Ataxin-3 with an Abnormally Expanded Polyglutamine Chain Disrupts Dendritic Development and Metabotropic Glutamate Receptor Signaling in Mouse Cerebellar Purkinje Cells. *Cerebellum*, 13, pp.29–41.

Kordasiewicz, H.B. et al., 2012. Sustained Therapeutic Reversal of Huntington's Disease by Transient Repression of Huntingtin Synthesis. *Neuron*, 74(6), pp.1031–1044.

Lagalwar, S and Orr, H., 2013. Regulation of Ataxin-1 Phosphorylation and Its Impact on Biology. *Methods in molecular biology (Clifton, N.J.)*, 1010, pp.3–17.

Lai, S. et al., 2011. 14-3-3 Binding to ataxin-1(ATXN1) regulates its dephosphorylation at Ser-776 and transport to the nucleus. *Journal of Biological Chemistry*, 286(40), pp.34606–34616.

Lam, Y.C. et al., 2006. ATAXIN-1 Interacts with the Repressor Capicua in Its Native Complex to Cause SCA1 Neuropathology. *Cell*, 127(7), pp.1335–1347.

Lein, E.S. et al., 2007. Genome-wide atlas of gene expression in the adult mouse brain. *Nature*, 445(7124), pp.168–76.

Lim, J. et al., 2008. Opposing effects of polyglutamine expansion on native protein complexes contribute to SCA1. *Nature*, 452(7188), pp.713–8.

Lin, X. et al., 2000. Polyglutamine expansion down-regulates specific neuronal genes before pathologic changes in SCA1. *Nature neuroscience*, 3(2), pp.157–163.

Liu, G. et al., 2013. Report Transient Inhibition of TrkB Kinase after Status Epilepticus Prevents Development of Temporal Lobe Epilepsy. *NEURON*, 79(1), pp.31–38.

Liu, J. et al., 2010. Cholesterol involvement in the pathogenesis of neurodegenerative diseases Jun-Ping. *Molecular and Cellular Neuroscience*, 43(1), pp.33–42.

Lochner, A. & Moolman, J.A., 2006. The many faces of H89: A review. *Cardiovascular Drug Reviews*, 24(3–4), pp.261–274.

López-Otin, C. et al., 2013. Review The Hallmarks of Aging. *Cell*, 153(6), pp.1194–1217.

Lorenzetti, D. et al., 2000. Repeat instability and motor incoordination in mice with a targeted expanded CAG repeat in the Sca1 locus. *Hum Mol Genet*, 9(5), p.779–85.

Madhusudan et al., 1994. cAMP-dependent protein kinase: crystallographic insights into substrate recognition and phosphotransfer. *Protein science : a publication of the Protein Society*, 3(2), pp.176–87.

Manning, G. et al., 2002. The Protein Kinase Complement of the Human Genome. *Science*, 298(5600), pp.1912–34.

Manning, G. et al., 2002. Evolution of protein kinase signaling from yeast to man. *TRENDS in Biochemical Sciences*, 27(10), pp.514–520.

Masuda, A., Takeda, J. & Ohno, K., 2016. FUS-mediated regulation of alternative RNA processing in neurons : insights from global transcriptome analysis. *Wiley Interdisciplinary Reviews: RNA*, pp.2–5.

Matilla, a et al., 1998. Mice lacking ataxin-1 display learning deficits and decreased hippocampal paired-pulse facilitation. *The Journal of neuroscience : the official journal of the Society for Neuroscience*, 18(14), pp.5508–5516.

McBride, J.L. et al., 2008. Artificial miRNAs mitigate shRNA-mediated toxicity in the brain: implications for the therapeutic development of RNAi. *Proceedings of the National Academy of Sciences of the United States of America*, 105(15), pp.5868–5873.

Miller, T.M. et al., 2013. An antisense oligonucleotide against SOD1 delivered intrathecally for patients with SOD1 familial amyotrophic lateral sclerosis: A phase 1, randomised, first-in-man study. *The Lancet Neurology*, 12(5), pp.435–442.

Morgan, D.J. et al., 2008. Tissue-specific PKA inhibition using a chemical genetic approach and its application to studies on sperm capacitation. *Proceedings of the National Academy of Sciences of the United States of America*, 105(52), pp.20740–20745.

Müller, K. et al., 2012. Impaired motor coordination and disrupted cerebellar architecture in Fgfr1 and Fgfr2 double knockout mice. *Brain Research*, 1460, pp.12–24.

Nakao, H. et al., 2007. Metabotropic glutamate receptor subtype-1 is essential for motor coordination in the adult cerebellum. *Neuroscience Research*, 57(4), pp.538–543.

Narayanan, R., Dougherty, K.J. & Johnston, D., 2010. Calcium Store Depletion Induces Persistent Perisomatic Increases in the Functional Density of h Channels in Hippocampal Pyramidal Neurons. *Neuron*, 68(5), pp.921–935.

Niles, J.O. & Schawarze, R., 2000. mGluR1 in Cerebellar Purkinje Cells Essential for Long-Term Depression, Synapse Elimination, and Motor Coordination. *Science*, 288(5472), pp.1832–1835.

Niswender, C.M. et al., 2002. Protein Engineering of Protein Kinase A Catalytic Subunits Results in the Acquisition of Novel Inhibitor Sensitivity. *The Journal of biological chemistry*, 277(32), pp.28916–28922.

Notartomaso, S. et al., 2013. Pharmacological enhancement of mGlu1 metabotropic glutamate receptors causes a prolonged symptomatic benefit in a mouse model of spinocerebellar ataxia type 1. *Molecular Brain*, 6(48), pp.1–17.

Orr, H.T. et al., 1993. Expansion of an unstable trinucleotide CAG repeat in spinocerebellar ataxia type 1. *Nature genetics*, 4(3), pp.221–6.

Park, J. et al., 2013. RAS-MAPK-MSK1 pathway modulates ataxin 1 protein levels and toxicity in SCA1. *Nature*, 498(7454), pp.325–31.

Pink, M.D. & Acqua, M.L.D., 2010. Subcellular Targeting of PKA through AKAPs : Conserved Anchoring and Unique Targeting Domains. In *Handbook of Cell Signaling*. Elsevier Inc., pp. 1329–1336.

Power, E.M., English, N.A. & Empson, R.M., 2016. Are Type 1 metabotropic glutamate receptors a viable therapeutic target for the treatment of cerebellar ataxia? *The Journal of physiology*, 0(April 2015), pp.1–10.

Qi, M. et al., 1996. Impaired hippocampal plasticity in mice lacking the Cbeta1 catalytic subunit of cAMP-dependent protein kinase. *Proceedings of the National Academy of Sciences of the United States of America*, 93(4), pp.1571–6.

Riley, B.E. et al., 2004. The effects of the polyglutamine repeat protein ataxin-1 on the UbL-UBA protein A1Up. *The Journal of biological chemistry*, 279(40), pp.42290–301.

Rinaldo, L. & Hansel, C., 2013. Muscarinic acetylcholine receptor activation blocks long-term potentiation at cerebellar parallel fi ber – Purkinje cell synapses via cannabinoid signaling. *Proc. Natl. Acad. Sci.*, 110(27), pp.11181–11186.

Roux, P.P. & Blenis, J., 2004. ERK and p38 MAPK-Activated Protein Kinases : a Family of Protein Kinases with Diverse Biological Functions. *MICROBIOLOGY AND MOLECULAR BIOLOGY REVIEWS*, 68(2), pp.320–344.

Ruegsegger, C. et al., 2016. Impaired mTORC1-Dependent Expression of Homer-3 Influences SCA1 Pathophysiology. *Neuron*, 89(1), pp.129–146.

Ruiz de Almodovar, C. et al., 2010. Matrix-Binding Vascular Endothelial Growth Factor (VEGF) Isoforms Guide Granule Cell Migration in the Cerebellum via VEGF Receptor Flk1. *The Journal of neuroscience*, 30(45), pp.15052–15066.

Sánchez-Hernández, N. et al., 2016. The in vivo dynamics of TCERG1 , a factor that couples transcriptional elongation with splicing. *RNA*, 22(4), pp.571–582.

Schauble, S. et al., 2007. Identification of ChChd3 as a Novel Substrate of the cAMP-dependent Protein Kinase (PKA) Using an Analog-sensitive Catalytic Subunit. *The Journal of biological chemistry*, 282(20), pp.14952–14959.

Schut, J.W., 1951. Hereditary Ataxia A Survey of Certain Clinical , Pathologic and Genetic Features with Linkage Data on Five Additional Hereditary Factors. *The American Journal of Human Genetics*, 3(2), pp.93–110.

Serra, H.G. et al., 2004. Gene profiling links SCA1 pathophysiology to glutamate signaling in Purkinje cells of transgenic mice. *Human Molecular Genetics*, 13(20), pp.2535–2543.

Serra, H.G. et al., 2006. RORa-Mediated Purkinje Cell Development Determines Disease Severity in Adult SCA1 Mice. *Cell*, 127(4), pp.697–708.

Shim, H.G. et al., 2016. mGlu 1 receptor mediates homeostatic control of intrinsic excitability through I h in cerebellar Purkinje cells. *Journal of Neurophysiology*, 115, pp.2446–2455.

Sillevis Smitt, P. et al., 2016. Paraneoplastic cerebellar ataxia due to autoantibodies against a glutamate receptor. *New England Journal of Medicine*, 342(1), pp.21–27.

Skalhegg, B S, Huang, Y, Su, T, Idzerda, R, McKnight, S, Burton, K., 2002. Mutation of the C Subunit of PKA Leads to Growth Retardation and Sperm Dysfunction. *Molecular Endocrinology*, 16(3), pp.630–639.

Skinner, P.J. et al., 2001. Altered Trafficking of Membrane Proteins in Purkinje Cells of SCA1 Transgenic Mice. *American Journal of Pathology*, 159(3), pp.905–913.

Smyth, L.A. & Collins, I., 2009. Measuring and interpreting the selectivity of protein kinase inhibitors. *Journal of Chemical Biology*, 2(3), pp.131–151.

Sugi, T. et al., 2011. 1NM-PP1 Treatment of Mice Infected with Toxoplasma gondii. *Parasitology*, 73(1), pp.1377–1379.

Taylor, S.S. et al., 2012. Assembly of allosteric macromolecular switches: lessons from PKA. *Nature reviews. Molecular cell biology*, 13(10), pp.646–58.

Tsai, C. et al., 2004. is functionally linked to the silencing mediator of retinoid and thyroid hormone receptors. *Proc. Natl. Acad. Sci.*, 101(12), pp.4047–4052.

Tsuda, H. et al., 2005. The AXH Domain of Ataxin-1 Mediates Neurodegeneration through Its Interaction with Gfi-1 / Senseless Proteins. *Cell*, 122, pp.633–644.

Tu, J.C. et al., 1998. Homer Binds a Novel Proline-Rich Motif and Links Group 1 Metabotropic Glutamate Receptors with IP3 Receptors. *Neuron*, 21, pp.717–726.

Tunquist, B.J. et al., 2008. Loss of AKAP150 perturbs distinct neuronal processes in mice. *Proc. Natl. Acad. Sci.*, 105(34), pp.12557–12562.

Turnham, R.E. & Scott, J.D., 2016. Protein kinase A catalytic subunit isoform PRKACA; History, function and physiology. *Gene*, 577(2), pp.101–108.

Uhler, M.D. et al., 1986. Isolation of cDNA clones coding for the catalytic subunit of mouse cAMP-dependent protein kinase. *Proceedings of the National Academy of Sciences of the United States of America*, 83(5), pp.1300–4.

Uhler, M.D., Chrivia, J.C. & McKnight, G.S., 1986. Evidence for a second isoform of the catalytic subunit of cAMP-dependent protein kinase. *The Journal of biological chemistry*, 261, pp.15360–15363.

Uhler, M.D. & McKnight, G.S., 1987. Expression of cDNAs for two isoforms of the catalytic subunit of cAMP-dependent protein kinase. *Journal of Biological Chemistry*, 262(31), pp.15202–15207.

Vanier, M.T., 2013. *Niemann – Pick diseases* 1st ed., Elsevier B.V. Available at: http://dx.doi.org/10.1016/B978-0-444-59565-2.00041-1.

Vig, P.J.S. et al., 2012. Suppression of calbindin-D28k expression exacerbates SCA1 phenotype in a disease mouse model. *Cerebellum*, 11(3), pp.718–732.

Walsh, DA, Van PAtten, S., 1994. Multiple pathway signal transduction by the cAMP-dependent protein kinase. *The FASEB Journal*, 8(15), pp.1227–1236.

Wang, H. et al., 2008. CAMKII ACTIVATION STATE UNDERLIES SYNAPTIC LABILE PHASE OF LTP AND SHORT-TERM MEMORY FORMATION. *Current Biology*, 18(20), pp.1546–1554.

Wang, H. et al., 2003. Inducible protein knockout reveals temporal requirement of CaMKII reactivation for memory consolidation in the brain. *Proceedings of the National Academy of Sciences of the United States of America*, 100(7), pp.4287–4292.

Wang, X. et al., 2009. TrkB Signaling Is Required for Both the Induction and Maintenance of Tissue and Nerve Injury-Induced Persistent Pain. *The Journal of neuroscience*, 29(17), pp.5508–5515.

Watase, K. et al., 2002. A long CAG repeat in the mouse Sca1 locus replicates SCA1 features and reveals the impact of protein solubility on selective neurodegeneration. *Neuron*, 34(6), pp.905–19.

Weisenhaus, M. et al., 2010. Mutations in AKAP5 Disrupt Dendritic Signaling Complexes and Lead to Electrophysiological and Behavioral Phenotypes in Mice. *PloS one*, 5(4), p.e10325.

Wong, W. & Scott, J.D., 2004. AKAP signalling complexes: focal points in space and time. *Nature reviews. Molecular cell biology*, 5(12), pp.959–70.

Xia, H. et al., 2004. RNAi suppresses polyglutamine-induced neurodegeneration in a model of spinocerebellar ataxia. *Nature Medicine*, 10(8), pp.816–820.

Yue, S. et al., 2001. The spinocerebellar ataxia type 1 protein , ataxin-1 , has RNA-binding activity that is inversely affected by the length of its polyglutamine tract. *Human molecular genetics*, 10(1), pp.25–30.

Zhong, H. et al., 2009. Article Subcellular Dynamics of Type II PKA in Neurons. *Neuron*, 62, pp.363–374.

Zhou, P., 2004. Determining protein half-lives. *Methods in molecular biology (Clifton, N.J.)*, 284, pp.67–77.

Zoghbi, H.Y. & Orr, H.T., 2009. Pathogenic mechanisms of a polyglutamine-mediated neurodegenerative disease, spinocerebellar ataxia type 1. *The Journal of biological chemistry*, 284(12), pp.7425–9.

Zu, T., Duvick LA, Kaytor, MD, Berlinger, MS, Zohgbi, HY, Clark, HB, Orr, H., 2004. Recovery from Polyglutamine-Induced Neurodegeneration in Conditional SCA1 Transgenic Mice. *Journal of Neuroscience*, 24(40), pp.8853–8861.

Appendix

Appendix 1: Publications associated with therapeutic effects of Ataxin1 clearance

Reference	Method of Ataxin1 knockdown	SCA1 model	% Ataxin1 knockdown	Behavior	Histopathology Molecular layer (ML)	Transcriptional changes	Notes
Zu et al., 2004	Tet-Off system	*Pcp2 cATXN1[82Q]*	Gene off after disease onset, ATXN1+ nuclear inclusions cleared within 2 days by IF	N/A	No ML atrophy	mGluR1 protein restored after 8 weeks gene off (but still down after 4 wks off)	
Serra et al., 2006	Tet-Off system	*Pcp2 cATXN1[82Q]*	Gene off during cerebellar development (P14, P21)	N/A	No ML atrophy	Genes down in disease: Grm1, Calbindin, Itpr1. Not measured in gene-off.	
Xia et al., 2004	AAV-RNAi	*Pcp2-ATXN1[82Q]* line BO5	Resolution of ATXN1+ nuclear inclusions within 1 week by IF	Partial rotarod recovery	No ML atrophy in transduced lobules		
Keiser et al., 2013	AAV-RNAi	*Pcp2-ATXN1[82Q]* line BO5	~70% hAtxn1 kd whole cerebellum	Rotarod: no deficit	Incomplete rescue ML atrophy	*Calbindin* restored to wt	
Keiser et al., 2014	AAV-RNAi	*Sca1*$^{154Q/2Q}$	20-30% kd *mAtxn1* whole cerebellum; 58% protein kd in microdissected transduced tissue	Rotarod: no deficit	ML n.s. from Wt	*Grm1 restored to wt*	
Keiser et al., 2016	AAV-RNAi	*Pcp2-ATXN1[82Q]* line BO5	48-71% *hAtxn1* kd whole cerebellum	Rotarod n.s. from wt	ML n.s. from Wt	*Grm1*, n.s. from wt	Dose achieving 23-28% kd improved rotarod, not ML, before disease onset; not therapeutic after disease onset
Orr lab (unpublished)	Antisense Oligonucleotides	*Sca1*$^{154Q/2Q}$	30% kd *mAtxn1* whole cerebellum; 50% kd PCL	Halts progression of rotarod deficits		Variable (n.s., but trend to improved expression)	Lifespan extended
Klement et al., 1998	Blocked nuclear entry	*Pcp2-ATXN1[82Q]-K772T*	No kd	Rotarod: no deficit. No overt ataxia out to 1yr old	No ML atrophy		
Emamian et al., 2003	Unstable unphosphorylated protein	*Pcp2-ATXN1[82Q]-A776*	Unstable protein compared to S776	Rotarod: no deficit	ML intact, but 30% atrophy after 37 wks. No PC loss.		
Park et al., 2013	Msk1 kinase KO	*Sca1*$^{154Q/2Q;}$ *Msk1*$^{-/-}$	<20% less protein (154Q and 2Q)	Rotarod: some rescue (Msk1$^{+/-}$;Msk2$^{+/-}$)	Improved Calbindin staining	N/A	

Appendix 2: Detailed summary of Keiser et al., 2016.

Age injection	AAV dose	Age tested	% Ataxin1 knockdown (whole cerebellum)	Rotarod	Histopathology Anterior	Histopathology Posterior	Transcriptional changes	Side effects
6 weeks	AAV-RNAi 8E8	30 weeks	23% mRNA knockdown	Better than Control; n.s. from wt	n.s. from wt	atrophy		
6 weeks	AAV-RNAi 8E9	30 weeks	53% mRNA knockdown		n.s. from wt	n.s. from wt		
6 weeks	AAV-RNAi 8E10	30 weeks	96% mRNA knockdown	No improvement	n.s. from wt	atrophy		GFAP+ Iba1+
12 weeks	AAV-RNAi 8E8	20 weeks	28% mRNA knockdown (but n.s.)	No improvement	atrophy	n.s. from wt	*Grm1*, *Pcp2*- Not restored	
12 weeks	AAV-RNAi 2.6E9	20 weeks	48% mRNA knockdown	Better than Control, but not to level of Wt				
12 weeks	AAV-RNAi 8E9	20 weeks	71% mRNA knockdown		n.s. from wt	n.s. from wt	*Grm1*, *Pcp2*- n.s. from wt	
12 weeks	AAV-RNAi 2.6E10	20 weeks	(~90%)	No improvement				
12 weeks	AAV-RNAi 8E10	20 weeks	(~90%)	No improvement	atrophy		*Grm1*, *Pcp2*- Not restored	

Appendix 3: IPA of "Ataxia" Pink Module. Complete list of genes in the Gq signaling pathway.

FVB/wt + ATXN1[82Q];CαM120A vs. ATXN1[82Q]			
Pink Module_Top Canonical Pathway_Gaq Signaling			
Gene Symbol - mouse (Entrez Gene)	Entrez Gene Name	Type(s)	Location
Chrm1	cholinergic receptor muscarinic 1	G-protein coupled receptor	Plasma Membrane
Fgfr1	fibroblast growth factor receptor 1	kinase	Plasma Membrane
Itpr2	inositol 1,4,5-trisphosphate receptor type 2	ion channel	Cytoplasm
Klb	klotho beta	enzyme	Plasma Membrane
Nfatc3	nuclear factor of activated T-cells 3	transcription regulator	Nucleus
Nfkbia	NFKB inhibitor alpha	transcription regulator	Cytoplasm
Pik3c2g	phosphatidylinositol-4-phosphate 3-kinase catalytic subunit type 2 gamma	kinase	Cytoplasm
Plcb2	phospholipase C beta 2	enzyme	Cytoplasm
Plcg2	phospholipase C gamma 2	enzyme	Cytoplasm
Ppp3r2	protein phosphatase 3 regulatory subunit B, beta	phosphatase	Cytoplasm
Rgs4	regulator of G-protein signaling 4	other	Cytoplasm
Rhod	ras homolog family member D	enzyme	Cytoplasm

Appendix 4: IPA of "Ataxia" Pink Module. Complete list of genes in the fMLP Signaling in Neutrophils pathway.

FVB/wt + ATXN1[82Q];CαM120A vs. ATXN1[82Q]			
Pink Module_Top Canonical Pathway_fMLP Signaling in Neutrophils			
Gene Symbol - mouse (Entrez Gene)	Entrez Gene Name	Type(s)	Location
Fgfr1	fibroblast growth factor receptor 1	kinase	Plasma Membrane
Itpr2	inositol 1,4,5-trisphosphate receptor type 2	ion channel	Cytoplasm
Klb	klotho beta	enzyme	Plasma Membrane
Ncf1	neutrophil cytosolic factor 1	enzyme	Cytoplasm
Nfatc3	nuclear factor of activated T-cells 3	transcription regulator	Nucleus
Nfkbia	NFKB inhibitor alpha	transcription regulator	Cytoplasm
Nox1	NADPH oxidase 1	ion channel	Cytoplasm
Pik3c2g	phosphatidylinositol-4-phosphate 3-kinase catalytic subunit type 2 gamma	kinase	Cytoplasm
Plcb2	phospholipase C beta 2	enzyme	Cytoplasm
Ppp3r2	protein phosphatase 3 regulatory subunit B, beta	phosphatase	Cytoplasm

Appendix 5: IPA of "Ataxia" Pink Module. Complete list of genes in the Phagosome Formation pathway.

FVB/wt + ATXN1[82Q];CαM120A vs. ATXN1[82Q]			
Pink Module_Top Canonical Pathway_phagosome formation			
Gene Symbol - mouse (Entrez Gene)	Entrez Gene Name	Type(s)	Location
Fcer2a	Fc fragment of IgE receptor II	transmembrane receptor	Plasma Membrane
Fgfr1	fibroblast growth factor receptor 1	kinase	Plasma Membrane
Klb	klotho beta	enzyme	Plasma Membrane
Mrc1	mannose receptor, C type 1	transmembrane receptor	Plasma Membrane
Pik3c2g	phosphatidylinositol-4-phosphate 3-kinase catalytic subunit type 2 gamma	kinase	Cytoplasm
Plcb2	phospholipase C beta 2	enzyme	Cytoplasm
Plcg2	phospholipase C gamma 2	enzyme	Cytoplasm
Rhod	ras homolog family member D	enzyme	Cytoplasm
Tlr8	toll like receptor 8	transmembrane receptor	Plasma Membrane
Tlr13	toll-like receptor 13	other	Cytoplasm

Appendix 6: IPA of "Ataxia" Pink Module. Complete list of genes in the Leukocyte Extravasation Signaling pathway.

FVB/wt + ATXN1[82Q];CαM120A vs. ATXN1[82Q]			
Pink Module_Top Canonical Pathway_Leukocyte Extravasation Signaling			
Gene Symbol - mouse (Entrez Gene)	Entrez Gene Name	Type(s)	Location
Arhgap9	Rho GTPase activating protein 9	other	Cytoplasm
Cldn10	claudin 10	other	Plasma Membrane
Ctnna1	catenin alpha 1	other	Plasma Membrane
Fgfr1	fibroblast growth factor receptor 1	kinase	Plasma Membrane
Itgal	integrin subunit alpha L	transmembrane receptor	Plasma Membrane
Klb	klotho beta	enzyme	Plasma Membrane
Mmp28	matrix metallopeptidase 28	peptidase	Extracellular Space
Ncf1	neutrophil cytosolic factor 1	enzyme	Cytoplasm
Nox1	NADPH oxidase 1	ion channel	Cytoplasm
Pik3c2g	phosphatidylinositol-4-phosphate 3-kinase catalytic subunit type 2 gamma	kinase	Cytoplasm
Plcg2	phospholipase C gamma 2	enzyme	Cytoplasm
Rassf5	Ras association domain family member 5	other	Plasma Membrane
Vcl	vinculin	enzyme	Plasma Membrane

Appendix 7: IPA of "Ataxia" Pink Module. Complete list of genes in the FcRIIB Signaling in B Lymphocytes pathway.

FVB/wt + ATXN1[82Q];CαM120A vs. ATXN1[82Q]			
Pink Module_Top Canonical Pathway_FcRIIB Signaling in B Lymphocytes			
Gene Symbol - mouse (Entrez Gene)	Entrez Gene Name	Type(s)	Location
Cd79a	CD79a molecule	transmembrane receptor	Plasma Membrane
Dok1	docking protein 1	kinase	Plasma Membrane
Fgfr1	fibroblast growth factor receptor 1	kinase	Plasma Membrane
Klb	klotho beta	enzyme	Plasma Membrane
Pik3c2g	phosphatidylinositol-4-phosphate 3-kinase catalytic subunit type 2 gamma	kinase	Cytoplasm
Plcg2	phospholipase C gamma 2	enzyme	Cytoplasm

Appendix 8: IPA of "Disease Progression" Turquoise Module. Complete list of genes in the Axonal Guidance Signaling pathway.

FVB/wt + ATXN1[82Q];CαM120A vs. ATXN1[82Q]			
Turquoise Module_Top Canonical Pathway_Axonal Guidance Signaling			
Gene Symbol - mouse (Entrez Gene)	Entrez Gene Name	Type(s)	Location
Ablim2	actin binding LIM protein family member 2	other	Cytoplasm
Actr3	ARP3 actin related protein 3 homolog	other	Plasma Membrane
Adam11	ADAM metallopeptidase domain 11	peptidase	Plasma Membrane
Adam15	ADAM metallopeptidase domain 15	peptidase	Plasma Membrane
Adam23	ADAM metallopeptidase domain 23	peptidase	Plasma Membrane
Adamts1	ADAM metallopeptidase with thrombospondin type 1 motif 1	peptidase	Extracellular Space
Adamts9	ADAM metallopeptidase with thrombospondin type 1 motif 9	peptidase	Extracellular Space
Akt2	AKT serine/threonine kinase 2	kinase	Cytoplasm
Arhgef6	Rac/Cdc42 guanine nucleotide exchange factor 6	other	Cytoplasm
Arpc2	actin related protein 2/3 complex subunit 2	other	Cytoplasm
Arpc1b	actin related protein 2/3 complex subunit 1B	other	Cytoplasm
Arpc5l	actin related protein 2/3 complex subunit 5 like	other	Cytoplasm
Baiap2	BAI1 associated protein 2	kinase	Plasma Membrane
Bcar1	BCAR1, Cas family scaffolding protein	enzyme	Plasma Membrane
Bdnf	brain derived neurotrophic factor	growth factor	Extracellular Space
Bmp1	bone morphogenetic protein 1	peptidase	Extracellular Space
Bmp8a	bone morphogenetic protein 8a	cytokine	Extracellular Space
Cdk5	cyclin dependent kinase 5	kinase	Nucleus
Cfl1	cofilin 1	other	Nucleus
Cops5	COP9 signalosome subunit 5	transcription regulator	Nucleus
Crkl	CRK like proto-oncogene, adaptor protein	kinase	Cytoplasm
Efna2	ephrin A2	kinase	Plasma Membrane
Efna3	ephrin A3	kinase	Plasma Membrane
Efnb2	ephrin B2	other	Plasma Membrane
Epha8	EPH receptor A8	kinase	Plasma Membrane
Ephb4	EPH receptor B4	kinase	Plasma Membrane

(continued from previous page)

FVB/wt + ATXN1[82Q];CαM120A vs. ATXN1[82Q]			
Turquoise Module_Top Canonical Pathway_Axonal Guidance Signaling			
Gene Symbol - mouse (Entrez Gene)	Entrez Gene Name	Type(s)	Location
Erbb2	erb-b2 receptor tyrosine kinase 2	kinase	Plasma Membrane
Farp2	FERM, ARH/RhoGEF and pleckstrin domain protein 2	other	Cytoplasm
Fzd9	frizzled class receptor 9	G-protein coupled receptor	Plasma Membrane
Fzd10	frizzled class receptor 10	G-protein coupled receptor	Plasma Membrane
Gab1	GRB2 associated binding protein 1	kinase	Cytoplasm
Gli1	GLI family zinc finger 1	transcription regulator	Nucleus
Gli3	GLI family zinc finger 3	transcription regulator	Nucleus
Gnai1	G protein subunit alpha i1	enzyme	Plasma Membrane
Gnal	G protein subunit alpha L	enzyme	Cytoplasm
Gnao1	G protein subunit alpha o1	enzyme	Plasma Membrane
Gnaq	G protein subunit alpha q	enzyme	Plasma Membrane
Gnaz	G protein subunit alpha z	enzyme	Plasma Membrane
Gnb1	G protein subunit beta 1	enzyme	Plasma Membrane
Gng7	G protein subunit gamma 7	enzyme	Plasma Membrane
Gng11	G protein subunit gamma 11	enzyme	Plasma Membrane
Gng13	G protein subunit gamma 13	enzyme	Plasma Membrane
Grb2	growth factor receptor bound protein 2	kinase	Cytoplasm
Hras	HRas proto-oncogene, GTPase	enzyme	Plasma Membrane
Irs1	insulin receptor substrate 1	enzyme	Cytoplasm
Kalrn	kalirin, RhoGEF kinase	kinase	Cytoplasm
Klc1	kinesin light chain 1	other	Cytoplasm
Limk2	LIM domain kinase 2	kinase	Cytoplasm
Lrrc4c	leucine rich repeat containing 4C	other	Plasma Membrane
Map2k1	mitogen-activated protein kinase kinase 1	kinase	Cytoplasm
Mbtps2	membrane bound transcription factor peptidase, site 2	peptidase	Cytoplasm
Mmp8	matrix metallopeptidase 8	peptidase	Extracellular Space
Mylpf	myosin light chain, phosphorylatable, fast skeletal muscle	other	Cytoplasm

(continued from previous page)

FVB/wt + ATXN1[82Q];CαM120A vs. ATXN1[82Q]			
Turquoise Module_Top Canonical Pathway_Axonal Guidance Signaling			
Gene Symbol - mouse (Entrez Gene)	Entrez Gene Name	Type(s)	Location
Ngef	neuronal guanine nucleotide exchange factor	other	Cytoplasm
Notum	NOTUM, palmitoleoyl-protein carboxylesterase	enzyme	Extracellular Space
Ntf3	neurotrophin 3	growth factor	Extracellular Space
Ntrk2	neurotrophic receptor tyrosine kinase 2	kinase	Plasma Membrane
Pappa	pappalysin 1	peptidase	Extracellular Space
Pdgfd	platelet derived growth factor D	growth factor	Extracellular Space
Pgf	placental growth factor	growth factor	Extracellular Space
Pik3cg	phosphatidylinositol-4,5-bisphosphate 3-kinase catalytic subunit gamma	kinase	Cytoplasm
Pik3r1	phosphoinositide-3-kinase regulatory subunit 1	kinase	Cytoplasm
Pik3r5	phosphoinositide-3-kinase regulatory subunit 5	kinase	Cytoplasm
Pik3r6	phosphoinositide-3-kinase regulatory subunit 6	kinase	Cytoplasm
Plcb3	phospholipase C beta 3	enzyme	Cytoplasm
Plcb4	phospholipase C beta 4	enzyme	Cytoplasm
Plcd3	phospholipase C delta 3	enzyme	Cytoplasm
Plcd4	phospholipase C delta 4	enzyme	Cytoplasm
Prkar2b	protein kinase cAMP-dependent type II regulatory subunit beta	kinase	Cytoplasm
Prkcg	protein kinase C gamma	kinase	Cytoplasm
Prkcz	protein kinase C zeta	kinase	Cytoplasm
Prkd1	protein kinase D1	kinase	Cytoplasm
Ptch1	patched 1	transmembrane receptor	Plasma Membrane
Ptch2	patched 2	transmembrane receptor	Plasma Membrane
Pxn	paxillin	other	Cytoplasm
Rac2	ras-related C3 botulinum toxin substrate 2 (rho family, small GTP binding protein Rac2)	enzyme	Cytoplasm
Robo2	roundabout guidance receptor 2	transmembrane receptor	Plasma Membrane
Rras2	related RAS viral (r-ras) oncogene homolog 2	enzyme	Plasma Membrane

(continued from previous page)

FVB/wt + ATXN1[82Q];CαM120A vs. ATXN1[82Q]			
Turquoise Module_Top Canonical Pathway_Axonal Guidance Signaling			
Gene Symbol - mouse (Entrez Gene)	Entrez Gene Name	Type(s)	Location
Sema3d	semaphorin 3D	other	Extracellular Space
Sema4c	semaphorin 4C	other	Plasma Membrane
Sema4d	semaphorin 4D	transmembrane receptor	Plasma Membrane
Sema4g	semaphorin 4G	other	Plasma Membrane
Sema5a	semaphorin 5A	transmembrane receptor	Plasma Membrane
Sema6b	semaphorin 6B	other	Plasma Membrane
Sema7a	semaphorin 7A (John Milton Hagen blood group)	transmembrane receptor	Plasma Membrane
Shank2	SH3 and multiple ankyrin repeat domains 2	other	Plasma Membrane
Shh	sonic hedgehog	peptidase	Extracellular Space
Srgap1	SLIT-ROBO Rho GTPase activating protein 1	other	Cytoplasm
Tlr9	toll like receptor 9	transmembrane receptor	Plasma Membrane
Tuba8	tubulin alpha 8	other	Cytoplasm
Tuba4a	tubulin alpha 4a	other	Cytoplasm
Tubb2b	tubulin beta 2B class IIb	other	Cytoplasm
Unc5b	unc-5 netrin receptor B	transmembrane receptor	Plasma Membrane
Unc5d	unc-5 netrin receptor D	other	Plasma Membrane
Vasp	vasodilator-stimulated phosphoprotein	other	Plasma Membrane
Vegfb	vascular endothelial growth factor B	growth factor	Extracellular Space
Vegfc	vascular endothelial growth factor C	growth factor	Extracellular Space
Was	Wiskott-Aldrich syndrome	other	Cytoplasm
Wipf1	WAS/WASL interacting protein family member 1	other	Cytoplasm
Wnt3	Wnt family member 3	other	Extracellular Space
Wnt16	Wnt family member 16	other	Extracellular Space
Wnt10a	Wnt family member 10A	other	Extracellular Space
Wnt10b	Wnt family member 10B	other	Extracellular Space
Wnt8b	Wnt family member 8B	other	Extracellular Space
Wnt9a	Wnt family member 9A	other	Extracellular Space

Appendix 9: IPA of "Disease Progression" Turquoise Module. Complete list of genes in the B Cell Receptor Signaling pathway.

FVB/wt + ATXN1[82Q];CαM120A vs. ATXN1[82Q]			
Turquoise Module_Top Canonical Pathway_B Cell Receptor Signaling			
Gene Symbol - mouse (Entrez Gene)	Entrez Gene Name	Type(s)	Location
Akt2	AKT serine/threonine kinase 2	kinase	Cytoplasm
Apbb1ip	amyloid beta precursor protein binding family B member 1 interacting protein	other	Cytoplasm
Bad	BCL2 associated agonist of cell death	other	Cytoplasm
Bcl10	B-cell CLL/lymphoma 10	transcription regulator	Cytoplasm
Bcl2a1b	BCL2 related protein A1	other	Cytoplasm
Bcl2l1	BCL2 like 1	other	Cytoplasm
Blnk	B-cell linker	other	Cytoplasm
Btk	Bruton tyrosine kinase	kinase	Cytoplasm
Calm3	calmodulin 1	other	Nucleus
Camk2a	calcium/calmodulin dependent protein kinase II alpha	kinase	Cytoplasm
Camk2b	calcium/calmodulin dependent protein kinase II beta	kinase	Cytoplasm
Cd22	CD22 molecule	transmembrane receptor	Plasma Membrane
Cd79b	CD79b molecule	transmembrane receptor	Plasma Membrane
Cfl1	cofilin 1	other	Nucleus
Creb5	cAMP responsive element binding protein 5	transcription regulator	Nucleus
Creb3l4	cAMP responsive element binding protein 3 like 4	transcription regulator	Nucleus
Ebf1	early B-cell factor 1	transcription regulator	Nucleus
Fcgr3	Fc fragment of IgG receptor IIa	transmembrane receptor	Plasma Membrane
Fcgr2b	Fc fragment of IgG receptor IIb	transmembrane receptor	Plasma Membrane
Foxo1	forkhead box O1	transcription regulator	Nucleus
Gab1	GRB2 associated binding protein 1	kinase	Cytoplasm
Gab2	GRB2 associated binding protein 2	other	Cytoplasm
Grb2	growth factor receptor bound protein 2	kinase	Cytoplasm
Gsk3a	glycogen synthase kinase 3 alpha	kinase	Nucleus
Hras	HRas proto-oncogene, GTPase	enzyme	Plasma Membrane
Inpp5d	inositol polyphosphate-5-phosphatase D	phosphatase	Cytoplasm

(continued from previous page)

FVB/wt + ATXN1[82Q];CαM120A vs. ATXN1[82Q]			
Turquoise Module_Top Canonical Pathway_B Cell Receptor Signaling			
Gene Symbol - mouse (Entrez Gene)	Entrez Gene Name	Type(s)	Location
Irs1	insulin receptor substrate 1	enzyme	Cytoplasm
Jun	Jun proto-oncogene, AP-1 transcription factor subunit	transcription regulator	Nucleus
Lyn	LYN proto-oncogene, Src family tyrosine kinase	kinase	Cytoplasm
Map2k1	mitogen-activated protein kinase kinase 1	kinase	Cytoplasm
Map3k1	mitogen-activated protein kinase kinase kinase 1	kinase	Cytoplasm
Map3k5	mitogen-activated protein kinase kinase kinase 5	kinase	Cytoplasm
Map3k6	mitogen-activated protein kinase kinase kinase 6	kinase	Other
Map3k8	mitogen-activated protein kinase kinase kinase 8	kinase	Cytoplasm
Map3k10	mitogen-activated protein kinase kinase kinase 10	kinase	Cytoplasm
Map3k12	mitogen-activated protein kinase kinase kinase 12	kinase	Cytoplasm
Mapk9	mitogen-activated protein kinase 9	kinase	Cytoplasm
Mapk12	mitogen-activated protein kinase 12	kinase	Cytoplasm
Pag1	phosphoprotein membrane anchor with glycosphingolipid microdomains 1	other	Plasma Membrane
Pik3cg	phosphatidylinositol-4,5-bisphosphate 3-kinase catalytic subunit gamma	kinase	Cytoplasm
Pik3r1	phosphoinositide-3-kinase regulatory subunit 1	kinase	Cytoplasm
Pik3r5	phosphoinositide-3-kinase regulatory subunit 5	kinase	Cytoplasm
Pik3r6	phosphoinositide-3-kinase regulatory subunit 6	kinase	Cytoplasm
Ptpn6	protein tyrosine phosphatase, non-receptor type 6	phosphatase	Cytoplasm
Ptprc	protein tyrosine phosphatase, receptor type C	phosphatase	Plasma Membrane
Rac2	ras-related C3 botulinum toxin substrate 2 (rho family, small GTP binding protein Rac2)	enzyme	Cytoplasm
Rras2	related RAS viral (r-ras) oncogene homolog 2	enzyme	Plasma Membrane
Syk	spleen associated tyrosine kinase	kinase	Cytoplasm
Synj1	synaptojanin 1	phosphatase	Cytoplasm
Synj2	synaptojanin 2	phosphatase	Cytoplasm
Tlr9	toll like receptor 9	transmembrane receptor	Plasma Membrane
Vav1	vav guanine nucleotide exchange factor 1	transcription regulator	Nucleus

Appendix 10: IPA of "Disease Progression" Turquoise Module. Complete list of genes in the Huntington's Disease Signaling pathway.

FVB/wt + ATXN1[82Q];CαM120A vs. ATXN1[82Q]			
Turquoise Module_Top Canonical Pathway_Huntington's Disease Signaling			
Gene Symbol - mouse (Entrez Gene)	Entrez Gene Name	Type(s)	Location
Akt2	AKT serine/threonine kinase 2	kinase	Cytoplasm
Arfip2	ADP ribosylation factor interacting protein 2	other	Cytoplasm
Bcl2l1	BCL2 like 1	other	Cytoplasm
Bdnf	brain derived neurotrophic factor	growth factor	Extracellular Space
Capn9	calpain 9	peptidase	Cytoplasm
Capn10	calpain 10	peptidase	Cytoplasm
Casp3	caspase 3	peptidase	Cytoplasm
Casp4	caspase 4	peptidase	Cytoplasm
Casp7	caspase 7	peptidase	Cytoplasm
Casp9	caspase 9	peptidase	Cytoplasm
Casq1	calsequestrin 1	other	Cytoplasm
Cdk5	cyclin dependent kinase 5	kinase	Nucleus
Cdk5r1	cyclin dependent kinase 5 regulatory subunit 1	kinase	Nucleus
Creb5	cAMP responsive element binding protein 5	transcription regulator	Nucleus
Creb3l4	cAMP responsive element binding protein 3 like 4	transcription regulator	Nucleus
Ctsd	cathepsin D	peptidase	Cytoplasm
Dlg4	discs large MAGUK scaffold protein 4	kinase	Plasma Membrane
Dnajc5	DnaJ heat shock protein family (Hsp40) member C5	other	Plasma Membrane
Gab1	GRB2 associated binding protein 1	kinase	Cytoplasm
Gnaq	G protein subunit alpha q	enzyme	Plasma Membrane
Gnb1	G protein subunit beta 1	enzyme	Plasma Membrane
Gng7	G protein subunit gamma 7	enzyme	Plasma Membrane
Gng11	G protein subunit gamma 11	enzyme	Plasma Membrane
Gng13	G protein subunit gamma 13	enzyme	Plasma Membrane
Gosr1	golgi SNAP receptor complex member 1	transporter	Cytoplasm
Gpaa1	glycosylphosphatidylinositol anchor attachment 1	enzyme	Cytoplasm

(continued from previous page)

FVB/wt + ATXN1[82Q];CαM120A vs. ATXN1[82Q]			
Turquoise Module_Top Canonical Pathway_Huntington's Disease Signaling			
Gene Symbol - mouse (Entrez Gene)	Entrez Gene Name	Type(s)	Location
Grb2	growth factor receptor bound protein 2	kinase	Cytoplasm
Grm1	glutamate metabotropic receptor 1	G-protein coupled receptor	Plasma Membrane
Grm5	glutamate metabotropic receptor 5	G-protein coupled receptor	Plasma Membrane
Hdac7	histone deacetylase 7	transcription regulator	Nucleus
Hdac10	histone deacetylase 10	transcription regulator	Nucleus
Hdac11	histone deacetylase 11	transcription regulator	Nucleus
Hras	HRas proto-oncogene, GTPase	enzyme	Plasma Membrane
Hspa2	heat shock protein family A (Hsp70) member 2	other	Cytoplasm
Hspa14	heat shock protein family A (Hsp70) member 14	peptidase	Cytoplasm
Ift57	intraflagellar transport 57	other	Cytoplasm
Irs1	insulin receptor substrate 1	enzyme	Cytoplasm
Itpr1	inositol 1,4,5-trisphosphate receptor type 1	ion channel	Cytoplasm
Jun	Jun proto-oncogene, AP-1 transcription factor subunit	transcription regulator	Nucleus
Map3k10	mitogen-activated protein kinase kinase kinase 10	kinase	Cytoplasm
Mapk9	mitogen-activated protein kinase 9	kinase	Cytoplasm
Napa	NSF attachment protein alpha	transporter	Cytoplasm
Napg	NSF attachment protein gamma	transporter	Cytoplasm
Nsf	N-ethylmaleimide sensitive factor, vesicle fusing ATPase	transporter	Cytoplasm
Pik3cg	phosphatidylinositol-4,5-bisphosphate 3-kinase catalytic subunit gamma	kinase	Cytoplasm
Pik3r1	phosphoinositide-3-kinase regulatory subunit 1	kinase	Cytoplasm
Pik3r5	phosphoinositide-3-kinase regulatory subunit 5	kinase	Cytoplasm
Pik3r6	phosphoinositide-3-kinase regulatory subunit 6	kinase	Cytoplasm
Plcb3	phospholipase C beta 3	enzyme	Cytoplasm
Plcb4	phospholipase C beta 4	enzyme	Cytoplasm
Polr2c	RNA polymerase II subunit C	enzyme	Nucleus
Polr2g	RNA polymerase II subunit G	enzyme	Nucleus
Polr2i	RNA polymerase II subunit I	transcription regulator	Nucleus

(continued from previous page)

FVB/wt + ATXN1[82Q];CαM120A vs. ATXN1[82Q]			
Turquoise Module_Top Canonical Pathway_Huntington's Disease Signaling			
Gene Symbol - mouse (Entrez Gene)	Entrez Gene Name	Type(s)	Location
Polr2l	RNA polymerase II subunit L	enzyme	Nucleus
Prkcg	protein kinase C gamma	kinase	Cytoplasm
Prkcz	protein kinase C zeta	kinase	Cytoplasm
Prkd1	protein kinase D1	kinase	Cytoplasm
Rest	RE1 silencing transcription factor	transcription regulator	Nucleus
Rph3a	rabphilin 3A	transporter	Plasma Membrane
Tlr9	toll like receptor 9	transmembrane receptor	Plasma Membrane
Ube2s	ubiquitin conjugating enzyme E2 S	enzyme	Nucleus
Vamp3	vesicle associated membrane protein 3	other	Plasma Membrane
Vti1b	vesicle transport through interaction with t-SNAREs 1B	transporter	Plasma Membrane

Appendix 11: IPA of "Disease Progression" Turquoise Module. Complete list of genes in the Superpathway of Cholesterol Biosynthesis pathway.

FVB/wt + ATXN1[82Q];CαM120A vs. ATXN1[82Q]			
Turquoise Module_Top Canonical Pathway_Superpathway of Cholesterol Biosynthesis			
Gene Symbol - mouse (Entrez Gene)	Entrez Gene Name	Type(s)	Location
Cyp51	cytochrome P450 family 51 subfamily A member 1	enzyme	Cytoplasm
Dhcr24	24-dehydrocholesterol reductase	enzyme	Cytoplasm
Fdft1	farnesyl-diphosphate farnesyltransferase 1	enzyme	Cytoplasm
Fdps	farnesyl diphosphate synthase	enzyme	Cytoplasm
Hadha	hydroxyacyl-CoA dehydrogenase/3-ketoacyl-CoA thiolase/enoyl-CoA hydratase (trifunctional protein), alpha subunit	enzyme	Cytoplasm
Hadhb	hydroxyacyl-CoA dehydrogenase/3-ketoacyl-CoA thiolase/enoyl-CoA hydratase (trifunctional protein), beta subunit	enzyme	Cytoplasm
Hmgcs1	3-hydroxy-3-methylglutaryl-CoA synthase 1	enzyme	Cytoplasm
Idi1	isopentenyl-diphosphate delta isomerase 1	enzyme	Cytoplasm
Lbr	lamin B receptor	enzyme	Nucleus
Lss	lanosterol synthase (2,3-oxidosqualene-lanosterol cyclase)	enzyme	Cytoplasm
Msmo1	methylsterol monooxygenase 1	enzyme	Cytoplasm
Nsdhl	NAD(P) dependent steroid dehydrogenase-like	enzyme	Cytoplasm
Pmvk	phosphomevalonate kinase	kinase	Cytoplasm
Sqle	squalene epoxidase	enzyme	Cytoplasm
Tm7sf2	transmembrane 7 superfamily member 2	enzyme	Cytoplasm

Appendix 12: IPA of "Disease Progression" Turquoise Module. Complete list of genes in the CREB Signaling in Neurons pathway.

FVB/wt + ATXN1[82Q];CαM120A vs. ATXN1[82Q]			
Turquoise Module_Top Canonical Pathway_CREB Signaling in Neurons			
Gene Symbol - mouse (Entrez Gene)	Entrez Gene Name	Type(s)	Location
Adcy8	adenylate cyclase 8	enzyme	Plasma Membrane
Akt2	AKT serine/threonine kinase 2	kinase	Cytoplasm
Calm3	calmodulin 1	other	Nucleus
Camk2a	calcium/calmodulin dependent protein kinase II alpha	kinase	Cytoplasm
Camk2b	calcium/calmodulin dependent protein kinase II beta	kinase	Cytoplasm
Creb5	cAMP responsive element binding protein 5	transcription regulator	Nucleus
Creb3l4	cAMP responsive element binding protein 3 like 4	transcription regulator	Nucleus
Gab1	GRB2 associated binding protein 1	kinase	Cytoplasm
Gnai1	G protein subunit alpha i1	enzyme	Plasma Membrane
Gnal	G protein subunit alpha L	enzyme	Cytoplasm
Gnao1	G protein subunit alpha o1	enzyme	Plasma Membrane
Gnaq	G protein subunit alpha q	enzyme	Plasma Membrane
Gnaz	G protein subunit alpha z	enzyme	Plasma Membrane
Gnb1	G protein subunit beta 1	enzyme	Plasma Membrane
Gng7	G protein subunit gamma 7	enzyme	Plasma Membrane
Gng11	G protein subunit gamma 11	enzyme	Plasma Membrane
Gng13	G protein subunit gamma 13	enzyme	Plasma Membrane
Grb2	growth factor receptor bound protein 2	kinase	Cytoplasm
Gria1	glutamate ionotropic receptor AMPA type subunit 1	ion channel	Plasma Membrane
Gria3	glutamate ionotropic receptor AMPA type subunit 3	ion channel	Plasma Membrane
Grid2	glutamate ionotropic receptor delta type subunit 2	ion channel	Plasma Membrane
Grik1	glutamate ionotropic receptor kainate type subunit 1	ion channel	Plasma Membrane
Grin1	glutamate ionotropic receptor NMDA type subunit 1	ion channel	Plasma Membrane
Grm1	glutamate metabotropic receptor 1	G-protein coupled receptor	Plasma Membrane
Grm3	glutamate metabotropic receptor 3	G-protein coupled receptor	Plasma Membrane
Grm5	glutamate metabotropic receptor 5	G-protein coupled receptor	Plasma Membrane

(continued from previous page)

FVB/wt + ATXN1[82Q];CαM120A vs. ATXN1[82Q]			
Turquoise Module_Top Canonical Pathway_CREB Signaling in Neurons			
Gene Symbol - mouse (Entrez Gene)	Entrez Gene Name	Type(s)	Location
Grm7	glutamate metabotropic receptor 7	G-protein coupled receptor	Plasma Membrane
Hras	HRas proto-oncogene, GTPase	enzyme	Plasma Membrane
Irs1	insulin receptor substrate 1	enzyme	Cytoplasm
Itpr1	inositol 1,4,5-trisphosphate receptor type 1	ion channel	Cytoplasm
Map2k1	mitogen-activated protein kinase kinase 1	kinase	Cytoplasm
Notum	NOTUM, palmitoleoyl-protein carboxylesterase	enzyme	Extracellular Space
Pik3cg	phosphatidylinositol-4,5-bisphosphate 3-kinase catalytic subunit gamma	kinase	Cytoplasm
Pik3r1	phosphoinositide-3-kinase regulatory subunit 1	kinase	Cytoplasm
Pik3r5	phosphoinositide-3-kinase regulatory subunit 5	kinase	Cytoplasm
Pik3r6	phosphoinositide-3-kinase regulatory subunit 6	kinase	Cytoplasm
Plcb3	phospholipase C beta 3	enzyme	Cytoplasm
Plcb4	phospholipase C beta 4	enzyme	Cytoplasm
Plcd3	phospholipase C delta 3	enzyme	Cytoplasm
Plcd4	phospholipase C delta 4	enzyme	Cytoplasm
Polr2c	RNA polymerase II subunit C	enzyme	Nucleus
Polr2g	RNA polymerase II subunit G	enzyme	Nucleus
Polr2i	RNA polymerase II subunit I	transcription regulator	Nucleus
Polr2l	RNA polymerase II subunit L	enzyme	Nucleus
Prkar2b	protein kinase cAMP-dependent type II regulatory subunit beta	kinase	Cytoplasm
Prkcg	protein kinase C gamma	kinase	Cytoplasm
Prkcz	protein kinase C zeta	kinase	Cytoplasm
Prkd1	protein kinase D1	kinase	Cytoplasm
Rras2	related RAS viral (r-ras) oncogene homolog 2	enzyme	Plasma Membrane
Tlr9	toll like receptor 9	transmembrane receptor	Plasma Membrane